Understanding the endoplasmic reticulum – mitochondrial crosstalk in the alveolar epithelium in lung fibrosis

Inaugural Dissertation

submitted to the Faculty of Medicine in partial fulfilment of the requirements

for the degree of Dr. biol. hom. of the Faculty of Medicine

of the Justus Liebig University Giessen

by Bickelhaupt, Jessica, geb. Knöll

from Groß-Umstadt, Germany

Giessen, 2023

From the Center for Interstitial and Rare Lung Diseases

of the Faculty of Medicine, Justus Liebig University Giessen

Director: Prof. Dr. Günther, Andreas

First Supervisor: Prof. Dr. Günther, Andreas

Second Supervisor: Prof. Dr. Pullamsetti, Soni

Date of Doctoral Defense: 23.01.2024

Index

1 Introduction

1.1 Idiopathic Pulmonary Fibrosis

Idiopathic Pulmonary Fibrosis (IPF) is a chronic and progressive lung disease belonging to the group of Idiopathic Interstitial Pneumonias (IIP), one of the most frequent forms of Diffuse Parenchymal Lung Disease (DPLD). The etiology remains unknown, but several age-related factors as well as harmful environmental factors, such as smoking, play a major role in the pathogenesis. IPF is a devastating disease mostly affecting the elderly, with a median survival rate of two to three years after diagnosis [Barkauskas, C.E. et al. 2014]. Currently there are two drugs available for the therapy of IPF, pirfenidone and nintedanib. They may slow down disease progression, but do not reverse the disease process. At present, lung transplantation is the only curative treatment for IPF [Kalchiem-Dekel, O. et al. 2018]. Consequently, median survival remains quite low. The pathogenesis of IPF still remains to be fully elucidated, but chronic alveolar epithelial cell type II (AECII) injury and apoptosis, disturbed epithelial-mesenchymal crosstalk, activation of fibroblasts and excessive collagen deposition represent major events [Kalchiem-Dekel, O. et al. 2018, Klymenko, O. et al. 2019, Lawson, W.E. et al. 2008, Selman, M. et al. 2004, Selman, M. et al. 2006]. With regard to AECII injury, “maladaptive”, pro-apoptotic, endoplasmic reticulum (ER) stress - in part due to induction and nuclear overexpression of CHOP - have been reported in AECIIs of patients with sporadic and familial IPF [Korfei, M. et al. 2008, Lawson, W.E. et al. 2008].

Progressive decline in lung function, first during exercise, later on at rest, is observed in all IPF patients. This is a very general symptom which may results from cardiac or other lung diseases as well, leading to misdiagnosis [American Thoracic Society. 2000]. Other common symptoms in addition to dyspnea are dry, non-productive cough as well as finger clubbing. Some late stage patients show signs of right ventricular failure, which could lead to the development of pulmonary hypertension [Lynch, D.A. et al. 2018]. As mentioned before, aging is one major risk factor for the pathogenesis of IPF [Selman, M. et al. 2010].

Histologically, IPF lungs show a pattern of ‘Usual Interstitial Pneumonia’ (UIP) which is characterized by hyperplastic alveolar epithelium next to dense fibrosis, typically characterized by fibroblastic foci heterogeneity with fibrotic areas directly adjacent to

normal appearing tissue, and loss of alveolar architecture (**Figure 1**) [Lai, C.K. et al. 2006, Mueller-Mang, C. et al. 2007, Wolters, P.J. et al. 2014]. Inflammatory changes may be seen, but are usually not prominent.

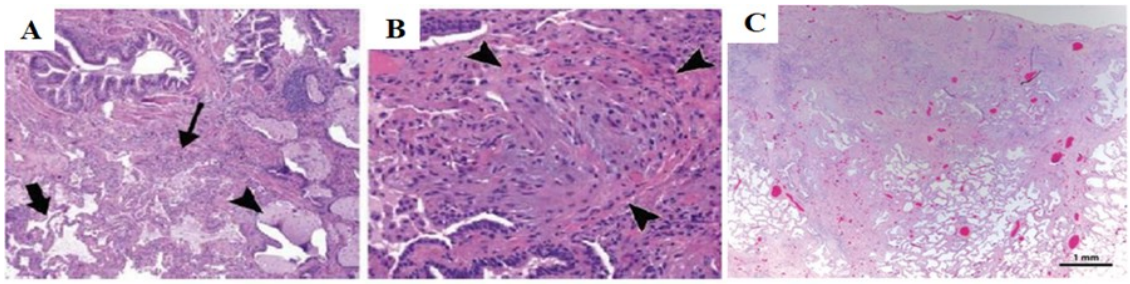

Figure 1 Histologic features of UIP
For details see text **[Mueller-Mang, C. et al. 2007, Wolters, P.J. et al. 2014]**

As already mentioned, pathogenesis of IPF is still elusive. There are two main hypotheses of IPF pathogenies: an older inflammatory hypothesis and a more recent alveolar epithelial cell injury hypothesis.

The inflammatory hypothesis proposed that chronic; uncontrolled inflammation would lead to proliferation of fibroblasts, promoting fibrosis. The cause and the mechanisms of such chronic inflammation have not been fully understood [Noble, P.W. et al. 2005]. Several studies suggested herpesvirus infection as a trigger of fibrosis [Lok, S.S. et al. 2002]. Also, such theory was supported by obvious signs of inflammation in computed tomography (CT), in histological samples and in bronchoalveolar lavage (BAL). On the other hand, conventional anti-inflammatory therapies did not elicit beneficial effects in clinical trials of IPF. All this indicated that inflammation may have little or no impact on the pathogenesis of IPF [Keane, M.P. et al. 2006].

According to a more recent theory, repeated, prolonged alveolar epithelial injury and aberrant wound healing could lead to IPF [American Thoracic Society. 2000, Barkauskas, C.E. et al. 2014]. Injury to AECIIs leads to proliferation of interstitial fibroblasts and their differentiation into myofibroblasts [Li, X. et al. 2017]. These fibroblasts produce an excessive amount of collagen and other extracellular matrix (ECM) components that lead to the development of fibrotic patches [Kim, K.K. et al. 2006]. This epithelial injury concept is supported by several studies in animal models where AECs have been shown to be vulnerable to apoptotic stimuli, leading to lung injury and subsequent fibrosis [B Moore, B. et al. 2013, Braakman, I. et al. 2011, Günther, A. et al. 2012]. The most frequently used animal model of lung fibrosis is the bleomycin (BLM) induced injury

model, with either single or repetitive doses that result in AECII hyperplasia, DNA damage, oxidative stress and ER stress supporting inflammation and ECM deposition [Korfei, M. et al. 2008, Tanjore, H. et al. 2012]. Also the amiodarone (AD) murine model shows AECII hyperplasia, AECII apoptosis and both lysosomal and ER stress [Mahavadi, P. et al. 2014, Mahavadi, P. et al. 2015]. Another animal model is the asbestosis model displaying histopathological signs of UIP as well as alveolar epithelial injury after single intratracheal application [Sanchez, V.C. et al. 2009]. The fluorescein isothiocyanate (FITC) model displays AECII injury, additional FITC conjugates can be visualized by fluorescence [Roberts, S.N. et al. 1995]. Taken together all these animal models supported AECII injury in lung fibrosis [Moore, B.B. et al. 2008]. To be mentioned, the administration of silica particles may also lead to the development of interstitial lung fibrosis in murine lungs, referred to as silicosis [Davis, G.S. 1986]. It is not a AECII injury model, but it is used to study the innate immune responses in fibrotic lung injury. Intratracheal application of silica leads to a persistent, toxic and inflammatory response [Barbarin, V. et al. 2005].

1.2 The Pulmonary Surfactant

The alveolar surface is covered by two types of epithelial cells, alveolar cells types I (AECI) and AECII. The vast majority of the surface is covered by AECI. These are flattened cells that maintain a thin barrier between blood and air. Their main feature is to facilitate gas exchange. AECII are cuboidal epithelial cells and their main function is the synthesis, storage and secretion of the pulmonary surfactant [Andreeva, A.V. et al. 2007]. Compounds of the innate immune defence system are also produced by AECIIs. Genetic lineage-tracing experiments have showed that surfactant protein C positive (*SFTPC*-positive) AECII can self-renew and transdifferentiate into AECI [Barkauskas, C.E. et al. 2013]. Indeed, AECIIs have a high potential to proliferate [Uhal, B.D. 1997]. Pulmonary surfactant is a complex mixture of lipids and proteins which prevents alveolar collapse by reducing surface tension at the air-water interphase. In premature infants with respiratory distress syndrome (RDS), a lack of surfactant has been identified to cause respiratory failure. Biochemically, pulmonary surfactant contains approximately 90% lipids, mainly amphiphilic phospholipids. Some of them are produced in the ER of the AECII. 10% of surfactant is represented by proteins, namely the surfactant proteins SP-A, SP-B, SP-C and SP-D [Griese, M. 1999].

SP-B and SP-C are small and light proteins, which are extremely hydrophobic, whereas SP-A and SP-D are big, hydrophilic, collectin-like glycoproteins. SP-C is the only surfactant protein which is expressed exclusively by AEC II in lungs and therefore serves as a marker for AECII. The surfactant proteins are processed and stored in the lamellar bodies in the AECII. These lysosome related organelles are then secreted to release surfactant via exocytosis [Weaver, T.E. et al. 2002]. Almost two thirds of the entirely surfactant pool is found within alveolar space, where it lowers the surface tension at the air-liquid interface [Committee on Fetus and Newborn et al. 2014]. Surfactant can be found in large amounts in the bronchoalveolar lavage (BAL) fluid. BAL therefore represents a main source to study surfactant composition [Mahavadi, P. 2009]. Some lipid components can be recycled by AECII from uptaken surfactant [Haller, T. et al. 1998, Weaver, T.E. et al. 2002].

In the ER of AECII, SP-C is synthesized as a 21 kDa propeptide (pro SP-C) including peptide domains on both the amino- and the carboxyl-terminal ends of the mature protein [Günther, A. et al. 2012]. Several proteolytic cleavage processes of the propeptide, which take place during the journey of the protein through trans-Golgi network, multivesicular bodies and laminar bodies, result in a 3.7 kDa mature SP-C that will be co-secreted with the lipids via laminar bodies into the alveolar space [Conkright, J.J. et al. 2001, Günther, A. et al. 2012, Solarin, K.O. et al. 2001].

1.3 Familial Interstitial Pneumonia

While IPF may occur sporadically, it may also develop in the context of heritable genetic predispositions. Human genetic studies have revealed associations between mutations in genes encoding surfactant proteins (*SFTPA2*, *SFTPC*) and the development of Familial Interstitial Pneumonia (FIP). Clinical, radiological as well as pathological characteristics of FIP are indistinguishable from those of IPF except for a younger age of onset for FIP [Thomas, A.Q. et al. 2002]. Also mutations in telomerase or telomere-related genes (*TERC*, *TERT*) have been ascribed to underlie FIP [Armanios, M.Y. et al. 2007]. Telomeres are associated proteins of repetitive sequence (TTAGGG) stabilizing the ends of chromosomes [Yildirim, H. et al. 2020]. The telomere sequence is shortened after every cell cycle due to the activity of the DNA polymerase, however the telomerase elongates the telomeres by de novo addition of TTAGGG repeat sequences to the telomere ends [Greider, C.W. et al. 1989]. The telomerase consists of the telomerase reverse transcriptase (TERT) and the telomerase RNA component (TERC) which is used as a

template [Gavory, G. et al. 2002]. Mutations in the genes of these subunits lead to a defective function of the telomerase and thereby to telomere shortening. This has been reported to be a reason for increased susceptibility to lung fibrosis and other clinical syndromes/conditions such as aplastic anaemia or dysceratosis congenita. After getting exposed to an injurious stimulus, shortened telomeres promote lung fibrosis due to development of replicative senescence and impaired tissue repair [Bilgili, H. et al. 2019].

Lung fibrosis may also develop due to mutations in genes encoding components of several, lysosomal cargo protein complexes in patients with Hermansky-Pudlak syndrome (HPS). HPS is a group of autosomal recessive disorders, which clinically show occulocutaneous albinism, platelet storage pool deficiency, ceroid lipofuscinosis and an early death caused by severe fibrotic lung disease in some forms. The cause of this severe disease could be functionally impaired lysosome related organelles (LROs), but still need to be fully elucidated. Patients with HPS type 1, 2 and 4 mutations display pathological features similar to those of IPF patients and are grouped together as HPS associated interstitial pneumonia (HPSIP) [Fulton, A.B. 1999, Pierson, D.M. et al. 2006].

Mutations in the BRICHOS domain of the SP-C gene in patients with familial interstitial lung disease have been described [Amin, R.S. et al. 2001, Brasch, F. et al. 2004, Cameron, H.S. et al. 2005, Nogee, L.M. et al. 2001]. The BRICHOS domain is a highly conserved homologous region in several proteins that belongs to the British and Danish dementia (BRI) family as well as to proteins like CA11, Chondromodulin-1 (ChM-I) and SP-C. The BRICHOS domain consists of around 100 amino acids [Mulugeta, S. et al. 2005]. At this stage, more than 60 mutations of SP-C have been reported [Mulugeta, S. et al. 2015]. Loss of function mutations of the SP-B gene lead to fatal neonatal respiratory disease, SP-A and SP-C deficiency have been associated with interstitial lung disease. These SP-C gene mutations in the BRICHOS domain leads to alternate splicing of SP-C mRNA, resulting in structurally altered carboxyl terminal and misfolded proteins. These misfolded proteins cannot be cleaved to generate mature SP-C. As a consequence, the misfolded pro-SP-C accumulates in the ER of the cell or it will be transferred to the cytosol leading to a toxic gain of function, maladaptive ER stress response and finally to chronic injury of AECII. It also appears that the misfolded pro SP-C can bind to wildtype SP-C in vitro, leading to aggregation and loss of functional SP-C (**Figure 2**) [Günther, A. et al. 2012, Nogee, L.M. et al. 2001] .

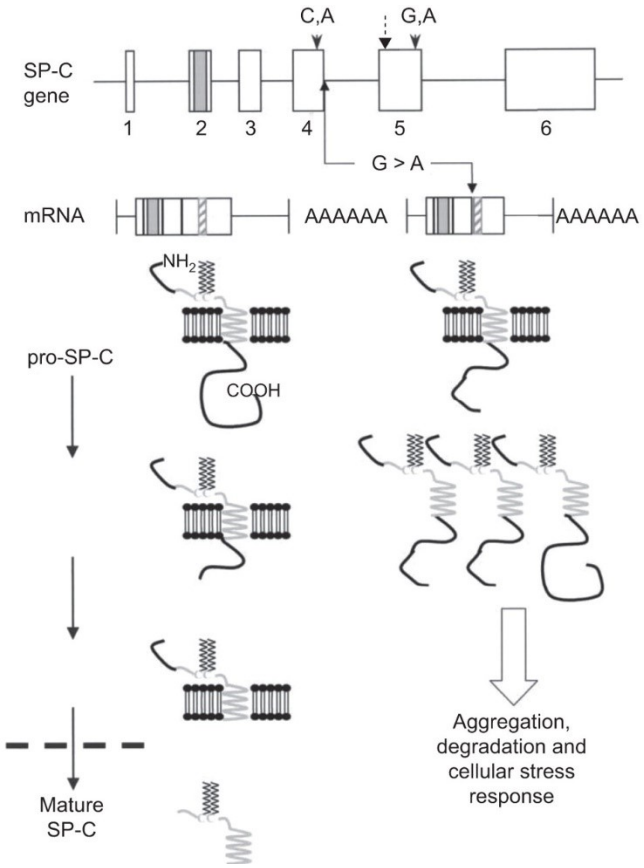

Figure 2 Surfactant protein (SP)-C mutations lead to protein misfolding
SP-C mutation leads to alternate splicing of SP-C mRNA, resulting in defective proprotein. This in turn leads to accumulation and seems to cause pro-apoptotic ER stress. Adapted from **[Günther A et al. 2012]**

These findings strongly suggest an important role of these two proteins in normal lung function. In 2003, Bridges et al. have generated a transgenic mouse model with SP-C$^{\Delta exon4}$ mutation to study lung development. These mice displayed defective lung morphogenesis resulting in fetal death. This study confirmed that mutation in the SP-C gene leads to protein misfolding and aberrant surfactant processing, which is essential for proper lung morphogenesis [Bridges, J.P. et al. 2003]. Another mutation of the SP-C gene (*SFTPC*) leads to an SP-C deficiency and also demonstrates abnormal lamellar bodies [Azuma, A. 2005]. Nureki et al. have developed a knock-in mouse model for the SP-C^{I73T} mutation. In this SP-C missense variant the substitution g.1286T>C results in a change of isoleucine to threonine at position 73 in the SP-C proprotein (SP-C^{I73T}) [Nureki, S.-I. et al. 2018]. This *SFTPC* mutation is associated with interstitial lung disease (ILD) [Cameron, H.S. et al. 2005].These mice display accumulation of misprocessed proSP-C^{I73T} protein resulting in early mortality after four to seven days. These mice also reflect multiple features of human IPF marked by diffuse parenchymal lung injury, inflammation alongside to AECII stress as well as fibrotic tissue remodeling. In addition altered

autophagy was observed in AECII after induction of SP-C^{I73T} mutation by tamoxifen [Nureki, S.-I. et al. 2018]. Nureki et al have demonstrated that mutation in SP-C gene especially the *STFPC*^{I73T} mutation drives AECII injury and aberrant repair.

Early studies of patients with mutations in SP-C give a hint towards ER stress as a main trigger in pulmonary fibrosis. In 2001 Nogee et al. reported a heterozygous substitution of A for G in the first base of intron 4 of the human SP-C gene (c.460+1A>G) that causes a lack of mature SP-C protein in infants with nonspecific interstitial pneumonia [Hamvas, A. et al. 2004, Nogee, L.M. et al. 2001]. This mutation resulted in alternate splicing of the SP-C mRNA leading to a deletion of exon 4(Δexon4). This in turn leads to misfolding of pro SP-C by removal of conserved structures in the BRICHOS domain in the C-terminus of pro SP-C. The BRICHOS domain is important for the effective translocation to the ER. Therefore mutations in the BRICHOS domain lead to mutant proteins that are left in the cytosol of the cell and accumulate there as aggresomes [Russo, S.J. et al. 1999]. SP-C protein is known to form homomers. In that mutant form is not only able to bind to other SP-C mutant molecules but also to wild-type pro SP-C (SP-C^{WT}) leading to aggresome formation and implying a dominant-negative effect on the trafficking of wild-type pro SP-C [Kabore, A.F. et al. 2001, Wang, W.-J. et al. 2003].

In vitro studies of the Δexon4 mutation have revealed ER stress and caspase 4 mediated apoptosis in AECII like cell lines (A549, MLE12) [Beers, M.F. et al. 1998, Mulugeta, S. et al. 2007]. As mentioned previously, the transgenic mouse model of *SFTPC*$^{\Delta exon4}$ mutation under human *SFTPC* promotor showed abnormal lung morphogenesis during lung development with abnormal surfactant processing and accumulation of misfolded proteins in the ER, resulting in fetal death [Bridges, J.P. et al. 2003]. Another transgenic mouse model employing a tet-on system for conditional expression of L188Q *SFTPC* mutation specifically in alveolar type II cells was generated. Mice with this mutation displayed modest ER stress in AECII, but this did not lead to AECII apoptosis or pulmonary fibrosis. Only additional treatment with low doses of bleomycin resulted in extensive AECII death via activation of caspase-4 and in development of lung fibrosis [Lawson, W.E. et al. 2011]. By a second hit with an additional stressor the AECII undergo full apoptosis resulting in pulmonary fibrosis. The findings in familial cases of IPF have pointed towards an important role of AECII injury in the early stage of IPF. Furthermore, ER stress has also been observed in IPF patient lungs without *SFTPC* mutations [Korfei, M. et al. 2008, Lawson, W.E. et al. 2008].

Two quality control systems are affected by SP-C$^{\Delta exon4}$ mutation: the unfolded protein response (UPR), which is activated by ER overload of accumulated misfolded proteins; and the ubiquitin/proteasome system (UPS), which ubiquitinates and degrades misfolded and damaged protein via the proteasome (**Figure 3**) [Mulugeta, S. et al. 2005].

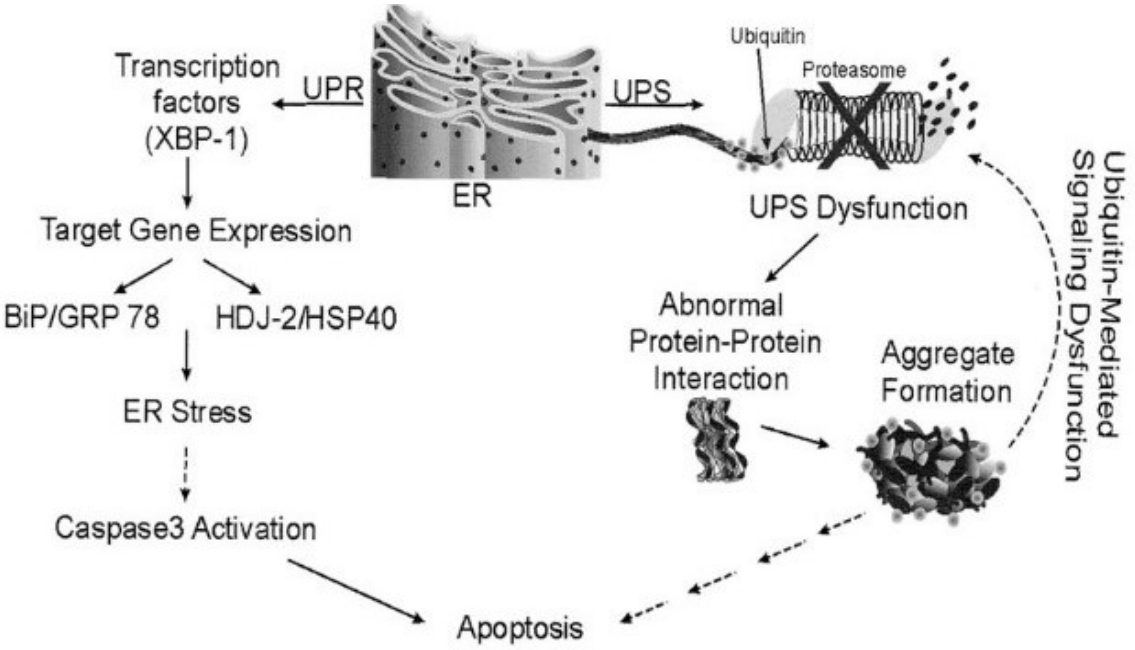

Figure 3 Dual effect of the SP-C BRICHOS domain mutant leading to cellular dysfunction.

At least two separate subcellular systems are affected by BRICHOS domain mutant expression: the UPR and UPS pathways. Reprinted with permission of the American Thoracic Society. Copyright © 2023 American Thoracic Society. All rights reserved. From **[Mulugeta S et al. 2005]**

Under normal conditions, propeptides of secretory or transmembrane proteins are modified and properly folded in the ER and translocated to the Golgi apparatus. Misfolded proteins however, are initially retained in the ER to facilitate proper folding. When the misfolded proteins accumulate, ER stress occurs, leading to UPR activation. When the capacity for ER accumulation is exceeded, the ER cannot keep the misfolded proteins any longer, so that protein translocate to the cytosol. This overwhelms the UPR, which is no longer able to degrade all misfolded proteins, resulting in the accumulation of mutant SP-C in the cytosol and the formation of aggresomes and the induction of caspase 3 and finally apoptosis. These aggregates can interact with different cellular targets and may interfere in normal cell processes Additionally, nonfunctional heteromeric aggresomes of mutant SP-C with SP-C^{WT} can bind ubiquitin leading to inhibition of ubiquitin-mediated signaling function and disturb the UPS system. All this interference with cellular quality control mechanisms lead to a disrupted cell function and, finally, cell death [Bridges, J.P. et al. 2003, Johnston, J.A. et al. 1998].

1.4 Unfolded Protein Response (UPR)

The ER is responsible for proper folding and posttranslational modifications of secreted and membrane proteins, production of steroids, synthesis of lipids, storage and production of glycogen and calcium homeostasis [Berridge, M.J. 2002]. Initial proteins, which are supposed to be secreted, are delivered to the ER by polypeptide chains that act as a signal-anchor. In the ER polypeptides will be folded correctly into three-dimensional conformation for proper functions of the protein. Proteins are further modified, e.g. glycosylated, and then processed through the secretory pathway. The chaperone-based process of protein folding requires high Ca^{2+} levels. This Ca^{2+} is typically stored inside the ER lumen in the sarcoplasmic reticulum (SR) [Braakman, I. et al. 2011]. The folding of proteins in the ER is supported by chaperone proteins like immunoglobulin binding protein (BiP), also known as glucose regulated protein-78 (GRP78). Under stress conditions like calcium depletion, metabolic stress, reduced energy stores or accumulation of unfolded, misfolded, or mutant proteins, BiP is dissociated from its receptor and initiates the unfolded protein response (UPR). Persistent ER stress activates the ER-associated degradation (ERAD) pathway, which usually results in improved protein folding accelerated removal of misfolded proteins, reduced ER burden, maintained cellular homeostasis and thereby avoid once of cell death [Hetz, C. 2012].

The cause of ER stress in IPF still remains elusive, but common environmental exposures such as herpesviruses, inhaled particulates, and cigarette smoke are known to induce ER stress and contribute to AECII vulnerability [Baumgartner, K.B. et al. 1997, Bonner, J.C. 2007]. The main function of the UPR is to restore ER capacity, therefore activating transcription factors, which reduce protein translation and enhance ER chaperone production to improve protein folding as well as metabolism and redox proteins. The UPR also promotes protein degradation via ERAD and maintains cellular homeostasis to prevent apoptosis through accumulation of misfolded proteins which disturb cellular functions [Lee, A.S. 2005, Zhang, L. et al. 2017]. When these UPR mechanisms fail and correct protein folding is not achieved or if ER stress persists, the cell undergoes cell death [Han, J. et al. 2013].

The UPR pathways can be activated by three ER transmembrane stress sensors: PKR-like ER kinase (PERK; also known as EIF2ZAK3), activating transcription factor 6α (ATF6α) and inositol requiring enzyme 1α (IRE1α; also known as ERN1) [B Moore, B. et al. 2013]. Under normal conditions the stress sensors are bound to the chaperone BiP (GRP78) and

are hence in an inactivate state. As mentioned before, BiP/GRP78 is one of the major ER chaperones and belongs to the family of heat shock proteins. It mediates proper protein folding in the ER. If proteins are folded correctly, they get dissociated from BiP and will be transferred to the Golgi apparatus. Upon accumulation of misfolded proteins, the bound BiP dissociates from the three stress receptors PERK, ATF6 and IRE1α to facilitate proper folding. The now free sensors are activated and start signaling cascades [Jäger, R. et al. 2012]. These three pathways are described below in more detail:

The activation of PERK leads to its autophosphorylation and dimerization [Liu, C.Y. et al. 2000]. PERK then phosphorylates and thereby inactivates the α-subunit of eukaryotic translational initiation factor 2 (eIF2α). The eIF2 complex is required for the initiation of protein synthesis, therefore inhibition eIF2α leads to protein synthesis arrest. Phosphorylated eIF2α also regulates the expression of ATF3 and C/EBP homologous protein (CHOP) via ATF4 [Brush, M.H. et al. 2003, Harding, H.P. et al. 2000]. Under persistent ER stress, ATF4 induces growth arrest and DNA damage inducible gene 34 (GADD34) leads to dephosphorylation of eIF2α [Gorman, A.M. et al. 2012, Novoa, I. et al. 2001]. When BiP is released from ATF6 during ER stress, it translocates ATF6 to the Golgi apparatus, where it is cleaved by site 1 and site 2 proteases [Shen, J. et al. 2004]. The cleaved product passages into the nucleus where it binds to cis-acting ER stress response elements (ERSE) and activates the transcription of ER protein-folding chaperones such as BiP, GRP94, calnexin as well as ER-associated protein degradation (ERAD) components [Wang, Y. et al. 2000]. In mammalian cells ATF6 exists in two isoforms, ATF6α and ATF6β. It induces X-box binding protein 1 (XBP-1) expression, which is an a transcription factor, that is activated by IRE-1α [Gorman, A.M. et al. 2012, Yoshida, H. et al. 2001]. The transmembrane protein IRE-1α is an intrinsic serine/ threonine kinase, meaning that it phosphorylates proteins with threonine or serine residues and also has endonuclease activity, which will be activated under ER stress. In mammals two homologues of IRE-1 exist, IRE1α and IRE1β, which homodimerize upon BiP release. After dimerization IRE-1 displays an RNase activity, which cleaves a 26-nucleotide long intron sequence from the transcription factor XBP-1. Spliced XBP-1 then translocates to the nucleus and binds to ERSE and promotes the transcription of ERAD target genes (**Figure 4**) [Gorman, A.M. et al. 2012, Hiller, M.M. et al. 1996].

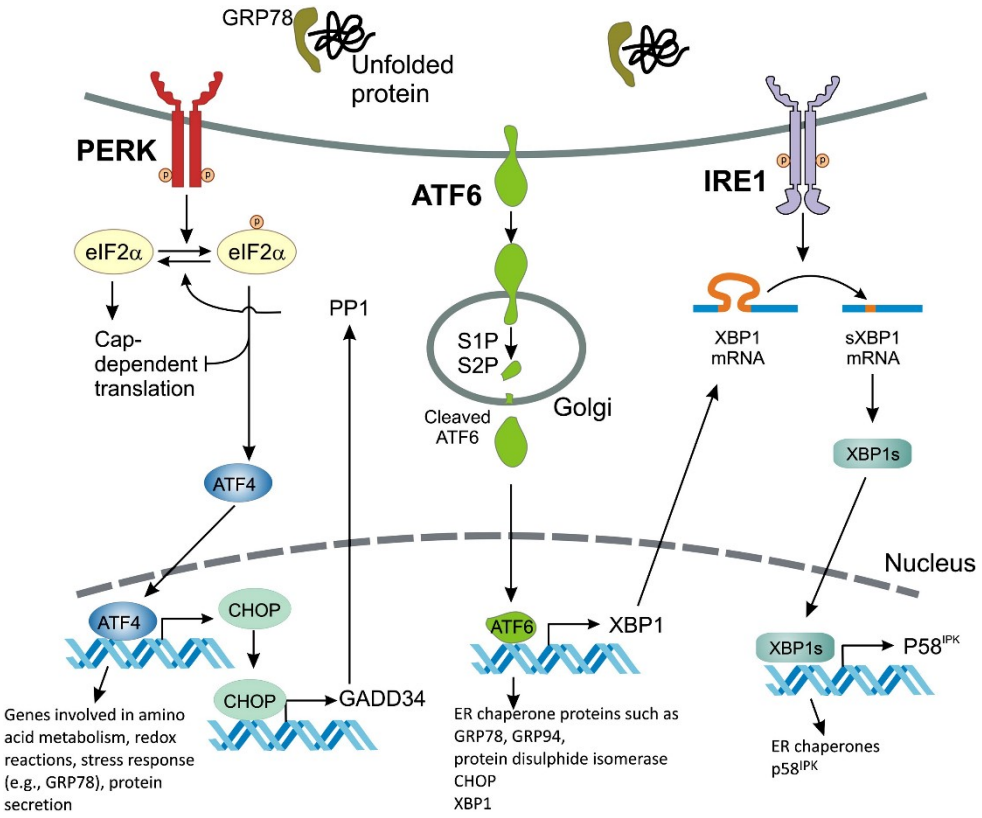

Figure 4 The UPR is mediated by three ER stress sensors
Schematic illustration of ER stress and UPR. Adapted from **[Gorman AM et al. 2012]**

If ER stress response is prolonged, then ERAD pathway will be activated. The exact mechanism by which ERAD recognizes and degrades misfolded proteins is not yet clear. But it is known that it takes place in five different steps: 1) Recognition of misfolded proteins by chaperones like calnexin (CNX) or BiP; 2) ER-degradation enhances α-mannosidase-like protein (EDEM) facilitate the release of the misfolded protein from calnexin and target them for degradation; 3) protein disulfide isomerase (PDI) facilitates the retro-translocation of misfolded proteins from the ER into the cytosol via translocons; 4) Then misfolded proteins will be ubiquitinated via enzymatic reactions mediated by E1 (ubiquitin activating enzyme), E2 (ubiquitin conjugating enzyme), and E3 (ubiquitin ligase); and 5) transport of ubiquitinated proteins into the proteasome for their degradation [Yoshida, H. 2007].

UPR pathway is induced to attenuate ER stress and protect the cell. However, prolonged or severe ER stress can result in cellular apoptosis through extrinsic and intrinsic pathways [Gorman, A.M. et al. 2012]. In the case of an intrinsic pathway, stimuli like calcium influx from the ER to the cytosol causes the release of cytochrome c from the mitochondria into cytosol. In the cytosol cytochrome c forms a complex known as the

apoptosome with Apaf-1 and procaspase-9 in the presence of ATP/dATP to process and activate initiator caspase [Wang, X. 2001]. In the case of an extrinsic pathway a ligand binds to death receptors like Fas, TNFR1 or DR3,4,5 with the help of adaptor proteins like Fas-associated protein with death domain (FADD). Activation of these cell surface receptors leads to recruitment of initiator procaspase-8 which will be cleaved by a complex that induces caspase-8 [Ashkenazi, A. et al. 1998]. Once activated, the upstream initiator caspases cleave and activate downstream effector caspases such as caspase -3,-6 and -7, which in turn cleave death substrates and induce apoptosis [Earnshaw, W.C. et al. 1999]. The extrinsic pathway is linked together with the intrinsic pathway through caspase-8 cleavage of BH3-only protein Bid that activates the mitochondrial pathway in order to induce apoptosis [Wang, X. 2001]. Both pathways require calcium influx from the ER to the cytosol as well as the activity of inflammatory caspase-4. Under ER stress initiator caspase-9 cleaves procaspase-3 and effector caspase-3 in turn mediates cell death pathways [Zhang, L. et al. 2017].

CHOP is another transcription factor that is involved in ER stress induced apoptosis. CHOP can be activated by all three UPR sensor receptors. ATF4, ATF6 and XBP-1 have binding sites in the CHOP gene promoter [Ma, Y. et al. 2002, Zinszner, H. et al. 1998]. Our group showed an increased AECII apoptosis and fibroblast proliferation as well as extensive collagen production as a result of CHOP overexpression *in vitro* in alveolar epithelial cells [Klymenko, O. et al. 2019]. After induction CHOP is translocated into the nucleus and bound on an ERSE element in order to upregulate pro-apoptotic genes such as BH-3 only protein Bim [Puthalakath, H. et al. 2007] and downregulate anti-apoptotic genes namely BCL2 [McCullough, K.D. et al. 2001]. Tanaka et al. have demonstrated transient increase of CHOP mRNA expression as well as protein expression in an early phase in bleomycin induced pulmonary fibrosis mice model. In addition, Chop knock-out (KO) mice display significant decrease of inflammation, apoptosis and fibrosis in bleomycin induced pulmonary fibrosis compared with the WT mice. These results suggest that CHOP plays a role in the development and exacerbation of BLM-induced pulmonary fibrosis in mice models [Tanaka, Y. et al. 2015].

In human IPF lung tissue our group has demonstrated apoptotic proteins in the same AECII fibrotic region which also expressed ER stress markers including CHOP [Korfei, M. et al. 2008]. This study suggests induction of ER stress may trigger profibrotic phenotype via enhanced AEC injury and death [Lawson, W.E. et al. 2011, Lin, J.H. et al.

2008]. Recently, a study by Baek et al. [Baek, H.A. et al. 2012] has revealed that UPR activation may also be involved in myofibroblast differentiation of lung fibroblasts. This confirms the link between ER stress and profibrotic cell phenotypes. Taken together it is known that ER stress leads to AECII vulnerability, which are then sensitive to additional environmental injury, which leads to aberrant epithelial repair and all together promotes fibrosis (**Figure 5**) [Tanjore, H. et al. 2012].

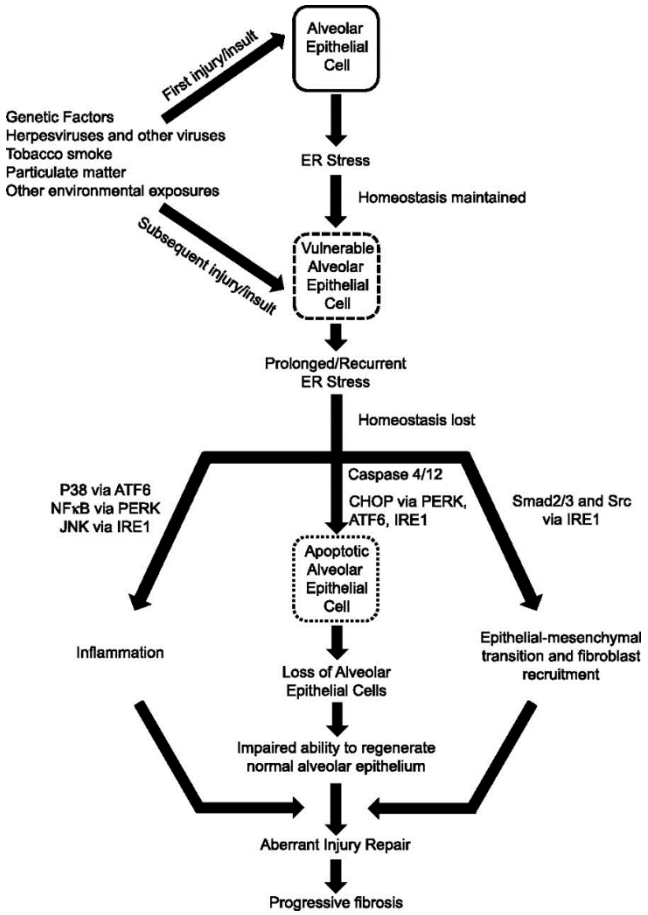

Figure 5 Schematic presentation of proposed mechanisms by which ER stress may contribute to the development of pulmonary fibrosis. Adapted from **[Tanjore H et al. 2012]**

1.5 Autophagy in the pathogenesis of IPF

Another mechanism through which cells cope with ER stress is autophagy [B'chir, W. et al. 2014]. Autophagy is a major cell quality process it degrades proteins, cellular components and organelles via the lysosomal pathway. Autophagy is also involved in recycling processes. In the case of degradation of misfolded protein, autophagy indirectly regulates cell survival. Till now, three types of autophagy are known: macroautophagy, microautophagy and chaperone-mediated autophagy (**Figure 6**) [Murrow, L. et al. 2013, Wirawan, E. et al. 2012].

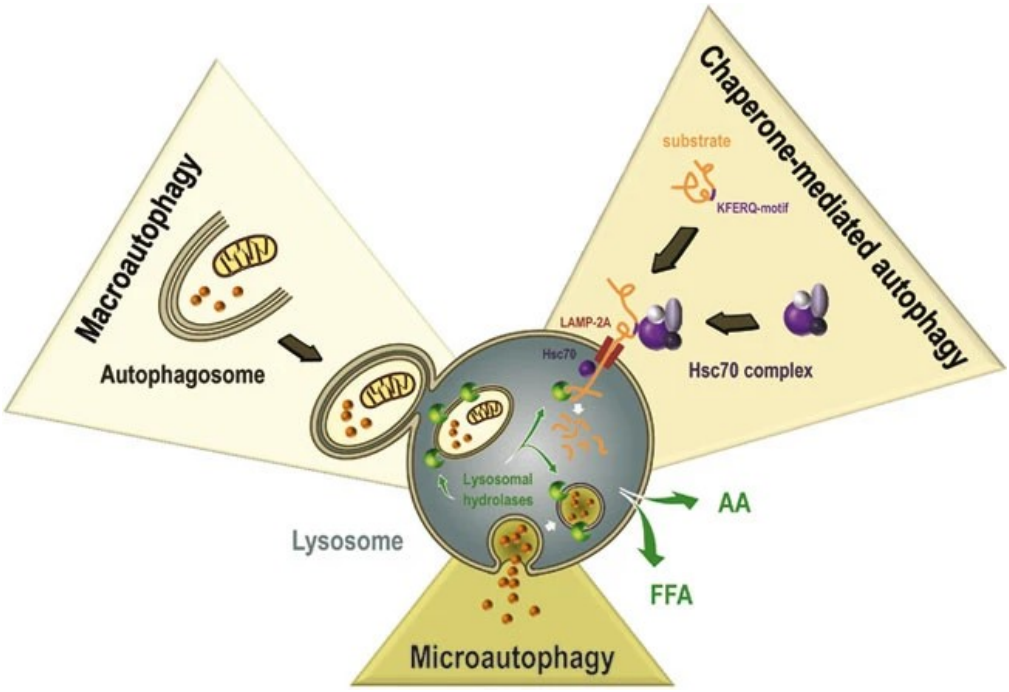

Figure 6 Schematic representation of the different types of autophagy

Chaperone-mediated autophagy sequesters cytosolic proteins selected by KFERQ-like motif and directly targeted them to the lysosomes for degradation. During microautophagy the engulfed cytoplasmic proteins are invaginated by lysosomal membranes and then broken down. Macroautophagy is a process in which the proteins are engulfed in specialized vacuoles, called autophagosomes, which transport the proteins to the lysosomes. Adapted from **[Wirawan E et al. 2012]**

During Chaperone-mediated autophagy (CMA) cytosolic proteins are individually selected by a pentapeptide recognition motif (KFERQ-like motif) [Yorimitsu, T. et al. 2005]. Chaperones like the heat shock-cognate protein 70 (HSC 70) recognize the motif and bind to it. After binding the substrate is translocated to the lysosomal surface, where it interacts with the lysosome-associated membrane protein type 2A (LAMP 2A) [Cuervo, A.M. et al. 1996]. HSC 70 and other chaperones mediated unfolding of the protein to facilitate the translocation into the lysosomal lumen, where it is degraded. Microautophagy is a non-selective degradation process, where the lysosomal membrane

directly invaginates proteins, which are engulfed by cytoplasmic cargo. This process is mediated by autophagic tubes, which are present at the membrane [Li, W. et al. 2012]. During macroautophagy, mainly referred as autophagy, the substrate is engulfed by an isolation membrane called phagophore. The phagophore forms double membrane vesicles known as autophagosomes. These autophagosmes fuse then with the lysosome forming autolysosomes to degraded enclosed substrate [Fader, C.M. et al. 2009]. Autophagy can be induced by cellular stress conditions including nutrient starvation, hypoxia conditions, invading microbes, tumor formation and long-lived proteins that accumulate in the ER [Deegan, S. et al. 2013].

Recent studies have demonstrated that that autophagy is involved at various levels in the pathogenesis of pulmonary fibrosis. It has been demonstrated that autophagy is either not activated or insufficiently in patients with IPF [Araya, J. et al. 2013, Patel, A.S. et al. 2012]. They also have shown that in the bleomycin mouse model, the administration of rapamycin, an autophagy inducer, leads to significant reduction of lung fibrosis [Patel, A.S. et al. 2012]. Other studies have revealed that the cytokines transforming growth factor beta 1 (TGF-β1) and interleukin 17A (IL-17A) have been attributed to inhibition of autophagy and therefore promotes chronic inflammation and progression of lung fibrosis [Mi, S. et al. 2011, Patel, A.S. et al. 2012]. Another study revealed decreased expression of the Bcl-2 binding protein Beclin 1 in IPF fibroblasts [Ricci, A. et al. 2013]. These and other studies suggest that regulation of autophagy activity may also be a new target for the treatment of pulmonary fibrosis [Haspel, J.A. et al. 2011]. The lung tissues of IPF patients show a decrease in the number of autophagosomes, accumulation of p62 and decreased LC3B level as well as ubiquitinated proteins, suggesting a blocked autophagic flux and insufficient autophagy. It appears as if autophagosome are not able to fuse with the lysosome in IPF (**Figure 7**) [Kesireddy, V.S. et al. 2019, Kota, A. et al. 2017, Lv, X. et al. 2020, Mahavadi, P. et al. 2015, Patel, A.S. et al. 2012]. Along the same line, Kesireddy et al. have reported that MAP1LC3B knock-out mice are susceptible to lung injury and fibrosis, which indicates the pathologic relevance of autophagy in the development of lung fibrosis [Kesireddy, V.S. et al. 2019].

Several studies have linked ER stress to autophagy [Ding, W.-X. et al. 2007, Høyer-Hansen, M. et al. 2007, Khaminets, A. et al. 2015, Oh, S.-H. et al. 2009]. As a compensatory cell survival mechanism, autophagy can be activated by mild to moderate ER stress, whereas due to severe or prolonged ER stress, the adaption program switches

to cell death program [Rashid, H.-O. et al. 2015]. However, it is not clear whether ER stress-mediated autophagy protects cells from undergoing apoptosis. Some data suggest that it may also induce cell death [Ogata, M. et al. 2006, Schröder, M. et al. 2005].

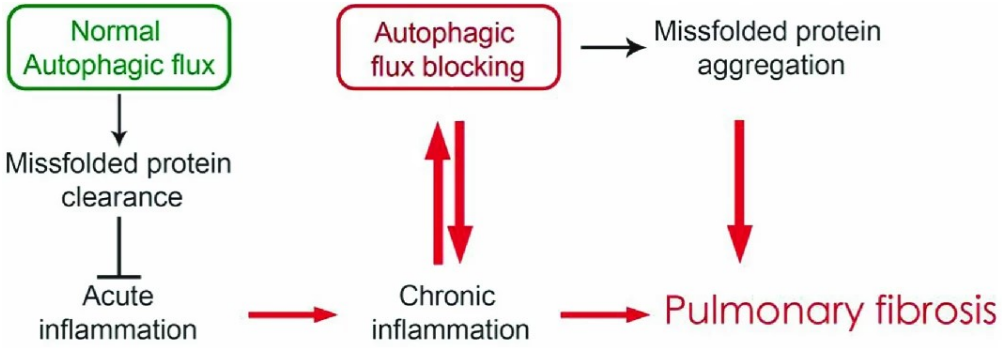

Figure 7 Blocking autophagic flux promotes pulmonary fibrosis
Normal autophagy promotes the clearance of damaged proteins and inhibit acute inflammatory responses. However, when pulmonary fibrosis occurs, acute inflammation gradually turns into chronic inflammation. This results in blockage of autophagic flux and damaged proteins and the extracellular matrix cannot be removed promoting pulmonary fibrosis. Adapted from **[Lv X et al. 2020]**

1.6 Mitochondrial alterations in the pathogenesis of IPF

Mitophagy targets mitochondria for turnover and removes damaged and dysfunctional mitochondria that can lead to cellular stress and apoptosis [Ding, W.-X. et al. 2012]. Mitophagy occurs through PTEN-induced putative kinase 1 (PINK1)-Parkin signaling. PINK1 senses mitochondrial membrane depolarization and recruits Parkin, which labels the dysfunctional mitochondria for trafficking to the autophagosome [Youle, R.J. et al. 2011]. Defective mitophagy and altered mitochondrial biogenesis has been associated with IPF (**Figure 8**) [Bueno, M. et al. 2015, Sosulski, M.L. et al. 2015, Zank, D.C. et al. 2018]. Mora et al. have discovered Pink1 deficiency, resulting in an accumulation of dysmorphic and dysfunctional mitochondria in AECIIs from human IPF lungs [Mora, A.L. et al. 2017]. This has been associated with the upregulation of ER stress markers and low expression of PINK1, the regulator of mitochondrial homeostasis [Bueno, M. et al. 2015]. ER stress has been shown to induce expression of ATF3, a transcriptional repressor of PINK1, in AECII [Bueno, M. et al. 2018]. Furthermore Bueno et al. have demonstrated that PINK1-deficient mice show increased susceptibility to apoptosis and lung fibrosis, developing similar dysmorphic and dysfunctional mitochondria and that ER stress is linked to mitochondrial function in the AECIIs [Bueno, M. et al. 2020]. Studies by Patel et al. confirmed this by showing that PINK1-deficient mice exhibited increased apoptosis in AECII [Patel, A.S. et al. 2015]. Also, Parkin deficiency is associated with

impaired mitophagy in IPF fibroblasts under profibrotic conditions. Supporting these data, Parkin-deficient mice develop more severe lung fibrosis [Zank, D.C. et al. 2018].

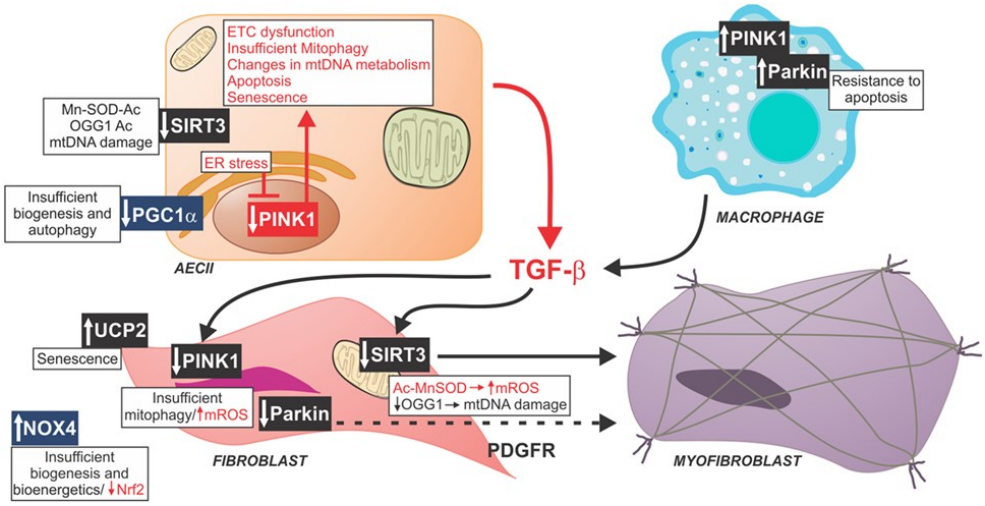

Figure 8 Schematic of profibrotic pathways mediated by mitochondrial dysfunction
Decrease PINK1 in AECII from fibrotic lungs has been associated with mitochondrial dysfunction and increased activation of TGF-β. Profibrotic macrophages shows increased mitophagy and resistance to apoptosis. TGF-β affects mitochondrial function in fibroblasts through decreasing PINK1 and Parkin. Adapted from **[Zank DC et al. 2018]**

Other studies have also confirmed the role of mitochondrial alterations in lung fibrosis. Hawkins et al. have demonstrated that a non-BRICHOS SP-C mutations (SP-C^{I73T}), which is also linked to familial pulmonary fibrosis, causes disrupted mitophagy within AECII. This results in an accumulation of dysfunctional and dysmorphic mitochondria [Hawkins, A. et al. 2015].On the contrary, pulmonary macrophages isolated from IPF lungs showed increased mitophagy as well as increased level of Pink1 and Parkin [Larson-Casey, J.L. et al. 2016].

1.7 Mitochondria-associated ER membranes (MAMs)

ER and mitochondria form tight physical junctions known as mitochondria associated ER membranes (MAMs). About 20% of the mitochondrial surface is in direct contact with the ER. This junction is stabilized by tethering complexes that are proteins anchored in the ER and mitochondrial outer membrane. This strong connection enables a dynamic and highly regulated communication between the ER and mitochondria [Rizzuto, R. et al. 1998]. The transfer of calcium (Ca^{2+}) and other metabolites between the ER and mitochondria is a major function of MAM contacts (**Figure 9**) [Vannuvel, K. et al. 2013]. The transfer is facilitated by MAM proteins inositol 1,4,5-trisphosphate receptor (IP3R),

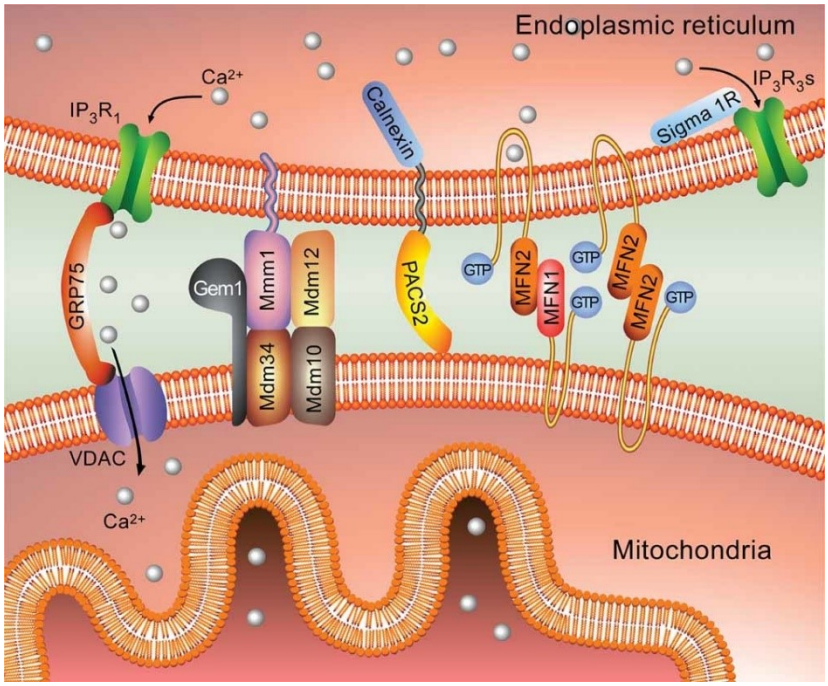

Figure 9 Illustration of the interactions of MAM proteins

IP3R3 and VDAC1 mediate the transport of Ca^{2+} from the ER to the mitochondria. PACS2 is a multifunctional protein, anchored in the ER membranes, that tethers the ER with mitochondria. Adapted from **[Vannuvel K et al. 2013]**

which is located at the ER, and voltage-dependent anion-selective channel (VDAC), which is localized on mitochondrial outer membranes [Bravo, R. et al. 2011, Vannuvel, K. et al. 2013]. Sigma-1 receptor, which is also located in the ER, stabilizes IP3R and so promotes Ca^{2+} exchange from ER to mitochondria in case of Ca^{2+} depletion in the ER. Ca^{2+} depletion of the ER as well as mitochondrial Ca^{2+} overload are both critical factors for cell death. Therefore these MAM proteins are important for maintaining cellular homeostasis by controlling ER–mitochondrial Ca^{2+} transfer [van Vliet, A.R. et al. 2014]. As mentioned before, other metabolites, including lipids, are also transferred between the ER and mitochondria through ER-mitochondria contacts [Bravo, R. et al. 2011, Vannuvel, K. et al. 2013]. Another ER-localized MAM-protein is phosphofurin acidic cluster sorting protein 2 (PACS2), which is associated with chaperone calnexin and fixed to the ER luminal face of MAM. PACS2 is important for MAM formation and stability and thereby also for the balance between homeostasis and cell death. In addition Simmen et al. have shown that PACS2 depletion is not only associated with decreased ER-mitochondrial interference, but may also induces mitochondrial fragmentation via a B cell associated protein 31 (BAP31), leading to physical dissociation of the mitochondria from the ER [Simmen, T. et al. 2005].

Disruption of the interaction between ER and mitochondria induces ER stress. Also, ER stress can lead to disrupted MAM contact sites. When such ER stress cannot be resolved, PACS2 initiates apoptosis by translocating from the ER to mitochondria, thereby promoting the formation of tBid, which in turn releases cytochrome c, followed by activation of caspase 3 [Simmen, T. et al. 2005, Werneburg, N.W. et al. 2012]. The multifunctional protein PACS2 could also play a role in the retention of chaperones in MAMs, as it is known that PACS2 binds the non-phosphorylated calnexin and thereby keeps it in place at the MAMs [Myhill, N. et al. 2008]. Some recent studies also show that prolonged pro-apoptotic ER stress can induce morphological changes of the mitochondrial network due to the close proximity [Rainbolt, T.K. et al. 2014].

As mentioned before, Ca^{2+} is a key regulator of apoptosis [Shi, J. et al. 2015] and MAM proteins facilitate Ca^{2+} exchange between ER and mitochondria. It is also known that in dying cells mitochondria undergo dynamin-related protein 1 (Drp1) dependent controlled fission, resulting in their punctate distribution [Brito, O.M. de et al. 2010, Frank, S. et al. 2001, Hom, J.R. et al. 2007]. Mitochondrial permeabilization is a complex mechanism and depends on a distinct balance of antiapoptotic members like B-cell lymphoma 2 (Bcl-2) and B-cell lymphoma 2 extra-large (Bcl-xL), or pro-apoptotic members such as BH3 interacting-domain death agonist (Bid), Bcl-2 homologous antagonist killer (Bak) and Bcl-2-associated X protein (Bax) [Su, J. et al. 2014]. Hom et al. have exposed rat liver cell lines to thapsigargin, a well-known ER stress inducer, by inhibition of SR/ER Ca^{2+}-ATPase (SERCA). This led to a fragmentation of mitochondria due to increased Ca^{2+} uptake by the mitochondria. This effect seems to be reversible, but under prolonged thapsigargin treatment the fragmentation of mitochondria becomes irreversible due to a depletion of Ca^{2+} in the ER and a mitochondrial Ca^{2+} overload [Hom, J.R. et al. 2007]. In the case of physical rupture of mitochondria, pro-apoptotic proteins such as cytochrome c and procaspases are released into the cytosol [Pradelli, L.A. et al. 2010]. This in turn triggers apoptosis.

ER stress can also induce mitochondrial stress, leading to a loss of mitochondrial membrane potential and thus to mitochondrial fragmentation and degradation via autophagy, the so called mitophagy [Ding, W.-X. et al. 2012]. Damaged mitochondria activate PINK1, which is sensitive for voltage changes. PINK1 then binds to Parkin leading to the induction of autophagy of those mitochondria. Under normal conditions, PINK1 is continuously processed and imported, leading to its degradation. During

mitochondrial fragmentation or mitochondrial stress, which results in mitochondrial membrane depolarisation, PINK1 is translocated onto the outer mitochondrial membrane (OMM) [Matsuda, N. et al. 2010]. The accumulation of PINK1 on the outer mitochondrial membrane leads to recruitment of Parkin, an E3 ligase, which in turn ubiquitinates mitochondrial proteins like Mitofusin 1 and 2 (MFN1/2) and VDAC [Gegg, M.E. et al. 2010]. Ubiquitinated proteins recruit p62, which then activates autophagosome formation and finally degradation of damaged mitochondria [Okatsu, K. et al. 2010]. Mitophagy can also be activated through the PERK–ATF4 pathway of the UPR [Bouman, L. et al. 2011].

1.8 ER and MAMs are a source of autophagosome formation

Autophagy is a crucial survival mechanism for the cell under stress conditions like starvation. Autophagy is initiated at the isolation membrane (phagophore) and this membrane is expanded to form the autophagosome [Lamb, C.A. et al. 2013]. In contrast to other biological pathways, the autophagosome is not always present in the cell, its formation will be initiated by activation of autophagy and will be degraded soon afterwards [Rubinsztein, D.C. et al. 2012]. The source of autophagosome formation has been an unsolved riddle. Some studies show that several autophagic proteins can be identified at the ER, suggesting it as a source of an autophagosome formation [Noda, T. et al. 2011]. According to ultrastructural analyses, autophagosome formation takes place near a specific region of the ER [Ylä-Anttila, P. et al. 2009]. This ER subdomain in the intracellular site is called omegasome [Hayashi-Nishino, M. et al. 2009]. Double FYVE domain-containing protein (DFCP1) serves as a specific marker of omegasome [Axe, E.L. et al. 2008]. The ULK1 complex, a scaffold of ATG proteins, is also located in the omegasome initating autophagosome formation in the tubulovesicular regions of the ER [Karanasios, E. et al. 2016]. ATG2 along with ATG8 and ATG18 binds to ER subdomain forming the phagophore [Kotani, T. et al. 2018]. Other ER membrane proteins called TMEM41b and VMP1 are also presumed to be involved in this process [Moretti, F. et al. 2018].

Next, it has been suggested that MAMs are the source of autophagosomal membranes [Hamasaki, M. et al. 2013]. By employing several methods, it was demonstrated that autophagy related proteins ATG14L and ATG5, which are necessary for autophagosome formation, accumulate at the MAM under stress conditions. Furthermore, Hamasaki et al. have demonstrated that depletion of PACS2 or MFN2 leads to a disruption of the contact site and, thereby, also to a defective autophagosome formation (by inhibition of ATG14L)

and LC3B formation and lipidation [Hamasaki, M. et al. 2013, Shibutani, S.T. et al. 2014]. Accordingly, Itakura et al. have identified syntaxin 17 (STX 17), an ER located soluble N-ethylmaleimide-sensitive factor-attachment receptor (SNARE) protein, to be involved in autophagy by controlling the fusion of the autophagosme with the lysosome. STX 17 relocated ATG14L to the MAM membrane under starvation-induced autophagy [Itakura, E. et al. 2012]. Nevertheless, besides the pathologic contribution of ER stress and mitochondrial dysfunction, there is not much known about altered ER–mitochondrial communication in disease pathogenesis, especially in IPF [Senft, D. et al. 2015, Vannuvel, K. et al. 2013].

2 Aim of the study

The pathophysiology of IPF is not fully understood, but it is well known that chronic AECII injury, disturbed epithelial-mesenchymal crosstalk, activation of fibroblasts and excessive collagen deposition are key factors for driving IPF. The concept of AECII injury is supported by scientifically appealing observations like severe and pro-apoptotic ER stress signaling and shortened telomere length in AECII in familial (e.g. SP-C mutations) and sporadic IPF cases. Recent studies have also underlined the importance of defective autophagy and dysfunctional mitochondria in driving alveolar epithelial cell apoptosis and thereby lung fibrosis. Although the distinct functions of the ER and mitochondria in AECII death are ascertained, the signaling network between these two dynamic organelles and their crosstalk with each other are still poorly understood in IPF. We hypothesize that the ER-mitochondrial crosstalk is severely altered under a) experimental ER stress and b) in lung fibrosis, where AECII display persistent, pro-apoptotic ER stress. To test this hypothesis, we identified the following objectives:

1. Fully understand the signaling mechanisms between ER and mitochondria under ER stress conditions and in lung fibrosis: Here, we plan to (i) exploit our *in vitro* model of inducible *Chop* overexpression in mouse lung epithelial (MLE 12) cells, (ii) study MAM protein expression in lung tissues of IPF patients compared to organ donors and (iii) generate stable cell lines overexpressing full length *SP-C* or *SP-C*$^{\Delta exon4}$ (BRICHOS domain mutation)

2. Investigate the effect of altered MAM proteins on cellular fate as well as cellular quality control mechanisms in the alveolar epithelial cells: To study this, we plan to perform gain / loss of function experiments for the identified MAM(s) from objective 1 and analyse the subsequent effects on apoptosis as well as autophagy.

3. Therapeutically target the ER-mitochondrial crosstalk: For this, we plan to identify drugs that may target one or more of the MAMs or associated proteins. Therapeutic efficacy of such drugs will be tested in precision cut lung slices (PCLS) from IPF patient lungs and downstream pathways will be studied.

3 Materials

3.1 Reagents

Products	Company
β-Estradiole	Sigma Aldrich, Germany
2-(4-(2-Hydroxyethyl)-1-piperazinyl)-ethansulfonic acid (HEPES)	Roth, Germany
2-Mercaptoethanol	Sigma Aldrich, Germany
4′,6-Diamidin-2-phenylindol (DAPI)	Sigma Aldrich, Germany
Acetic acid	Merck KGaA, Germany
Acrylamide/Bisacrylamide (30%/0.8%) solution, Rotiphorese® Gel 30	Roth, Germany
Agarose	Roth, Germany
Albumine, Bovine Serum Fraktion V (BSA)	Roth, Germany
Alexa Fluor™ 488 Antibody Labeling Kit	Invitrogen AG, USA
Ammoniumperoxodisulfate (APS)	Roth, Germany
Ampicillin sodium salt	Sigma Aldrich, Germany
BactoTM Agar	BD,USA
BactoTM Tryptone	BD,USA
BactoTM Yeast extract	BD,USA
Bafilomycin A 1	InvivoGen, France
Brillant Blue G	Sigma Aldrich, Germany
Bromphenol blue	Merck KGaA, Germany
Capsaicin	Sigma Aldrich, Germany
Chloroquine diphosphate salt	Sigma Aldrich, Germany
CutSmart® Buffer	New England BioLabs, USA
D-(+)-Glucose	Roth, Germany
D-(+)-Saccharose	Roth, Germany
Dako Fluorescent Mounting Medium	Dako, USA
Dako Glycergel Mounting Medium	Dako, USA
Dimethylsulfoxide (DMSO)	Roth, Germany
Di-Sodium hydrogenphosphate dehydrate (Na2HPO4•2H2O)	Merck KGaA, Germany
DMEM-F12	Gibco, Germany

Donkey Serum	PAN Biotech, Germany
Doxycyclinhyclat	Fargon, Germany
Dulbecco's Phosphate Buffered Saline (PBS)	Sigma Aldrich, Germany
Duolink® In Situ Orange Starter Kit Goat/Rabbit	Sigma Aldrich, Germany
Dynabeads™ M-280 Tosylactivated (30mg/mL)	Invitrogen AG, Germany
EndoFree® Plasmid Maxi Kit (10)	Qiagen, Germany
EpiQuik Nuclear Extraction Kit I	Epigentek, USA
Ethanol 70%	SAV Liquid Production GmbH, Germany
Ethanol 96%	Otto Fischar GmbH& Co. KG, Germany
Ethanol absolut	Otto Fischar GmbH& Co. KG, Germany
Ethylenediaminetetraacetic acid (EDTA)	Roth, Germany
Fetal Bovine/Calf Serum (FB/CS)	Sigma Aldrich, Germany
GelRed® Nucleic Acid Stain 10,000X in water	Biotium, USA
Geneticin (G-418)Sulphate	Gibco, Germany
Gibco DMEM-F12 Medium	Thermo Scientific, Germany
Gibco RPMI 1640 Medium	Thermo Scientific, Germany
Glycerol, glycerine	Sigma Aldrich, Germany
Glycine	Roth, Germany
GlycoBlue™ Coprecipitant	Invitrogen AG, Germany
Halt™ Protease Inhibitor Cocktail	Thermo Scientific, Germany
Hämalaunlösung sauer nach Mayer	Roth, Germany
HotStar HiFidelity Polymerase Kit 100 units	Qiagen, Germany
HotStar Taq® DNA Polymerase 1000 units	Qiagen, Germany
Hydrochloric acid (HCl)	Roth, Germany
Hydrocortisone	Sigma Aldrich, Germany
Hygromycin B Gold	InvivoGen, France
Immobilon® Western Chemiluminescent HRP Substrate	EMD Millipore Corporation, USA

Insuline-Transferrine-Sodium selenite / ITS solution I (100x)	PAN Biotech, Germany
Isopropanol (2-Propanol)	Roth, Germany
Kanamycin disulfate salt	Sigma Aldrich, Germany
L-Glutamine	Gibco, Germany
Lipofectamine® 200 Reagent	Invitrogen AG, Germany
MEM Non-Essential Amino Acids Solution (100x) (MEM NEAA)	Gibco, Germany
Methanol	Merck KGaA, Germany
Milk powder	Roth, Germany
Minimum Essential Media (100x) (MEM)	Gibco, Germany
MitoTracker® Red CMXRos	Life Technologies, USA
MycoZAP™	Lonza Group Ltd, Switzerland
N,N,N',N'-Tetramethyl ethylenediamine	Sigma Aldrich, Germany
NEBufferTM 3.1	New England BioLabs, USA
Nintedanib	Sigma-Aldrich, Germany
NucleoSpin® Tissue (250prep)	Macherey-Nagel, Germany
Oligo(dT) Primer	Roche, Germany
Omniscript® RT Kit	Qiagen, Germany
Opti-MEM medium	Gibco, Germany
PageRuler™ Prestained Protein Ladder	Thermo Scientific, Germany
Paraformaldehyde	Roth, Germany
pEGFP-C1 Vector	Addgene Europe, UK
Penicilline/Streptomycine	Gibco, Germany
Phenylmethylsulfonylfluoride (PMSF)	Thermo Scientific, Germany
Pierce™ BCA Protein Assay Kit	Thermo Scientific, Germany
Pierce™ IP Lysis Buffer	Thermo Scientific, Germany
Potassium Chloride (KCl)	Roth, Germany
Potassium dihydrogenphosphate (KH2PO4)	Merck KGaA, Germany
Proteinase K	PEQLAB Biotechnologie, Germany
QIAprep® Spin Miniprep Kit (250)	Qiagen, Germany
QIAquick® Gel Extraction Kit (50)	Qiagen, Germany

QIAquick® PCR Purification Kit (250)	Qiagen, Germany
Restriction endonucleases(XhoI, EcoRI, StuI, HindIII, ApaL I)	New England BioLabs, USA
RNase Inhibitor	Roche,Germany
S.O.C Medium	Invitrogen, Germany
Smart Ladder	Eurogentec, Germany
Sodium butyrate	Sigma Aldrich, Germany
Sodium Chloride (NaCl)	Roth, Germany
Sodium citrate tribasic dihydrate	Sigma Aldrich, Germany
Sodium dodecyl sulfate (SDS)	Roth, Germany
Sodium hydroxide (NaOH)	Merck KGaA, Germany
Storage Solution for pH and ORP electrodes	Hanna Instruments, Germany
T4 DNA ligase	New England BioLabs, USA
T4 DNA ligase buffer	New England BioLabs, USA
OneShot™ TOP10, competent cells	Invitrogen AG, Germany
Tris(hydroxymethyl)-aminomethane (Tris)	Roth, Germany
Triton-X-100	Sigma Aldrich, Germany
TRIzol™ Reagent	Invitrogen AG, Germany
Trypsin 0.50% (100x)	Gibco, Germany
Turbofect	Thermo Scientific, Germany
Tween® 20	Roth, Germany
ZytoChem (AP) Broad Spectrum (Permanent Red) Kit 80 Tests	Zytomed Systems, Germany
ZytoChem Plus AP-Fast Red Kit Broad Spectrum 80 Tests	Zytomed Systems, Germany

3.2 Equipment

Product	Company
Agarosegel electrophoresis chamber	Kreutz Labortechnik, Germany
Analytical Balance	Mettler Toledo, Germany
Bacteria culture incubator, Orbital incubator SI50	Stuart Equipment, UK
BD Microlance™ 3 cannulas 20 G 1 1/2 0,9 x 40 mm	Becton Dickinson, Germany
Cell culture centrifuge, Mikro 200R	Hettich, Germany
Cell culture Hood	Heraeus, Germany
Cell culture incubator HERAcell 150i	Thermo Scientific, Germany
Cell culture water bath	Julabo, Germany
Cell Scrapers	Sarstedt, Germany
Disposable Glass Pasteur Pipettes 230mm	VWR International, Germany
DynaMag 5	Invitrogen AG, Germany
ECL Chemostar	Intas, Germany
Electrophoresis Chamber	Bio Rad, Germany
Eppendorf Research® plus (IVD) pipette 100-1000µL	Eppendorf, Germany
Eppendorf Research® plus (IVD) pipette 10-100µL	Eppendorf, Germany
Eppendorf Research® plus (IVD) pipette 1-10µL	Eppendorf, Germany
Falcon Roller	Phoenix Instrument, Germany
Falcon tubes 15mL/50mL	Greiner bio-one, Germany
Feather sterile disposable scalpel No.10	GF Health Products, USA
Fluorescence microscope adapter	AHF Analysentechnik, Germany
Freezer -20°C	Bosch, Germany
Fridge +4°C	Liebherr, Germany
Glass bottles 250, 500, 1000mL	Roth, Germany
Haemocytometer coverslips Menzel-Glässer 20x26mm	Thermo Scientific, Germany
Haemocytometer Neubauer Chamber	Optik Labor, Germany

HeraFreeze Top -80°C	Thermo Scientific, Germany
IKA® VXR basic Vibrax® orbital shakers	IKA®-Werke GmbH, Germany
Immobilon®-P Transfer Membrane PVDF	Merkmillipore, Ireland
INCU-Line	VWR International, Germany
Image J software (version 1.52a)	National Institute of Health, USA
Kimble® dounce tissue grinder set 2mL	DWK Life Sciences, Germany
Leica M205 FA Fluorescent Stereoscope	Leica Microsystems, USA
Magnetic Stirrer UC151	Stuart Equipment, UK
Membrane Filter Express™ Plus 0.22µm	Merckmillipore, Ireland
Microplate reader Infinite® M200 Pro	Tecan Group Ltd, Switzerland
Microscope Nikon Eclipse TS100	Nikon GmbH, Germany
Microtest Plate 96 Well, F	Sarstedt, Germany
Microwave Severin MW 7825	Severin GmbH, Germany
MJ MiniTM Personal Thermal Cycler	Bio Rad, Germany
Multifuge centrifuge Rotina 380R	Hettich, Germany
Multipipette	Eppendorf, Germany
Nalgene Cyroware Cryogenic Vials	Nalge Company, USA
Nano Zoomer	Hamamatsu, Germany
NanoDrop One	Thermo Scientific, Germany
Oxygraph-2K	Oroboros Instruments, Austria
PCR SoftTubes, 0.2 mL, transparent	Biozym Biotech, Germany
PCR-Thermocycler Thermomix comfort	Eppendorf, Germany
pH/ORP Meter HI 2211	Hanna Instruments, Germany
Pipette 10mL	Greiner bio-one, Germany
Pipette tip 10µL, 100µL, 1000µL	Sarstedt, Germany
Pipetus®	Hirschmann Laborgeräte, Germany
Platesealer, Easyseal™ transparent, 79x135mm	Greiner bio-one, Germany
Platform rocker PMR-30	Grant Instruments Ltd, UK
Power Supply MP-300V	Major Science, USA
Power Supply, Consort EV265	AlphaMetrix Biotech, Germany
PowerPac™ Basic Power Supply	Bio Rad, Germany
Precellys® 24 homogenizer	Bertin Technologies, Germany
Pumpe 4010	Clinicon, Germany

Safe-Look tubes 0.5mL, 1.5mL (amber),2mL	Eppendorf, Germany
SproutTM Mini centrifuge	Heathrow Scientific, USA
Syringes Injekt® Solo 2mL, 5mL, 10mL, 20mL	B. Braun, Germany
Table balance FCB 3K0.1	Kern&Sohn GmbH, Germany
Table centrifuge Rotina 380R	Hettich, Germany
Tissue Culture Chambers (8-well on lumox®, detachable)	Sarstedt, Germany
Tissue Culture Dish 100mm, Standard	Sarstedt, Germany
Tissue Culture Dish 60mm, Standard	Sarstedt, Germany
Tissue Culture Plates 12 Well,Standard,F	Sarstedt, Germany
Tissue Culture Plates 6 Well,Standard,F	Sarstedt, Germany
Vortex machine	VWR International, Germany
Water bath	Julabo, Germany
Western blot unit	Bio-Rad, Germany
Whatmann™ Gel Blot Paper	GE Healthcare,UK

3.3 List of antibodies

Antibody	Company	Order number	Source	Use
Anti-ABCA3	Seven Hills Bioreagents, USA	WMAB-ABCA3-177	mouse	IF
Anti-ß-actin	Abcam, USA	ab8227	rabbit	WB
Anti-Calnexin (c-20)	Santa Cruz, USA	sc6465	goat	WB, IF; PLA
Anti-CHOP (D46F1)	Cell Signaling, USA	5554s	rabbit	WB, IF, IHC
Anti-cIAP-1	Biovision, USA	3180A-30T	rabbit	WB
Anti-cIAP-2/ HIAP-1	Novus Biologicals, USA	NBBP1-90132	rabbit	WB
Anti-COL1A1	Rockland Immunochemicals, Ireland	600-401-103-0.5		IF

Anti-cleaved caspase3 (D175) (5A1E)	Cell Signaling, USA	9664s	rabbit	WB, IF
Anti-GAPDH (14C10)	Cell Signaling, USA	2118s	rabbit	WB
Anti-GFP	Abcam, USA	ab5450	goat	WB
Anti-hcIAP	R&D Sytems, USA	AF8181	goat	WB
Anti-IP3R3	Novus Biologicals, USA	NBP1-21400	rabbit	WB;IF
Anti-Lamin A/C (N-18)	Santa Cruz, USA	sc15426	goat	WB
Anti-LC3B	Abcam, USA	ab192890	rabbit	WB, IF
Anti-LC3B	Cell Signaling, USA	2775s	rabbit	WB, IF
Anti-Myc tag	Abcam, USA	ab9132	goat	WB, IF, IP
Anti-p62/SQMSTM 1	Sigma-Aldrich, Germany	P0067	rabbit	WB, IF
Anti-PACS2	Abcam, USA	ab129402	rabbit	WB,IHC
Anti-PACS2	ProSci Inc.	8189	rabbit	WB
Anti-PACS2	Proteintech, USA	19508-1-AP	rabbit	WB, IF, IHC
Anti-Parkin	Abcam, USA	ab15494	rabbit	WB
Anti-PERK (H-300)	Santa Cruz, USA	sc13073	rabbit	WB,IF,IHC
Anti-PINK1	LSBio, USA	LS-C 296148	rabbit	WB
Anti-PINK1	Novus Biologicals, USA	NB 100-493	rabbit	WB
Anti-proSP-C	Biorbyt, UK	orb137602	rabbit	WB
Anti-proSP-C	Merck Millipore, Germany	ab3786	rabbit	WB
Anti-proSP-C	Seven Hills Bioreagents, USA	WRAB-09337	rabbit	WB
Anti-SigmaR1	Proteintech, USA	15168-1-AP	rabbit	WB,IF,IHC
Anti-TFEB	Proteintech, USA	13372-1-AP	rabbit	WB,IF

Anti-TOM20 (F-10)	Santa Cruz, USA	sc17764	mouse	WB, IF
Anti-TOM20 (FL-145)	Santa Cruz, USA	sc11415	rabbit	WB, IF, PLA
Anti-TRPV1	Invitrogen AG, USA	PA1-29421	rabbit	WB
Anti-VDAC1	Proteintech, USA	10866-1-AP	rabbit	WB, IF, IHC, PLA
Alexa Fluor® Plus 488 anti-Goat IgG	Invitrogen AG, USA	A-11055	donkey	IF
Alexa Fluor® Plus 488 anti-Mouse IgG	Invitrogen AG, USA	A-21202	donkey	IF
Alexa Fluor® Plus 488 anti-Rabbit IgG	Invitrogen AG, USA	A-21206	donkey	IF
Alexa Fluor® Plus 488 anti-Rat IgG	Invitrogen AG, USA	A-21208	donkey	IF
Alexa Fluor® Plus 555 anti-Goat IgG	Invitrogen AG, USA	A32816	donkey	IF
Alexa Fluor® Plus 555 anti-Mouse IgG	Invitrogen AG, USA	A32773	donkey	IF
Alexa Fluor® Plus 555 anti-Rabbit IgG	Invitrogen AG, USA	A32794	donkey	IF
HRP conjugat/ Anti-Goat Immunoglobulins	Agilent Dako, USA	P044901-2	rabbit	WB
HRP conjugat/ Anti-Mouse Immunoglobulins	Agilent Dako, USA	P026002-2	rabbit	WB

HRP conjugat/ Anti-Rabbit Immunoglobulins	Agilent Dako, USA	P021702-2	swine	WB
Goat control IgG	Abcam, USA	ab37373		IP

4 Methods

4.1 Human tissue

Lung tissue samples were obtained from patients with sporadic IPF and non diseased control subjects / healthy donors. Explanted lungs or lobes were obtained from the Department of Thoracic Surgery, Vienna, Austria (K. Hoetzenecker) and were collected in the frame of the European IPF Registry/Biobank (eurIPFreg/bank). Human lung samples were provided by the Biobank of the Universities of Giessen and Marburg Lung Center (UGMLC), member of the German Center for Lung Research (DZL) Platform Biobanking. All IPF diagnoses were made according to the American Thoracic Society (ATS)/European Respiratory Society (ERS) consensus criteria [Raghu, G. et al. 2011]. The study protocol was approved by the Ethics Committee of Justus Liebig University Giessen (111/08 and 58/15). Formalin fixed lung tissue blocks were obtained from eight patients with IPF (mean age 55 ± SD: 10.28) and 8 non diseased control subjects (Donors; mean age 39 ± SD: 13.91)

4.2 Animal experiments

Chop transgenic mice (mice with conditional overexpression of Chop) were created by P. Moreira, European Molecular Biology Laboratory (EMBL) Mouse Biology Unit, Italy. Background strain for these mice was C57BL/6. These mice were purchased from the Jackson Laboratory. All animal experimentation as described in this study were performed according to the Helsinki convention for the use and care of animals and was approved by Justus Liebig-University's committee on animal investigations and the federal authorities for animal research (Regierungspräsidium Giessen, Hessen, Germany, V54-19c2015h01 GI20/10-No. 19/2015).

4.3 Precision Cut Lung Slices

PCLS have been used as *ex vivo* model for studying therapeutic efficacy of capsaicin (explained in the upcoming sections) for IPF. This technique has several benefits compared to the standard culture system and also animal models, which cannot be transferred to humans completely. The three-dimensional structure lung tissue slice allows morphological insights into lung architecture. PCLS maintain relevant tissue structures, including respiratory structures and also immune cells. Another advantage is that PCLS can be taken into culture so that the components stay biologically active [Liu, G. et al. 2019].

After lung explanation the removed lung was inflated with warm 3% low-melting agarose in each segment. After inflation, the lung was allowed to cool on ice for 30 minutes for solidification of the agarose. The solidified agarose preserves the structure of airways and alveoli during slicing. The section blocks of lung tissue were cut into 500 µm thick sections using vibrating blade microtome (Thermo Fisher, Germany). The PCLS were cultured in Roswell Park Memorial Institute (RPMI) medium without phenolred (see table below) and left in cell culture incubator for 48 hours for the agarose to dissolve. The PCLS were then transferred into new culture plates and treated with capsaicin or nintedanib. Thereafter they were either fix in 2 mL formalin at 4°C overnight for preparing slides or were transferred into an eppendorf cup and shock frozen for biochemical studies. Supernatants were collected and shock frozen. Formalin fix PCLS were washed with PBS and transferred to previously labeled embedding cassettes for dehydration with a dedicated tissue processing machine. Thereafter PCLS were embedded in hot wax and cooled down for solidification. For further analysis 3 µm tick sections were cut with a microtome.

PCLS culture medium

Component	Final Concentration
RPMI 1640 (without phenolred)	500 mL
FCS	2% (v/v)
L-Glutamine 200 mM	1% (v/v)
Penicillin/Streptomycin	1% (v/v)
Amphotericin B	30 ng/mL
MycoZap™	2 ng/mL

4.4 Cell lines and Cell culture

Mouse lung epithelial cell line (MLE12) was obtained from American Type Culture Collection (ATCC), Manassas, USA. Human skin epithelial cell lines (melanoma, MEL188) were a kind gift from Prof. Dr. Timothy E. Weaver, Cincinnati Children's Hospital, Ohio, USA. Inducible mouse lung epithelial cells for Chop (MLE-12/pBI-L-Chop) were already generated by our group as described before [Klymenko et al. 2016]. 24 h after thawing, a fresh medium with selection antibiotics (1 µg/mL doxycycline, 100 µg/mL hygromycin, 100 µg/mL geneticin) were added to induce *Chop* expression

for 6, 12 or 24 h (+dox). Cells grown in normal growth medium (without antibiotics or doxycycline) for similar time points were treated as control group (-dox). All cells were grown in tissue culture plates in full medium based on Dulbecco's Modified Eagle Medium/Nutrient Mixture F-12 (DMEM-F12 Medium).

Medium for A549 and MEL188 cell line

Component	Final Concentration
DMEM-F12	500 mL
Penicillin/Streptomycin	2% (v/v)
FCS	10% (v/v)
MEM Vitamins	1% (v/v)
Non-essential MEM	1% (v/v)
L-Glutamine 200 mM	1% (v/v)

Medium for MLE12 cell line

Component	Final Concentration
DMEM-F12	500 mL
Penicillin/Streptomycin	2% (v/v)
FCS	2% (v/v)
ITS	1% (v/v)
1.25 M HEPES	0.8% (v/v)
L-Glutamine 200 mM	1% (v/v)
1 mM Hydrocortisone	10 ng/mL
1 mM β-Estradiole	10 ng/mL

Cells were harvested or transferred to a new plate to reach confluency of 80-90%. To detach cells from cell culture plates, cells were washed with PBS and flushed with 0.5% Trypsin for 2 min at 37°C. For neutralization of trypsin 2 mL culture medium was added. Cells were diluted 1:10 and plated on new cell culture plates for maintenance.

Transfections and treatment of cells with drugs were performed at 70% confluency using Lipofectamine® 2000 Reagent (Invitrogen AG, Germany). The experiment was performed in a 6-well dish using 4 µg PACS2-GFP (OriGene, Rockville, USA) or empty-GFP using 4 µl Lipofectamine® 2000 Reagent (Invitrogen, Germany) per well.

4.5 Drug treatment

Chop overexpressing MLE12 cells (+/-dox for 12 h) or MEL188 cells stably overexpressing SP-C^{WT} or SP-$C^{\Delta exon4}$ were treated with capsaicin (5 µM,10 µM, 25 µM, Sigma, #M2028) or vehicle (DMSO) for 8 h before processing them for immunoblotting or PLA. PCLS were treated for 24 h with capsaicin (10 µM, 25 µM) or the IPF therapy drug nintedanib (2 µM, Sigma, #SML2848). Sterile filtered DMSO served as vehicle control. About four to five IPF patient PCLS were cultured in one well of a 6-well dish for each treatment group and 'n' of three IPF patient PCLS were used.

4.5.1 Autophagy flux

30 mM stock solution of chloroquine (CQ; Chloroquine diphosphate salt, Sigma, #C6628) was prepared by dissolving 7.74 mg chloroquine in 500 µL aqua dest. 100 µM stock solution of bafilomycin A1 (Baf; Invivogen, # tlrl-baf1) was prepared by dissolving 10 µg bafilomycin A1 in 160 µL DMSO. MLE12 Chop cells were plated in 6-well cell culture dishes. The next day, the medium was replaced with a fresh culture medium and 2 µL Baf, CQ or vehicle (DMSO) was added to get a final concentration of 30 µM CQ or 100 nM respectively. One hour later, MLE12 cells were either not induced or were induced with doxycycline for Chop expression for 6 h. Cells were then harvested to perform immunoblots for LC3B and p62.

4.6 Isolation of RNA

RNA from human lung tissue or cells was extracted using 500 µL guanidine thiocyanate-acid phenol (TRIzol™, Invitrogen AG, Germany) and transferred to a 1.5 mL eppendorf cup. 100 µL chloroform was added to the homogenate/lysate and mixed. The solution was separated into aqueous and organic phase by incubating for 5 min at room temperature. Subsequent centrifugation at 13000 g for 15 min efficiently removed DNA and proteins from the aqueous phase containing RNA. The upper aqueous phase (~200 µL) containing RNA was collected in a new 2 mL eppendorf cup. For enrichment of RNA these steps were repeated by adding 100 µL chloroform. The non-degraded, pure RNA colored by 1 µL Glycoblue™ (Invitrogen AG, Germany) was obtained from the aqueous phase (~150 µL) by precipitation with 100 µL isopropanol and gentle inversion. After incubation at -80°C overnight the solution was centrifuged at 13000 g at room temperature (RT) for 1 hour and supernatant was discarded. RNA pellet was washed twice with 750 µL of 75% ethanol. The purified RNA was centrifuged again for 15 min at 13000 g and air dried at room temperature for 15 min. Finally, the pellet was dissolved

in an appropriate amount of RNase free water. RNA concentration was measured by using NanoDrop™ (Thermo Fisher, Germany) and stored at -80°C. To determine the concentration and purity of the RNA, the extinction at 260 nm and 280 nm was measured. An OD of 1 at 260 nm corresponds to 40 µg RNA/mL. The ratio of the OD at 260 nm and at 280 nm is a measure of RNA purity. In a protein-free solution the ratio OD260/OD280 is 2. Due to protein contaminations this coefficient is usually lower.

4.7 Reverse Transcription

For the preparation of complementary DNA (cDNA) from isolated total RNA reverse transcriptase (Omniscript® RT Kit, Qiagen, Germany) and Oligo dT primers (Roche, Germany) were used. 2 µg of total RNA were used per sample. The sample was filled up with RNase-free water to a total amount of 10 µL and 10 µL Master Mix were added.

Reverse-transcription reaction component

Component	Volume/reaction	Final Concentration
Master Mix		
10x Buffer RT	2 µL	1x
dNTP Mix (5 mM each dNTP)	2 µL	0.5 mM
Oligo dT primer (50 µM)	0.5 µL	1.25 µM
RNase Inhibitor (20 units/µL)	0.5 µL	0.5 units
Omniscript Reverse Transcriptase	1 µL	2 units
RNase-free water	variable	
Template RNA (2 µg)	variable	2 µg
Total reaction volume	20 µL	

For annealing Oligo dT primers, the RNA sample was incubated for 15 min at 22°C. Thereafter cDNA was synthesized at 37°C for 90 min. cDNA concentration was measured using NanoDrop and stored at -80°C.

4.8 Polymerase Chain Reaction

The polymerase chain reaction (PCR) allows amplification of DNA fragments due to repetitive cycles (20-40) of DNA synthesis using heat-stable DNA polymerase (HotStar HiFidelity or Taq® DNA polymerase, Qiagen, Germany). Each cycle consists of three reactions that take place under different temperatures. First template DNA was

denaturated into two single strands at 94°C for 20 min. They function as templates for the synthesis of new DNA using two specific oligonucleotides (primers), which hybridize to sense and antisense strands of the template DNA. Primer annealing was performed at 50-60°C for 30 sec depending on primer design. DNA polymerase started extension of DNA strands from the primers at 72°C (30 sec per 500 bp). High fidelity polymerase was used for better proofreading. The PCR was performed in a thermocycler, programmed as follows:

PCR reaction components

Component	**Volume/reaction**	**Final Concentration**
5x HotStar HiFidelity PCR Buffer (contains dNTPs)	10 µL	1x
Forward Primer	1 µL	1 µM
Reverse Primer	1 µL	1 µM
HotStar HiFidelity DNA Polymerase (2.5 units/µL)	2 µL	5 units
$MgSO_4$	1 µL	1.5 mM
RNase-free water	variable	
Template DNA (200 ng)	variable	200 ng
Total reaction volume	50 µL	

Program

Step		**Time**	**Temperature**
Polymerase activation	1x	20 min	94°C
3-step cycling	**40 cycles**		
Denaturation		30 sec	94°C
Annealing		30 sec	50-68°C (see **Table 2**)
Extension		30 sec(1 min/kb)	72°C
Final Extension step	1x	10 min	72°C

Name	Primer Sequence (5'→3')
ForSP-C-hu	TATTATAAAGCTTATGGATGTGGGCAGCAAAGAGGTCCTG
RevSP-C-hu	TATTATGAATTCCTAGATGTAGTAGAGCGGCACCTCGCCAC
ForSP-Cint1-hu	TACAAGTCCGGAATGGATGTGGGCAGCAAAGAGGTCCTG
RevSP-Cint1-hu	CTGCTGGTAGTCATACACCACGAGGCC
ForSP-Cint2-hu	GGCCTCGTGGTGTATGACTACCAGCAGATGGAATGCTCTCT GCAGGCCAAGCCC
RevSP-Cint2-hu	TATTATCTCGAGCTAGATGTAGTAGAGCGGCACCTCGCCAC
For_ß-actin	ACCCTGAAGTACCCCATCG
Rev_ß-actin	CAGCCTGGATAGCAACGTAC

Table 1. List of primers

Name	Annealing Temperature
SP-C-hu	66°C
SP-Cint1-hu	66°C
SP-Cint2-hu	68°C
ß-actin	53°C

Table 2. Annealing temperature of primers

4.9 Agarose gel electrophoresis

In order to separate and analyze RNA or DNA fragments, agarose gel electrophoresis was performed. 10 µL of DNA samples were mixed with 5x running buffer and loaded onto 2% (w/v) agarose gel. To prepare agarose gel agarose was mixed with 200 mL 1x TAE (Tris base, acetic acid and EDTA) buffer and 5 µL GelRed™. The electrophoresis was performed for 60 min at 150 V in 1x TEA buffer. The negatively charged DNA migrated through the electromagnetic field in the agarose gel and was separated by size (kb). DNA was visualized with GelRed™ by UV Light in ChemoStar Imager (Intas, Germany). The size of DNA was determined by a DNA molecular weight standard (SmartLadder, Eurogentec, Germany)

50x TAE buffer

Component	Final Concentration
Tris	2 M
Acetic acid	5% (v/v)
EDTA pH 8	50 mM
Water	up to 1 L

5x Running buffer

Component	Final Concentration
Glycerol	50% (v/v)
bromphenole blue	0.01% (w/v)
50x TAE buffer	2% (v/v)
Water	up to 10 mL

4.10 Isolation of proteins

4.10.1 Isolation of proteins from lung tissues

Proteins from lung tissue were isolated by homogenizing the tissues using Precellys® (Bertin Technologies, Germany). A small piece of frozen lung tissue was put into homogenization vials containing 1.4 mm and 2.8 mm ceramic beads and treated with 1 mL lysis buffer containing the protease inhibitor phenylmethylsulfonylfluorid (PMSF). Tissue was homogenized twice at 5000 rpm for 20 sec with a 5 sec resting phase in between. Lysate was transferred to eppendorf cup and centrifugated at 15000 rpm at 4°C to clear it. Supernatant was storage at -80°C.

4.10.2 Isolation of proteins from cells

For protein extraction 300 µL lysis buffer (buffer composition given below) containing 3 µL PMSF for a 100 mm TC Dish was applied to cells followed by scraping using Cell Scrapers®. Lysates were transferred to an eppendorf cup, sonicated and centrifuged at 15000 rpm at 4°C. Supernatants were transferred to new tubes and stored at -80°C.

Protein extraction buffer pH 7.4

Component	Final Concentration
Tris-HCl pH 7.5	50 mM
EDTA pH 8	5 mM
NaCl	150 mM
Triton-X-100	1% (w/v)
Sodium-deoxycholate	0.5% (w/v)
Water	up to 1 L

4.10.3 Mitochondrial enrichment from cells by differential centrifugation

Mitochondrial enrichment was performed via a two-step centrifugation: at low speed to remove intact cells from whole cell extracts followed by a high-speed centrifugation to concentrate mitochondria and separate them from other organelles [Djafarzadeh, S. et al. 2017]. For the experiment cells from two 100 mm TC Dish were directly scraped in the medium on ice and pulled together in a 50 mL falcon. After centrifugation at 1200 rpm at 4°C for 6 min supernatant was aspirated and cell pellet was resuspended in 1 mL PBS and transferred to an eppendorf cup. Subsequently cells were again spun down at 1200 rpm at 4°C for 6 min and supernatant was removed. Cell pellet was kept in liquid nitrogen. 10 µL PMSF were added to 1 mL freshly prepared hypoosmotic puffer. 300 µL of this mixture were used to resuspend cell pellets. Thereafter cells were homogenized with 25 strokes using Kimble® dounce homogenizer (2 mL volume) with loose-fitting pestle (Wheaton type B) (DWK Life Sciences, Germany) and transferred into a 2 mL eppendorf cup. Cells were homogenized again using BD Microlance™3 cannula (20 G, 0,9 x 40 mm) for 15 strokes. After homogenization cells were centrifuged at 830 g for 20 min at 4°C. Supernatant was transferred into new eppendorf cup and cell pellet was resuspended in 300 µL hypoosmotic buffer with PMSF (1:100). Cells were homogenized for a second time with 25 strokes using Kimble® dounce homogenizer type B. Thereafter, samples were centrifuged at 830 g for 10 min at 4°C. Supernatant was pooled together and centrifuged at 16800 g for 10 min at 4°C. Then supernatant is the cytosolic fraction. Pellet was washed three times with 500 µL hypoosmotic buffer and centrifuged at 16800 g for 10 min at 4°C. Mitochondria are now enriched in cell pellet that was resuspended in 60 µL. Both cytosolic and mitochondrial fractions were stored at -80°C until further use.

Hypoosmotic buffer pH 7.5

Component	Final Concentration
Saccharose	25 mM
HEPES	2 mM
EDTA	1.16 µM
Water	up to 50 mL

4.10.4 Nuclear extraction

Nuclear extraction was performed using EpiQuik™ Nuclear Extraction Kit I (Epigentek, USA). Cells were allowed to grow 70-80% confluency in a 100 mm TC Dish and then the medium was removed followed by washing twice with PBS. 3 mL of PBS were added to the plate, cells were then scraped and transferred to a 15 mL falcon. Cells were centrifuged for 5 min at 1000 rpm and the supernatant was discarded. The reagent nuclear pre-extraction buffer 1 (NE1) was diluted 1:10 with aqua dest. and kept on ice. Dithiothreitol (DTT) solution and Protease Inhibitor Cocktail (PIC) were added 1:1000 to diluted NE1. Cell pellet was resuspended in 100 µL NE1 solution and transferred to a 1.5 mL eppendorf cup. The cells were incubated on ice for 10 min followed by vortexing for 10 sec. Then the eppendorf cup was centrifuged for 1 min at 12000 rpm at 4°C. The supernatant is the cytosolic fraction and was carefully transferred into a new eppendorf cup. DTT solution and PIC were added 1:1000 to nuclear extraction buffer (NE2) solution. The pellet was resuspended in 50 µL NE2 solution and incubated for 15 min on ice. The sample was vortexed for 5 sec every 3 min to increase nuclear protein extraction. The suspension was centrifuged for 10 min at 14000 rpm at 4°C and the supernatant, which is the nuclear fraction, was transferred to a new 1.5 mL eppendorf cup. Samples were stored at -80°C.

4.11 Protein quantification

Protein concentration was determined by Bicinchoninic acid (BCA) assay (Pierce™ BCA Protein Assay Kit, Thermo Scientific, Germany). Colorimetric measurement was performed using microplate reader (Infinite® M200 Pro, Tecan Group Ltd, Switzerland). The total protein concentration is exhibited by a colour change of the sample solution compared to protein standard. Colour change from green to purple results in a BCA forming chelate complex with reduced Cu^{+} (Cupper-I-ion). The amount of Cu^{2+} reduced

is proportional to the amount of protein present in the solution. Protein standard was prepared by 2 mg/mL bovine serum albumin (BSA) as given in the following table. Samples were diluted 1:100 with sodium chloride (NaCl). 200 µL BCA reagent (160 µL Reagent A and 40 µL Reagent B) was added to 50 µL diluted samples in a 96 well plate, followed by incubation at 37°C for 30 min. Thereafter values were measured by a microplate reader at a wavelength of 492 nm.

BSA (µg/mL)	Standards (µL)	Dilution with 0.9% NaCl (µL)
A. 2000		
B. 1500	450 A	150
C. 1000	300 A	300
D. 750	300 B	300
E. 500	300 C	300
F. 250	300 E	300
G. 125	300 F	300
H. 62.5	300 G	300
I. 31.25	300 H	300
J. 15.625	300 I	300
K. 7.813	300 J	300
L. 0	0	300

4.12 SDS-polyacrylamide gel electrophoresis

Proteins were separated by Sodium dodecyl sulfate polyacrylamide gel electrophoresis (SDS-PAGE). Protein extracts was denaturated by adding 4x SDS sample buffer and reduced with 10% β-mercaptoethanol, followed by heating at 98°C for 12 min. Samples were briefly spun down before loading onto gel. Gel consists of 4% stacking gel and different concentrations of resolving gel depending on the size of the target protein, which is inversely proportional to the molecular weight of the protein. The sizes of proteins were determined by a protein molecular weight standard (PageRuler™, Thermo Scientific, Germany). The electrophoresis was performed in the presence of 1x SDS running buffer with 15 mA constant per gel. Gel was run until bromphenole blue line reached the bottom of the gel. Thereafter gel was used for Western blotting.

4xSDS sample buffer

Component	Final Concentration
Stacking gel buffer (Tris-HCl, pH 6.8)	156 mM
SDS	5% (w/v)
Glycerine	40% (v/v)
Bromphenole blue	0.01% (w/v)
Water	up to 100 mL

Gel Component

SDS PAGE	Resolving Gel				Stacking Gel
	8%	**10%**	**12%**	**15%**	**4%**
Rotiphorese	2.65 mL	3.33 mL	4 mL	5 mL	0.66 mL
dest. H_2O	3.85 mL	3.53 mL	3.2 mL	1.53 mL	3.29 mL
10% SDS	100 µL	100 µL	100 µL	100 µL	100 µL
Resolving gel buffer (1.125 M Tris/HCl, pH 8.8, 30% saccharose)	3.33 mL	3.33 mL	3.33 mL	3.33 mL	
Stacking gel buffer (0.625 M Tris/HCl, pH 6.8)					1 mL
10% APS	50 µL	50 µL	50 µL	50 µL	50 µL
TEMED	10 µL	10 µL	10 µL	10 µL	5 µL

1x SDS running buffer

Component	Final Concentration
Tris	25 mM
Glycin	192 mM
SDS	0.1% (w/v)
Water	up to 1 L

4.13 Western blotting

4.13.1 Electro blotting of proteins

Western blotting was performed in order to visualize and detect proteins of interest using the electrophoretic mobility of proteins to transfer them from the gel onto a membrane. After separating by SDS-PAGE proteins were transferred onto polyvinylidene fluoride (PVDF) Transfer Membrane (Merckmillipore, Ireland) by wet electroblotting. Before use the PVDF membrane was activated in methanol for 1 min. Transfer equipment was prepared in a "sandwich" layer way: two layers of Whatmann™ Gel Blot Paper (GE Healthcare, UK), followed by activated PVDF membrane, then the gel and again two layers of Whatmann™ Gel Blot Paper. All equipment was soaked with transfer buffer and placed into the electro blotting chamber. Transfer was performed in transfer buffer at 100 V for 90 min.

1x Transfer buffer

Component	Final Concentration
Tris	20 mM
Glycine	159 mM
Methanol	20% (v/v)
Water	up to 1 L

4.13.2 Immunological protein detection

The membrane was blocked with 5% non-fat dry milk in TBST buffer at room temperature for 1 h followed by incubation with primary antibody dissolved according to the data sheet, usually 1:500, in the 5% milk buffer at 4°C overnight. After washing three times with 1x TBST for 15 min at RT, the membrane was incubated for 1 h at RT with HRP-conjugated secondary antibody (Agilent Dako, USA) dissolved 1:2000 in 5% milk buffer. Thereafter the membrane was washed again three times for 15 min with 1x TBST. Proteins on the membrane were detected by Immobilon® Western Chemiluminescent HRP Substrate (EMD Millipore Corporation, USA) and the emitted chemiluminescence signal was detected with Enhanced Chemiluminescence (ECL) ChemoStar Imager (Intas, Germany).

1x TBST buffer

Component	Final Concentration
Tris	50 mM
NaCl	50 mM
Tween 20	0.1% (v/v)
HCl 32%	up to pH 7.5
Water	up to 1 L

If necessary to re-probe the membrane, the membrane was stripped twice with 0.2 M NaOH for 15 min after washing twice with TBST. Thereafter the membrane was prepared for immunological detection as described above.

4.14 Immunohistochemistry

Immunohistochemistry (IHC) was used to visualize localization of specific cellular components within cells and within their proper histological context by using appropriately labelled antibodies to bind specifically to their target antigens *in situ*. Visualising an antibody-antigen interaction can be accomplished in a number of ways. Lung tissues were fixed in paraformaldehyde as described earlier and sections of 3 µm thickness were used for immunohistochemical analysis. ZytoChem Plus AP-Fast Red Kit (Zytomed Systems, Germany) was used for this study. Lung tissue sections were deparaffinized at 60°C for 1 h and then cleared in xylene for 10 min. Sections were then rehydrated in ethanol with descending concentrations for 3 min each (99.6% > 96% > 80% > 70% > 50%) and kept in 1x PBS (Phosphate Buffered Saline). Antigen retrieval was performed by boiling with citrate buffer three times and the buffer was cooled down for 20 min, before heating it again. Sections were washed three times with 1x PBS and further steps were carried using ZytoChem Plus AP-Fast Red Kit. Briefly, sections were blocked with blocking solution for 7 min. After washing them three times with 1x PBS slides were incubated with primary antibodies with respective dilutions in 3% BSA at 4°C overnight. A negative control was prepared where primary antibody was omitted. Thereafter slides were washed again and incubated for 10 min at RT with 100 µL biotinylated secondary antibody, followed by washing. Three drops of enzyme conjugate (streptavidin / alkalic-phosphatase) were added to each section with 10 min incubation at RT. After washing one drop of fast red solution was dissolved in

one substrate buffer bottle (naphthol-phosphate buffer) and vortexed for 2 min. Four drops of freshly prepared substrate solution were added to each section and allowed to develop in the dark, with constant monitoring for the development of pink/red colour under a light microscope. All sections were treated at the same point of time to facilitate proper development and to avoid false results. When development reached the proper colour, the reaction was stopped by immersing the slides in distilled water. Nuclei staining was performed with haemalaun for 40 sec followed by washing the slides under running tap water. Sections were then mounted with pre-warmed glycerol mounting medium (Dako, USA) and allowed to dry. For scanning and analysing sections Nano Zoomer (Hamamatsu, Germany) was used and all scanned pictures of the stained sections were photographed and analyzed using NDP View 2.0 software.

10x PBS, pH 7.4

Component	Final Concentration
NaCl	1.37 M
KCl	26.8 mM
Na_2HPO_4*2 H_2O	64.6 mM
KH_2PO_4	14.7 mM
Water	up to 1 L

4.15 Immunofluorescence

4.15.1 Immunofluorescence on tissue

Immunofluorescence analysis was performed to identify cellular localization of proteins in tissue sections. 3 µM paraffin-embedded, formalin-fixed lung tissue sections were deparaffinised and antigen retrieval was performed as described above. Sections were washed three times with 1x PBS and then blocked with 5% Donkey Serum in PBS for 30 min at RT, followed by blocking with 3% BSA (bovine serum albumin) for 1 h. After blocking sections were incubated with primary antibodies with respective dilutions in 3% BSA at 4°C overnight. Also control sections were prepared by omitting primary antibody, followed by washing steps and incubation of the sections with fluorochrome-conjugated secondary antibodies (Alexa Fluor® Plus, Invitrogen AG, USA) 1:400 diluted in 3% BSA in the dark at room temperature. Thereafter sections were washed again and

stained for nuclei with 4′,6-Diamidin-2-phenylindole (DAPI, Sigma Aldrich, USA) for 2 min at RT. Sections were then washed again and mounted with a fluorescence mounting medium (Dako, USA) and allowed to dry. Sections were detected and processed by Leica M205 FA Fluorescent Stereoscope (Leica Microsystems, USA) and LAS-X-Core Software (3.7.4. version, LAS X Life Science, USA).

Citrate buffer, pH 6

Component	Final Concentration
$C_6H_5Na_3O_7$*2 H_2O	1 M
Tween 20	0.05% (v/v)
HCl 32%	up to pH 6
Water	up to 1 L

4.15.2 Immunofluorescence on cells

Immunofluorescence on cells was performed on tissue culture chamber slides (8-well on lumox®, detachable, Sarsteadt, Germany). 30,000 cells per well were seeded a day before use. The number of cells was calculated using Neubauer Chamber (Optik Labor, Germany). For Chop induction cells were treated with 1 µg/mL doxycycline for 12 h and 24 h, and if required stained with 0.1 mM MitoTracker® as a fluorescence dye for staining mitochondria for 15 min at 37°C under sterile conditions. Cells were then fixated with either methanol/acetone (1:1) for 5 min at -20°C or with 4% paraformaldehyde (PFA) for 15 min at 37°C. Cells fixed with PFA were permeabilized with 0.5% Triton X for 15 min at RT after washing them three times with 1x PBS. Thereafter steps were followed as described above (**4.15.1**).

4.16 Proximity Ligation Assay

Proximity ligation assay (PLA) allows detection of protein-protein interactions *in situ* (at distances <40 nm) at endogenous level. Protein targets can be readily detected and localized with single molecule resolution in unmodified cells and tissues. Typically, two primary antibodies raised in different species are used to detect two unique protein targets. A pair of oligonucleotide-labeled secondary antibodies (PLA probes) then binds to the primary antibodies. Next, hybridizing connector oligos join the PLA probes only if they are in close proximity to each other and ligase forms a closed, circle DNA template that is required for rolling-circle amplification (RCA). The PLA probe then acts as a primer

for a DNA polymerase. This allows up to 1000-fold amplified signal that is still tethered to the PLA probe, allowing localization of the signal. Lastly, labeled oligos hybridize to the complementary sequences within the amplicon, which are then visualized and quantified as discrete spots by microscopy image analysis. In this experimental setting we used Duolink® In Situ Orange Starter Kit Goat/Rabbit (Sigma Aldrich, Germany). Cells were spread on chamber slides and fixed with PFA as described above. To observe ER-Mitochondria interaction anti-calnexin antibody (goat, Santa Cruz) as an ER marker and either anti-VDAC1 (rabbit, Proteintech) or anti-TOM20 (rabbit, Santa Cruz) were used as mitochondrial makers. PLA was performed according to manufacturer's instructions. The results were viewed using Leica M205 FA Fluorescent Stereoscope (Leica Microsystems, USA) and LAS-X-Core Software (3.7.4. version, LAS X Life Science, USA). PLA results were quantified by Image J software (version 1.52a, NIH, USA) following user guide (https://imagej.nih.gov/ij/docs/guide/user-guide.pdf) and *Basic Intensity Quantification with ImageJ* by Christine Labno University of Chicago (https://www.unige.ch/medecine/bioimaging/files/1914/1208/6000/Quantification.pdf).

4.17 Co-Immunoprecipitation

Co-immunoprecipitation (Co-IP) is a method that is used to detect potential interactors of specific proteins from cell lysates or tissue homogenates. It involves incubating fresh lysates with magnetic beads or agarose-resin beads attached to antibody against the specific protein of interest (IP) or against a potential interacting partner of this protein (Co-IP). Co-immunoprecipitation help determine whether two proteins interact or not and can also give insight on unknown interacting proteins. Here cells were plated in a 10 cm TC-Dish followed by treatment and/or transfection or left untreated. One day before cell lysis, beads were prepared. For a 10 cm TC-Dish 2 mg Beads (66.6 µL) were transferred to an eppendorf cup and washed with 1 mL buffer B. In order to immobilize antibody on the beads 2 µg of target antibody was mixed with 58 µL buffer B and 38.67 µL buffer C and added to beads. A separate epi control was prepared using 2 µg control IgG from the same source. The mixture was incubated on roller overnight at room temperature. In order to preserve protein-protein interactions, 0.5 µL Halt™ Protease Inhibitor Cocktail (Thermo Scientific, Germany) was added to 500 µL Pierce™ IP lysis buffers (Thermo Scientific, Germany). Cells were washed once with ice cold PBS before adding 100°µL premixed lysis buffer to a 10 cm TC dish. Next cells were carefully scraped on ice and transferred to an epi. Cells were then incubated for 10 min on ice occasionally mixed after

every 3-4 min, followed by centrifugation at 13000 rpm for 10 min at 4°C. Supernatant was collected into a new eppendorf cup. To remove supernatant the eppendorf cup was placed on a magnetic stand to allow the beads to pellet. Next beads were washed with 1 mL buffer E. For the input 25 µL from cell lysate were removed and put in a separate epi, the remaining lysate was added to antibody coupled beads and incubated overnight at 4°C in a vertical rotor. The next day the eppendorf cup was placed on the magnetic stand and the supernatant was removed, followed by washing it three times with buffer E. The pellets were resuspended with 40 µL PBS. Samples were denaturated as previously described. For loading on SDS-gel 5 µL of input and 5-20 µL for immunoprecipitated samples was used.

Buffer B

Component	Final Concentration
NaH_2PO_4	0.2 M
Na_2HPO_4*2 H_2O	0.8 M
Water	up to 1 L

Buffer C

Component	Final Concentration
$(NH_4)_2SO_4$	1 M
Buffer B	up to 100 mL

Buffer D

Component	Final Concentration
BSA	0.5 %(w/v)
NaCl	0.15 M
Buffer B	up to 100 mL

Buffer E

Component	Final Concentration
Triton X-100	0.1 %(w/v)
NaCl	0.15 M
Buffer B	up to 100 mL

4.18 Cloning

In order to synthesize cDNA reverse transcription was performed using RNA isolated from human donor lungs as described earlier. Primers used for cloning full length human *SFTPC* in pEGFP-C1 vector (pCMV promoter driven, originally from Clontech) with GFP tag to the N-terminal of the multiple cloning site (EGFP-SP-C^{WT}) are given in **Table 1** (ForSP-C-hu, RevSP-C-hu). The reference sequence for SP-C^{WT} is Gene ID: 6440, *SFTPC*, *Homo sapiens* (NCBI, updated on 29-Jan-2021). An in-frame fusion protein was made through introduction of a HindIII site at the 5' end and an EcoRI site at the 3'end for cloning into pEGFP-C1 generating pCMV-EGFP-hSP-C^{WT} plasmid. Then the *SFTPC* gene was amplified using gene-specific primers for HotStar HiFidelity Polymerase. After amplification PCR products were purified using QIAquick® PCR Purification Kit (Qiagen, Germany), followed by digestion with restriction enzymes (HindIII, EcoRI, NEB, USA) at 37°C overnight. The same restriction enzymes were also used for digestion of the pEGFP-C1 Vector (Addgene Europe, UK) Restriction digested (RD) products were separated by agarose gel electrophoresis, followed by gel purification using QIAquick® Gel Extraction Kit (Qiagen, Germany) according to the manufacturer's instructions. Thereafter *SFTPC* gene was then cloned into pEGFP-C1 Vector via ligation reaction using NEB T4 DNA ligase (NEB, USA) at 16°C overnight.

Restriction Digestion

Component	Final Concentration
PCR purified product / Vector	48 µL / 5 µL
10x NEB Buffer	6 µL / 2 µL
Enzyme 1	2 µL / 1 µL
Enzyme 2	2 µL / 1 µL
Water	2 µL / 11 µL

Ligation Reaction

Component	Final Concentration
Gel extracted RD insert DNA	7 µL
Gel extracted RD vector DNA	1.5 µL
10x T4 DNA ligase buffer	1 µL
T4 DNA ligase	0.5 µL

4.19 Gene Splicing by Overlap Extension

Gene Splicing by Overlap Extension (SOEing) was used for site-directed mutagenesis to generate a plasmid with deletion of exon4 of the *SFTPC* gene (*SP-C$^{\Delta exon4}$*). This PCR-based method directly generates mutated DNA fragments without relying on restriction sites. As described by Horton et al. [Horton, R.M. 1995] and Wang et al. [Wang, W.-J. et al. 2003] gene Splicing by Overlap Extension (SOEing) was performed to generate *SP-C$^{\Delta exon4}$* by HighFidelity DNA Polymerase using specific primers (Metabion, Germany). For generating pCMV-EGFP-hSP-C$^{\Delta exon4}$, deletion of exon 4 from pCMV-EGFP-hSP-C^{WT} was achieved by overlap extension PCR with a two round, four-primer technique. Mutation variants of SP-C were obtained from Uniprot (http://www.uniprot.org/uniprot/P11686). Sequence alignments were performed using Blast/NCBI (https://blast.ncbi.nlm.nih.gov/Blast.cgi).

In step 1, exons 1-3 were amplified by single PCR using two primers: ForSP-Cint1-hu and RevSP-Cint1-hu (**Table 1**). In step 2, exon 5 was amplified through the 3' untranslated Poly A tail using a forward primer containing complete overlap with the 3' end of the reverse primer used to amplify exon 3 (ForSP-Cint2-hu, RevSP-Cint2-hu in **Table 1**). These two overlapping primary products were purified by PCR Purification Kit (Qiagen, Germany) and then they were mixed, denatured and reannealed by SOEing PCR. Expression PCR was performed according to the program above for 15 cycles without adding primers and an annealing temperature at 68°C. The 3′-end of the top strand of one fragment anneals onto the 3′-end of the bottom strand of the other fragment. This overlap can be extended to form the recombinant product and amplified using normal expression PCR as described above using specific primers (ForSP-Cint1-hu, RevSP-Cint2-hu, **Table 1**). Following digestion with HindIII and EcoRI, the hSP-C$^{\Delta exon4}$ insert was subcloned into pEGFPC1 using standard protocols to generate pCMV-EGFP-hSP-C$^{\Delta exon4}$ plasmid. Several clones were generated and sequenced. All further details are explained in results section.

4.20 Heat shock transformation

Transformation was performed using OneShot™ TOP10 competent *E.coli*. (Invitrogen AG, Germany). 10 µL of ligation mixture was pipetted into a vial of competent cells which were thawed on ice and mixed gently. Vials were incubated on ice for 30 min, followed by heat shock for 30 sec at 42°C and immediately placed back on ice for 2 min. Thereafter 250 µL S.O.C Medium was added to the vial and incubated in a horizontal

shaking incubator for1 h at 225 rpm. An aliquot of 20 µL was spread on a pre-warmed 50 µg/mL kanamycin containing agar dish. The dish was inverted and incubated at 37°C overnight. Individual bacterial colonies were picked from the dish and inoculated in LB Medium containing the appropriate antibiotics and incubated overnight at 37°C at 225 rpm. The next day glycerol stock was prepared 500 µL LB Medium was added to 600 µL sterile glycerol. Plasmids were subsequently isolated using QIAprep® Spin Miniprep Kit or EndoFree® Plasmid Maxi Kit (Qiagen, Germany). In order to evaluate the efficiency of cloning insert release was performed at 37°C overnight and an aliquot of purified plasmids from positive clones were sent to Eurofins Genomics Germany GmbH (former MyGATC) for sequencing using sequencing primers (GFP_forseq, SP-Cfor_midseq, SP-Cfrev_midseq, **Table 3**) The sequences were then compared to the reference insert sequence obtained from the NCBI (NCBI gene/NCBI-Blast; Gene ID: 6440). Positive clones were identified after confirming the correct sequence for both plasmids.

Sequencing primer

Name	**Primer Sequence (5'→3')**
GFP_forseq	ACTACCTGAGCACCCAGT
For_resNeo_seq	CAAGATGGATTGCACGCAGG
SP-Crev_N	GCAGGGCTCCCACAATC
Seq_flag_for	GACTACAAGGACGACGA
SP-Cfor_midseq	TACCACTGCCACCTTCTC
SP-Crev_midseq	GAGAAGGTGGCAGTGGTA

Table 3 List of primers for sequencing

Liquid Luria Bertani (LB) medium

Component	**Final Concentration**
Bacto tryptone	1% (w/v)
Yeast Extract	0.5% (w/v)
NaCl	1% (w/v)
Water	up to 1 L

Solid Luria Bertani (LB) medium for selective dishes

Component	Final Concentration
Bacto tryptone	1% (w/v)
Yeast Extract	5% (w/v)
NaCl	1% (w/v)
Agar	1.5% (w/v)
Water	up to 1 L

Insert Release

Component	Final Concentration
Miniprep	5 µL
10x NEB Buffer	2 µL
Enzyme 1	1 µL
Enzyme 2	1 µL
Water	11 µL

4.21 Epithelial cell lines with conditional, stable expression of genes

4.21.1 Transient transfection

Cells were transfected with 4 µg plasmid DNA using 4 µL Lipofectamine® 2000 Reagent (Invitrogen AG, Germany). Transfection was performed when cells reached 70% confluency. Plasmid DNA and transfection reagent were each diluted in 250 µL Opti-MEM Medium (Gibco, Germany) and allowed to rest for 5 min at RT. Thereafter DNA and transfection reagent were mixed and incubated for 20 min at RT for complex formation. Meanwhile cells were given fresh serum- and antibiotics-free DMEM medium (Gibco, Germany). Finally, 500 µL of the transfection mixture were then added as droplets onto the cells. After 4 h transfection mixture was replaced with full culture DMEM medium. The next day transfection efficiency was observed by GFP signal under a light microscope and cells were harvested and analyzed for gene and protein expression.

4.21.2 Stable transfection

For stable transfection MEL188 cells were seeded in 6 well plates in A549 medium and allowed to grow overnight. GFP-SP^{WT} Vector and GFP-SP-C$^{\Delta exon4}$ were linearized with restriction enzyme *ApaL I* and purified with PCR purification Kit (Qiagen, Germany).

Cells were transfected with linearized vector containing the neomycin resistance gene as described above. After 24 h post-transfection the medium was replaced with a fresh medium containing 600 µg/mL geneticin (G418, Gibco, Germany) and left for 10 days. The medium was replaced every second day. Stably transfected cells were identified by GFP under a fluorescence microscope and picked with a sterile pipette and transferred to 96 well plates. After two to three weeks with changing culture media containing 600 µg/mL geneticin every third day and transferring them to a bigger plate, only resistant cells were left over. If cells were able to grow in the wells in the presence of geneticin, the cells were regarded as transgenic cell line. In order to confirm the transfection efficiency resistant clones were harvested and analyzed for gene and protein expression. Positive clones were identified after confirming the correct sequence for both plasmids.

4.22 Cytotoxicity Assay

Cytotoxicity was measured using Lactate Dehydrogenase Activity Assay Kit (Sigma Aldrich, Germany). Lactate dehydrogenase (LDH) is an oxidoreductase enzyme that catalyses the interconversion of pyruvate and lactate. Cells release LDH into the bloodstream after tissue damage. Since LDH is a fairly stable enzyme, it has been widely used to evaluate the presence of damage and toxicity of tissue and cells. Quantification of LDH has a broad range of applications. In this kit, LDH reduces NAD to NADH, which is specifically detected by colorimetric (450 nm) assay. In this experimental setting LDH release is directly proportional to cell death level. LDH assay was performed according to the manufacturer's instructions. The experiment was performed in a 96 well plate. Cells were cultured in colourless DMEM-F12 Medium (Gibco, Germany) without phenolred. For measurement cell death 50 µL of cell supernatants were mixed with 50 µL reaction mix (48 µL LDH Assay Buffer and 2 µL LDH Substrate Mix) and the absorbance at 450 nm (A_{450}) was measured by microplate reader (Infinite® M200 Pro, Tecan Group Ltd, Switzerland). The raw data were analyzed using the following formula. For each sample two replicates were applied.

$$LDH\ activity\ [\frac{milliunits}{mL}] = \frac{(A_{450})final - (A_{450})inital}{(T_{final} - T_{inital})x\ V}$$

ΔA_{450} = amount of NADH generated by assay between T_{inital} and T_{final} [nmol]

T_{inital} -T_{final} = reaction time [min]; V = sample volume [mL]

4.23 Measurement of mitochondrial respiratory function

For measurement of respiratory activity (oxidative phosphorylation in mitochondria (OXPHOS)) of biological samples and quantitative data Oxygraph-2K (Oroboros Instruments, Austria) was used. High-Resolution Respirometry (HRR) provides a modern tool to study mitochondrial respiratory physiology which allows direct measurement of cellular metabolic function during health and disease. OXPHOS analysis uses respirometry as a fundamental approach to study oxygen consumption as an element of mitochondrial function in aerobic core metabolism. Oxygen flux times the driving force of the oxidation. In a closed oxygraph chamber, the oxygen concentration declines over time as a result of respiratory processes. Oxygen concentration remains constant over time and the slope is zero when all processes reacting with oxygen are fully inhibited. The oxygen consumption rate per unit volume (=oxygen flux, volume-specific) is proportional to the negative slope of oxygen concentration with time. For running the assay, cells were harvested at 80% confluent and transferred to cell culture medium with DMEM Medium with 0.2 M HEPES. Before cells were transferred to the chamber cells were counted and written in the software mask (Oroboros DatLab). For optimal conditions cell counts should be around two million. Two chambers allow comparing control and treated cells in the same experiment. The tightness of the chamber was checked and the experiment was run. It began with measuring the base level of oxygen consumption rate (OCR) after approximately 2 min. As 2 mM oligomycin, an ATP synthase inhibitor, was injected, the OCR is rapidly decreased. This was reversed by the careful titration of 1 nM uncoupling agent FCCP that dissipated the proton gradient and maximized the OCR. After the injection of 0.5 mM rotenone/antimycin A, a blocker of complex A, the OCR decreased again. Parameters were calculated out of the graph. Basal respiration showed the energetic demand of cells under basal conditions. The parameter after oligomycin injection showed ATP-linked respiration. Maximal respiration represented the maximum capacity that the electron respiratory chain could achieve. The maximal oxygen consumption rate was measured by injection of FCCP. Spare respiration was the difference between maximal and basal respiration, which reflected the capability of the cells to respond to changes in energetic demand and indicates the fitness of the cells. Non-mitochondrial respiration was the oxygen consumption due to cellular enzymes other than mitochondria after injection of rotenone and antimycin A.

4.24 Electron micoroscopy

The lung samples investigated by electron microscopy were taken from the Department of Thoracic Surgery, Vienna, Austria (W. Klepetko) and were collected in the frame of the European IPF Registry/Biobank (eurIPFreg/bank). All electron microscopic analysis was performed by Prof. Dr. Lars Knudsen (Hannover Medical School Germany). Tissue samples were fixed by immersion using a mixture of 1.5% Glutaraldehyde, 1.5% Paraformaldehyde in 0.15 M HEPES buffer. In order to increase the contrast of the membranes, the tissue was stained en-bloc based on the rOTO (reduced osmium tetroxide – thiocarbohydrazide–osmium tetroxide) protocol [Beike, L. et al. 2019, Deerinck, T.J. et al. 2010]. Ultrathin sections were cut at a thickness of approximately 60 nm and investigated using a transmission electron microscope (Morgagni, Philips, Eindhoven, The Netherlands).

4.25 Densitometry analysis

The relative expression level of proteins in blots was calculated by measuring bands density using Image J software (version 1.52a, NIH, USA). Integrated density values of respective proteins were normalized against those of β-actin or GAPDH values. The values of controls were then assumed as 1 and the fold change of a target protein was calculated.

4.26 Statistical analysis

Data were analyzed by GraphPad Prism 5.02 software and are expressed as mean ± SD. At least two independent experiments were performed from eight IPF or donors. About four to five PCLS from each IPF patient were pooled per treatment group and PCLS from three IPF patients were used. Statistical significance of differences between two groups was assessed using the Mann-Whitney U test. For the statistical comparison of differences between ≥ 3 groups, one-way ANOVA was used. Significance level is indicated by *$p < 0.05$, **$p < 0.01$, and ***$p < 0.001$, ns=not significant and data are expressed as mean ± SD.

5 Results

5.1 Regulation of ER-mitochondria interactions in cells with inducible Chop expression

5.1.1 Induction of Chop alone is sufficient to decrease ER-mitochondrial tethering

The pathomechanistic significance of ER and mitochondria have been well established in the apoptosis of AECII in IPF patients and in animal models of lung fibrosis. Based on this, we first asked if ER-mitochondrial crosstalk is altered under conditions of ER stress and in lung fibrosis. Our group showed that MLE12 cells with stable, inducible tet-on system (doxycycline, +dox) overexpression of the terminal ER stress pro-apoptotic transcription factor Chop is sufficient enough to drive their apoptosis and induce pro-fibrotic signaling [Korfei, M. et al. 2008]. We hence exploited the same system to study the ER-mitochondrial interface. Cells were either not induced (-dox) or were induced with doxycycline (+dox) followed by *Chop* expression for 12 and 24 hours, harvesting and

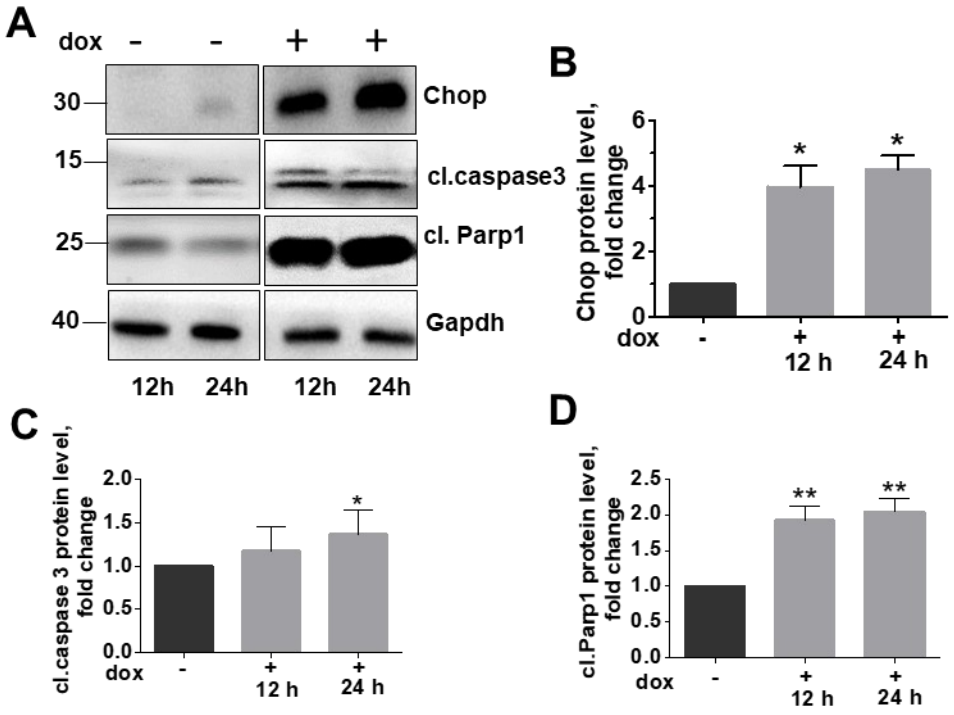

Figure 10 Induction of Chop increases apoptosis markers in alveolar epithelial cell line

A. MLE12 cells were either not induced or were induced with 1 µg/mL doxycycline for Chop expression for 12 and 24 hours, followed by immunoblots for the given proteins from total cell lysates. The positions of molecular weight markers are shown. **B.-D**. Quantification of significant increase in cl. caspase 3 protein levels (**C**) and cl. Parp1 protein level (**D**) upon Chop induction (**B**) obtained from (**A**). Relative protein amounts were normalized to Gapdh and their level in -dox cells was set as one. Statistical significance is indicated as: *p ≤ 0.05, **p ≤ 0.01

western blot analysis (**Figure 10 A**). First, as shown before, overexpression of *Chop* (**Figure 10 B**) resulted in a significant increase in the terminal apoptosis marker, cleaved caspase 3 (**Figure 10 C**) and cleaved Poly(ADP-ribose)-Polymerase 1 (Parp1) (**Figure 10 D**). In order to investigate if such Chop induction alone would also result in altered ER-mitochondrial tethering, co-immunofluorescence analysis for the ER protein calnexin (green) and mitochondrial dye (Mitotracker®, red) was performed (**Figure 11 A**). Such staining showed decreased co-localization (yellow) of ER with mitochondria in dox treated cells versus dox untreated cells (**Figure 11 B).**

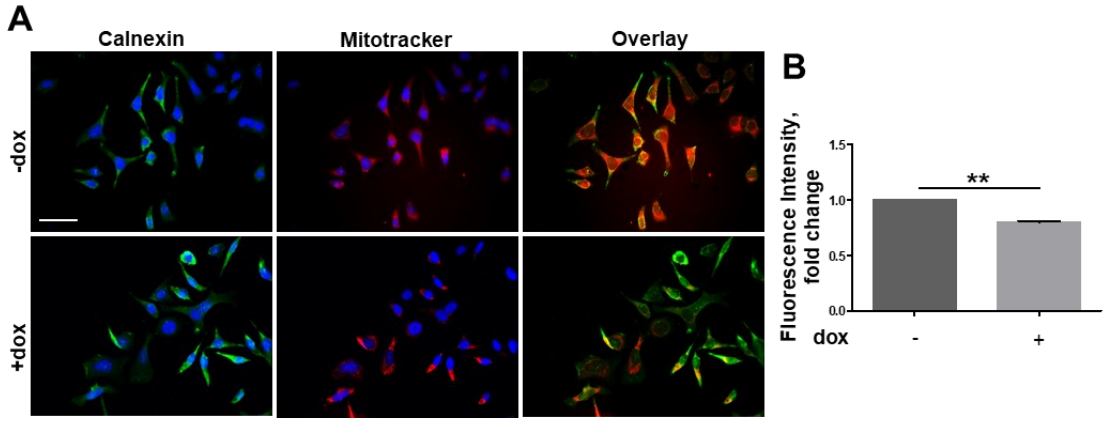

Figure 11 Induction of Chop alone decreases ER-mitochondrial contact

A. Representative immunofluorescence images of MLE12 cells either non-induced or induced with dox for 24 hours for Chop expression. Staining for ER (Calnexin, green) and mitochondria (Mitotracker red) is shown. Nuclei were stained with DAPI (blue), scale bar = 60 µm. **B.** Fluorescence intensity of co-localization was quantified using ImageJ, its intensity in -dox cells was set to one. Statistical significance is indicated as: $^{**}p \leq 0.01$

In order to study if the reduction in co-localization between ER-mitochondrial markers could be due to a reduced ER-mitochondrial tethering, we performed proximity ligation assay (PLA) using antibodies against the ER membrane protein calnexin and the mitochondrial membrane proteins, mitochondrial import receptor subunit, translocase of outer membrane (TOM20) or voltage-dependent anion-selective channel 1 (VDAC1). As can be seen in **Figure 12 A-C**, the fluorescence signal intensity significantly decreased in Chop induced cells with both TOM20/Calnexin and VDAC1/Calnexin pairs as compared with dox untreated cells lacking Chop expression. This clearly indicates that the proximity between ER-mitochondria decreased upon Chop induction.

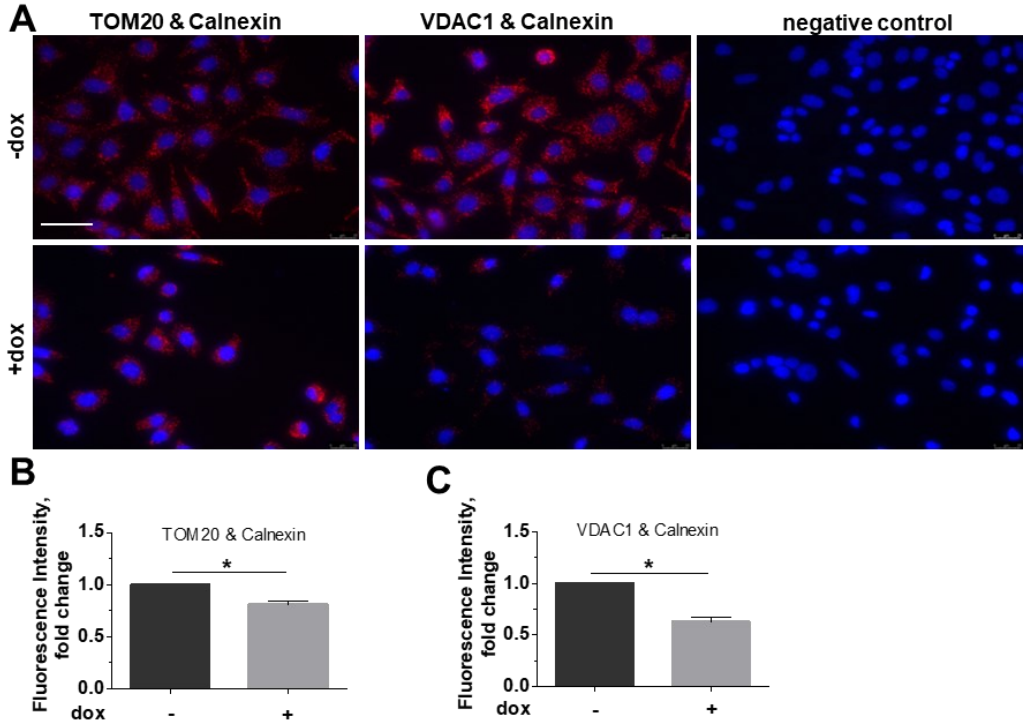

Figure 12 ER-Mitochondria tethering is impaired upon Chop overexpression

A. Proximity Ligation assay with antibodies against Calnexin and TOM20 or Calnexin and VDAC1 followed by fluorescence microscopy images are shown; scale bar = 60 µm. **B.&C.** Fluorescence intensity was quantified using ImageJ, its intensity in uninduced cells was set to one. Blots, stainings and analysis were performed from n = 3 and at least three technical replicates. Statistical significance is indicated as: *p ≤ 0.05

5.1.2 Induction of Chop decreases Pacs2 protein levels

As mentioned in the introduction, the MAM protein Pasc2 is important for ER-mitochondria tethering, as it anchors the ER membrane to the mitochondrial outer membrane [Li, C. et al. 2020]. Other important MAM proteins, namely SigmaR1 and IP3R3, are important Ca^{2+} channel modulators at the MAMs. Based on this information, we further investigated if altered MAM proteins are responsible for decreased ER-mitochondrial tethering that is observed in cells with Chop induction. For this, we performed immunoblots for SigmaR1, IP3R3 and Pacs2. Of the MAM proteins analyzed, we observed a significant decrease in Pacs2 protein (**Figure 13 A&B)** upon 12 and 24 hours of Chop induction. Protein levels of SigmaR1 and IP3R3 did not change significantly upon Chop induction (**Figure 13 C&D**).

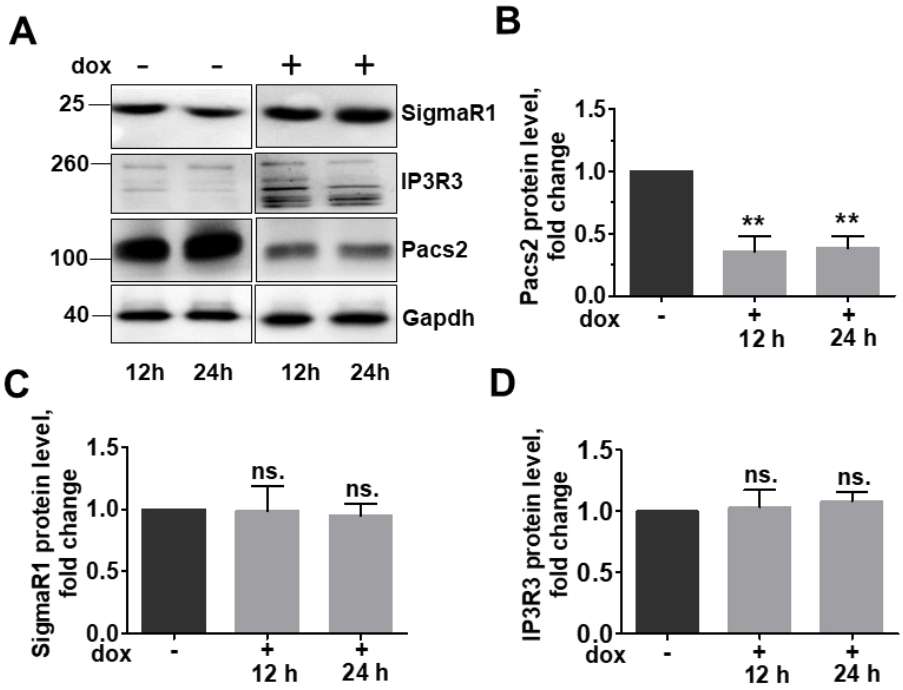

Figure 13 Altered MAM protein levels upon Chop overexpression

A. MLE12 cells were either not induced or were induced with 1 µg/ml doxycycline for Chop expression for 12 and 24 hours, followed by immunoblots for the given proteins from total lysates. **B.-D.** Quantification of significant decrease in Pacs2 (**B**), SigmaR1 (**C**) and IP3R3 protein level (**D**) upon Chop induction. Relative protein amounts were normalized to Gapdh and their level in –dox cells was set as one. Blots were performed from n = 3 and statistical significance is indicated as: **p ≤ 0.01 and ns.= not significant.

Supporting this, immunofluorescence analysis also revealed a significant decrease in Pacs2 protein in Chop induced cells (**Figure 14 Figure 12A&B**).

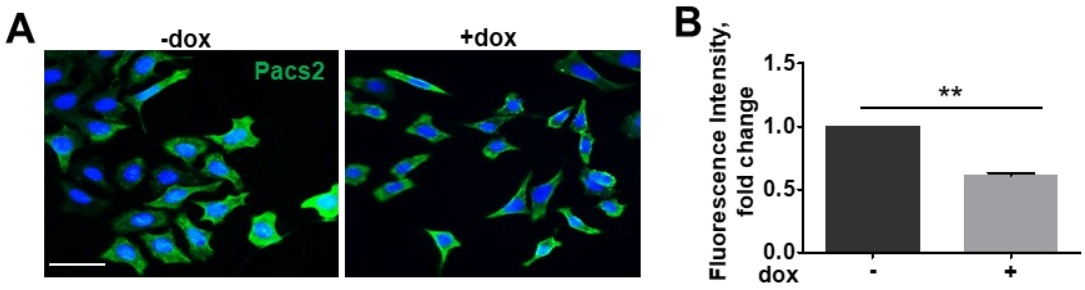

Figure 14 Pacs2 is decreased upon Chop overexpression

A. Representative immunofluorescence images of Pacs2 (green) in –dox or + dox treated cells for 24 hours. Nuclei were stained with DAPI (blue), scale bar = 60 µm. **B.** Fluorescence intensity was quantified using ImageJ, its intensity in -dox cells was set to one. Blots and analysis were performed from n=3 experiments and statistical significance is indicated as:**p ≤ 0.01.

Further, in order to rule out any direct effects of doxycycline treatment on ER-mitochondrial tethering, we also treated wildtype MLE12 cells with doxycycline and analyzed them for Pacs2 protein levels. Doxycycline treatment itself did not affect the protein levels of Pacs2 or Chop (**Figure 15 A&B**).

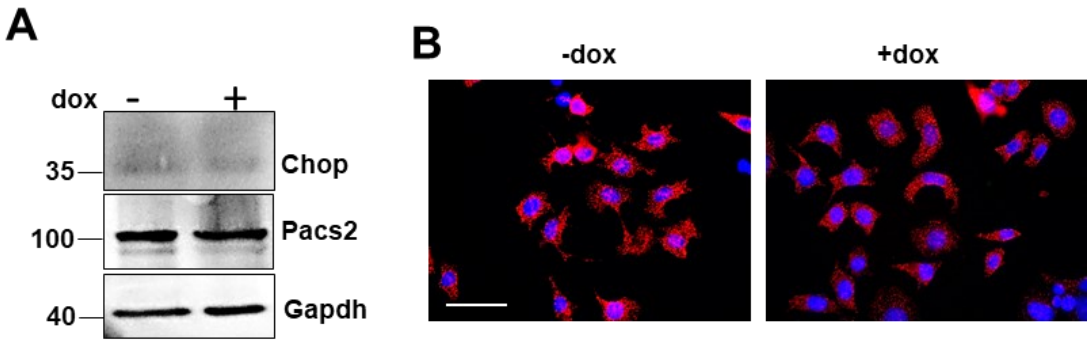

Figure 15 dox treatment has no effect on ER-mitochondrial contacts

A. Immunoblot analysis of Pacs2 in total cell lysates of healthy MLE12 cells with or without 1 µg/mL doxycycline. **B.** Proximity ligation assay of MLE12 cells – or + dox treatment with antibodies against Calnexin and VDAC1 followed by fluorescence microscopy, scale bar = 60 µm.

5.2 Regulation of MAM proteins in lung tissues of *Chop* overexpressing mice

Our group has recently identified that conditional overexpression of *Chop* in the AECII of mice results in the apoptosis of this cell type, creating a pro-fibrotic microenvironment in the lungs (Unpublished). In view of our data from in vitro *Chop* overexpression we next asked if a decrease in Pacs2 protein is also observed in this *in vivo* mouse model with conditional *Chop* overexpression. Mice were fed with doxycycline for 4 or 56 days, sacrificed using standard protocols and lung tissue homogenates of these mice were used for western blot analysis. As observed *in vitro*, overexpression of Chop resulted in significantly increased protein levels of cleaved caspase 3 already at day 4 that persisted also at day 56 (**Figure 16 A-C**). Pacs2 protein levels, on the other hand, were significantly decreased already at day 4 and also at day 56 post doxycycline treatment (**Figure 16 A&D**).

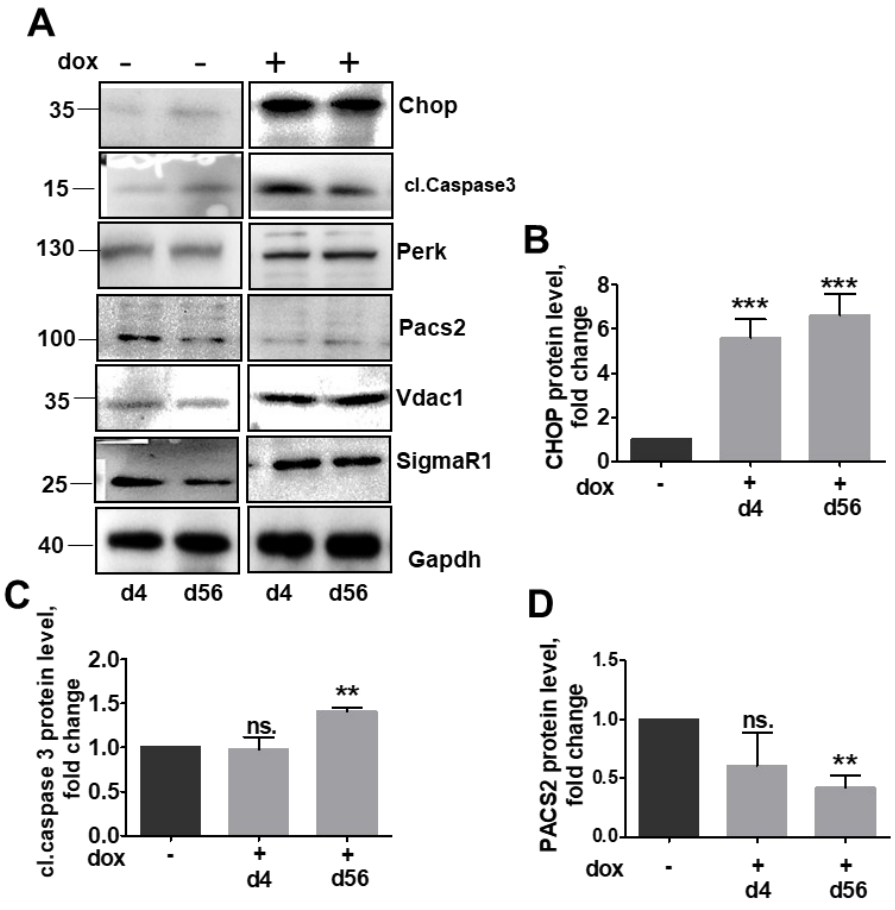

Figure 16 Regulation of MAM proteins in lung tissues of *Chop* mice

A. Chop mice were fed with doxycycline for four or 56 days, followed by sacrificing and tracheotomy. Mice lung tissue was homogenised, followed by Western Blot analysis. **B.-D.** Quantification of cl. caspase 3 (**C**) and Pacs2 (**D**) protein levels upon *Chop* induction **(B)** obtained from (**A**). Relative protein amounts were normalized to Gapdh and their level in control mice was set as one. Statistical significance is indicated as: **p ≤ 0.01, ***p ≤ 0.001, ns.= not significant.

5.3 Pacs2 is required to maintain ER-mitochondrial tethering in cells with Chop induction

Since the Pacs2 protein controls ER-mitochondria communication, we hypothesized that the decreased ER-mitochondrial tethering that was observed in Chop induced cells is a result of decreased Pacs2 protein levels. Hence, to test this, we either overexpressed empty myc or myc tagged *PACS2* in MLE12 cells using Lipofectamin® for four hours followed by 12 h Chop induction (+dox) non-induced (-dox). We then performed proximity ligation assay. As expected, mock and empty myc transfected cells showed lesser proximity of ER to mitochondria, as shown by the quantification of fluorescence intensity in *Chop* induced cells compared to non-induced *Chop* cells **(Figure 17 A&B**). However, in cells transfected with myc-*PACS2*, the fluorescence intensity in Chop induced cells was comparable to the fluorescence intensity observed in non-induced *Chop* cells (**Figure 17 A&B**). This indicated that overexpression of Pacs2 is sufficient to rescue ER-mitochondrial tethering under conditions of Chop induction.

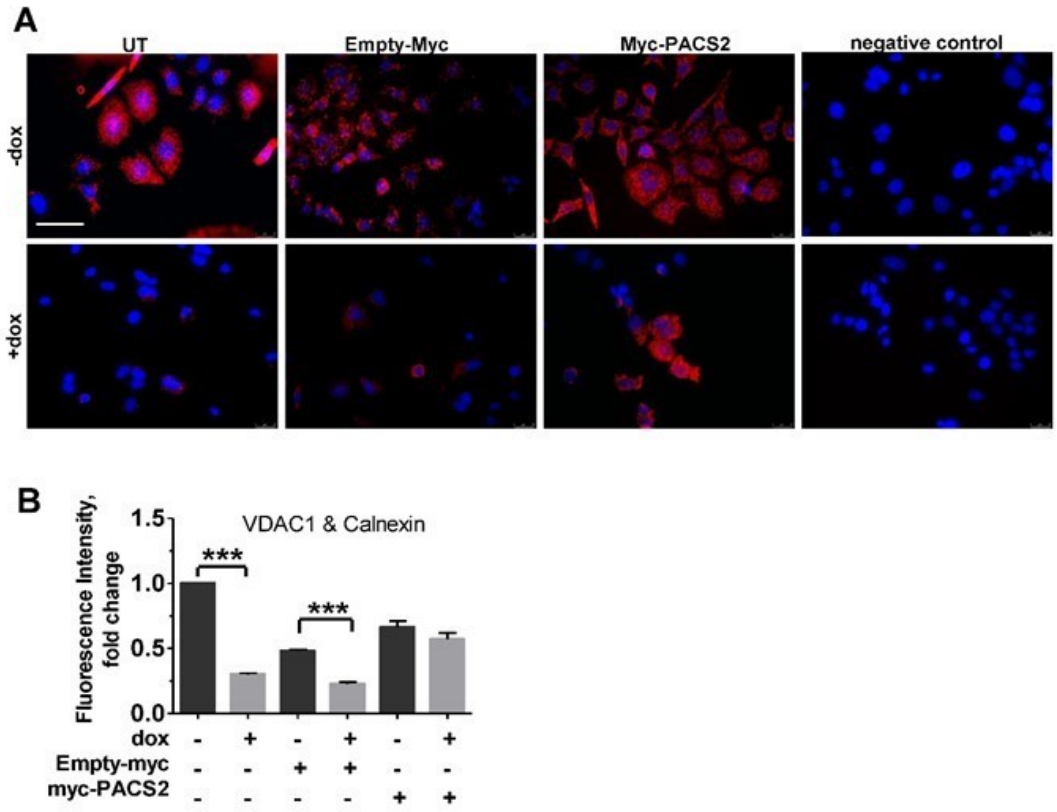

Figure 17 Pacs2 is required to maintain ER-mito tethering in Chop cells

A. MLE12 Chop cells were either mock transfected, or transfected with empty-Myc or Myc-PACS2 for 4 h followed by no dox (-dox) or with dox (+dox, 12 hours) treatment for *Chop* overexpression followed by proximity ligation assay with antibodies against Calnexin and VDAC1 followed by fluorescence microscopy, scale bar = 60 µm. **B.** Fluorescence intensity was quantified using ImageJ, its intensity in untreated -dox cells was set to one. Statistical significance is indicated as: ***p ≤ 0.001

We next analyzed if such Pacs2 overexpression may rescue Chop induced apoptosis. For this, we performed western blots for cleaved caspase3 after overexpressing empty-myc or myc-PACS2 in Chop induced cells [Simmen, T. et al. 2005, Werneburg, N.W. et al. 2012]. As expected, *Chop* induced cells with *PACS2* overexpression displayed a decrease in the terminal apoptosis marker cleaved caspase 3 as compared to Chop induced cells without *PACS2* overexpression (**Figure 18 A&B**). This result indicated improved cell viability due to *PACS2* overexpression under conditions of *Chop* induction.

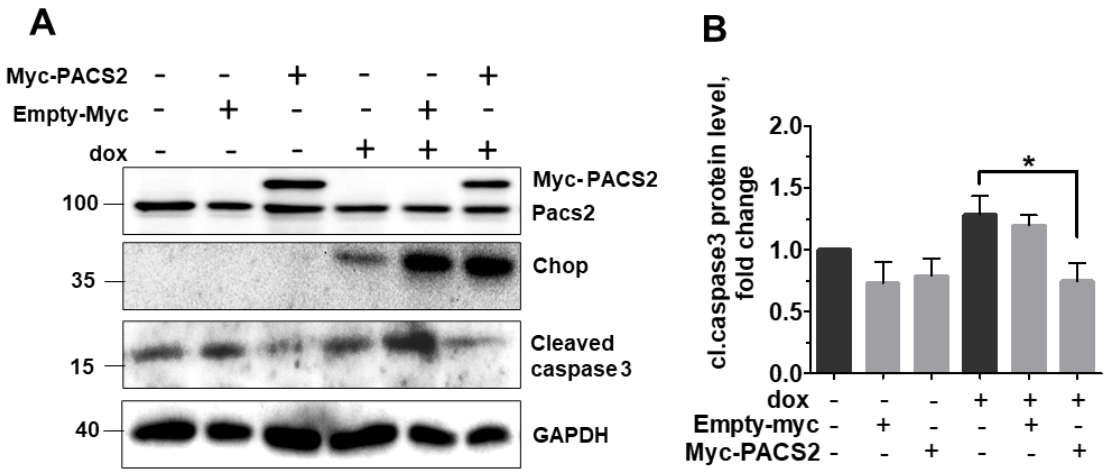

Figure 18 Pacs2 overexpression decrease cl. caspase 3 protein level in Chop cells

A. MLE12 Chop cells were either mock transfected, or transfected with empty myc or Myc-*PACS2* for 4 h followed by no dox (-dox) or with dox (+dox, 12 hours) treatment for Chop overexpression followed by immunoblots for the indicated proteins. **B.** Relative protein levels of cleaved caspase 3 protein level (**C**) were normalized to Gapdh and their level in -dox cells was set as one. Statistical significance is indicated as: *$p \leq 0.05$

5.3.1 Pacs2 is not degraded via the proteasome

Information about drugs that may interfere with Pacs2 protein expression or its signaling is not available till date. It is, however, known that Pacs2 may be ubiquitinated by cellular inhibitor of apoptosis (cIAP1/2) and therefore may be degraded via the proteasome. The cellular levels of cIAP 1/2 are inversely correlated with apoptosis [Guicciardi, M.E. et al. 2014]. Hence, we hypothesized that reduced Pacs2 in cells with Chop overexpression is a result of an increase in cIAP1/2 protein level. We therefore analyzed cIAP 1/2 protein levels in response to *Chop* overexpression but their protein level did not change in Chop induced cells as compared to non-*Chop* induced cells (**Figure 19 A&B**).

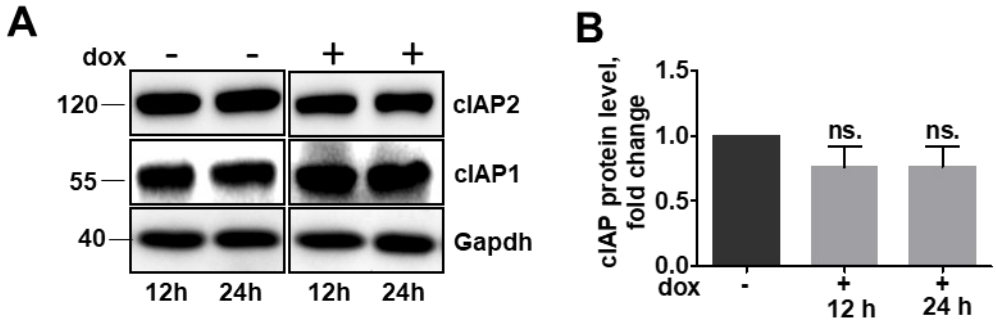

Figure 19 cIAP protein is not affected upon Chop overexpression

A. Immunoblot analysis in total cell lysates of MLE12 Chop cells either untreated or treated with dox for *Chop* expression for 12 and 24 hours for ciAP1/2. **B.** Densitometry analysis of ciAP normalized to Gapdh and their mean value in uninduced controls was set as one. Statistical significance is indicated as ns.= not significant.

Furthermore, treatment with the proteasome inhibitor MG132 did also not affect Pacs2 protein under conditions of Chop induction, indicating that it is not degraded via the proteasome. The Pacs2 protein level is not accumulated upon proteasome inhibition in Chop context (**Figure 20 A&B**).

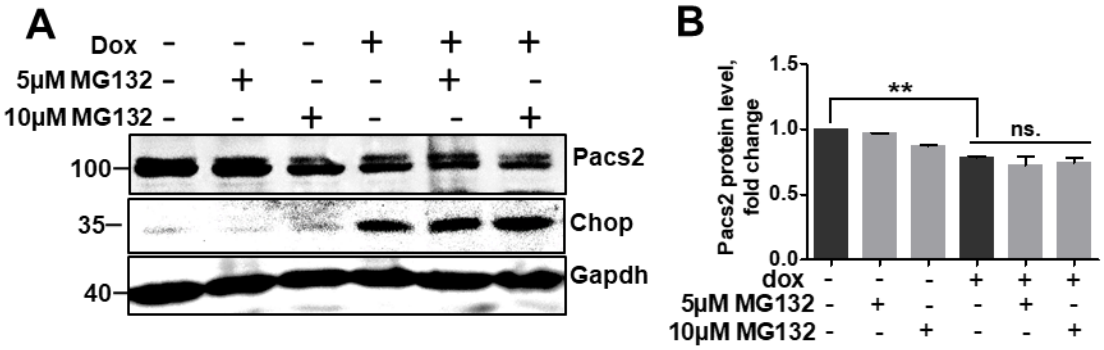

Figure 20 MG132 treatment of MLE12 Chop

A. MLE12 Chop were induced with 1 μg/mL doxycycline for 24h or not induced followed by treatment with 5 μM or 10 μM MG132 for 4 h followed by western blot analysis. Densitometry analysis of Pacs2 normalized to Gapdh and the mean value in uninduced controls was set as one. Statistical significance is indicated as**p ≤ 0.01 and ns.= not significant.

Both the WT PACS2 and a *de novo* missense variant of PACS2, p-Glu209Lys, were shown to interact with transient receptor potential vanilloid 1 (TRPV1), a ligand gated ion channel, suggesting that the interaction of the PACS2 missense variant with TRPV1 may indirectly contribute towards channelopathies [Olson, H.E. et al. 2018]. Members of TRP ion channel family have been shown to mediate cellular Ca^{2+} homeostasis, initiate ER stress and stimulate UPR and apoptosis, or autophagic survival in cells [Amantini, C. et al. 2017, Sukumaran, P. et al. 2016]. The activation of TRPV1 causes a Ca^{2+} and Na^{+} influx, with a higher selectivity for Ca^{2+} over Na^{+}, and is expressed at both, the ER membrane as well as in the plasma membrane.Trpv1 has a strong correlation to ER stress due to its expression on the ER membrane [Castro, J. et al. 2009]. These findings supported our assumption that PACS2 and TRPV1 are influenced by each other, and that imbalance in their interaction could lead to maladaptive ER stress. We hence asked if protein levels of Trpv1 are altered upon Chop induction. For this, MLE12 Chop cells were either not induced or induced with doxycycline for *Chop* expression for 12 and 24 hours, followed by western blots analysis. A significant decrease in Trpv1 was indeed noted in Chop induced cells (**Figure 21 A&B**). Supporting our observation, a study by Wang et al. have demonstrated that Trpv1 antagonist DWP05195 induces apoptosis through Chop pathway in human ovarian cancer cells [Wang, Y.-Y. et al. 2020]. Based on these findings it is possible that reduction of Trpv1 by Chop promotes apoptosis in our system.

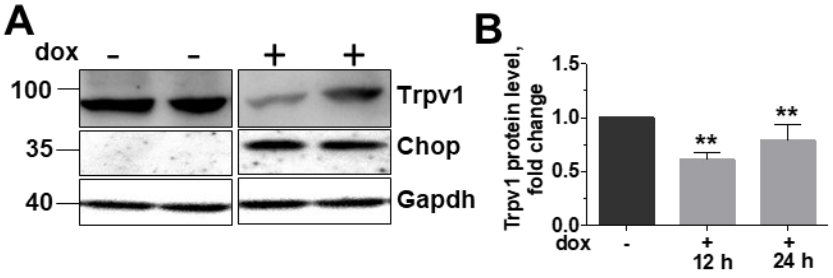

Figure 21 Trpv1 is altered in Chop overexpression

A. Immunoblot analysis in total cell lysates of MLE12 Chop cells either untreated or treated with dox for *Chop* expression for 12 and 24 hours for Trpv1. **B.** Densitometry analysis of Trpv1 normalized to Gapdh and their mean value in uninduced controls was set as one. Statistical significance is indicated as: **$p \leq 0.01$.

5.3.2 Pacs2 directly interact with Trpv1

It has been shown that Trpv1 and Pacs2 interact with each other in other cell types. We hence asked if such interaction may also be found in general in MLE12 cells, the background cell type for Chop induction. We hence performed immunoprecipitation experiments. For this, MLE12 cells were transfected with either empty myc or myc-*PACS2* followed by Co-IP with anti-myc antibody (**Figure 22**). Western Blot analysis verified a direct interaction of Pacs2 (myc-*PACS2*) with Trpv1 by pulling down myc-*PACS2*. Pulldown of empty myc did not forward any detectable Trpv1. This Co-IP further gave a hint towards the hypothesis that regulation of ER-mitochondria tethering may be affected by a Pacs2-Trpv1 interaction.

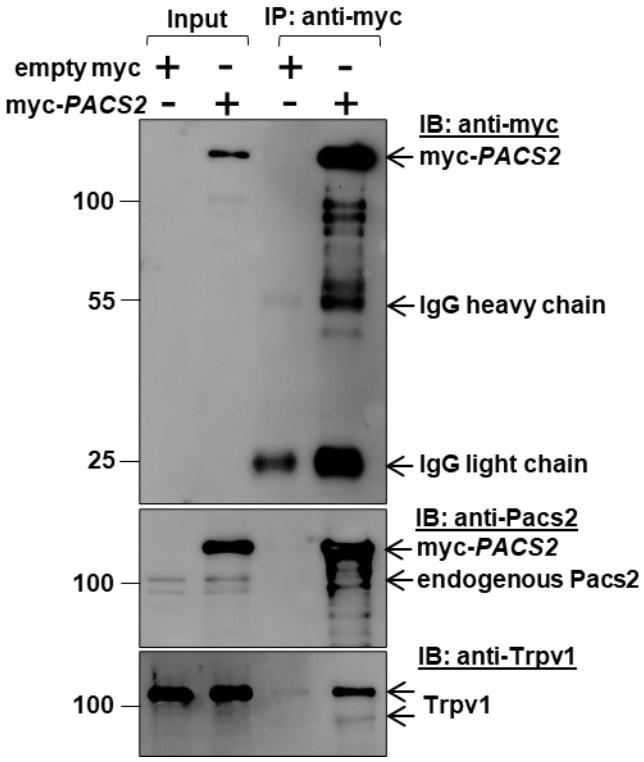

Figure 22 Pacs2 directly interacts with Trpv1

MLE12 were transfected with empty myc or myc-*PACS2*, followed by Co-IP with anti-myc. Western blot analysis with given antibodies.

5.3.3 Modulating the Pacs2-Trpv1 axis rescues Chop induced cells from apoptosis and ER-mitochondrial tethering

In accordance with the observation that Trpv1 and Pacs2 are interacting partners, we hypothesized that modulation of Trpv1 may influence Pacs2 protein levels as well. Vanilloids like capsaicin (CPS), a natural alkaloid and analgesic found in chili peppers, is a highly selective agonist of Trpv1 with nanomolar affinity. Upon exposure to CPS, Trpv1 receptors might undergo phosphorylation processes and contribute to its activation and increased protein levels [Yang, F. et al. 2017]. Cells overexpressing *Chop* were treated with 5, 10 and 25 µM CPS for 8 hours after *Chop* induction or non-induction for 12 h in order to investigate the effect of activated Trpv1 on Pacs2 in ER stress conditions. Non-toxic concentrations of CPS, as determined by LDH assay (**Figure 23 A),** were investigated. In cells with no dox treatment, CPS treatment did not show any significant differences in Trpv1 levels as compared to DMSO treatment. However, in dox treated and *Chop* induced cells a significant increase in Trpv1 protein levels was observed (**Figure 23 B&C**). Interestingly, CPS treatment also resulted in an increase in Pacs2

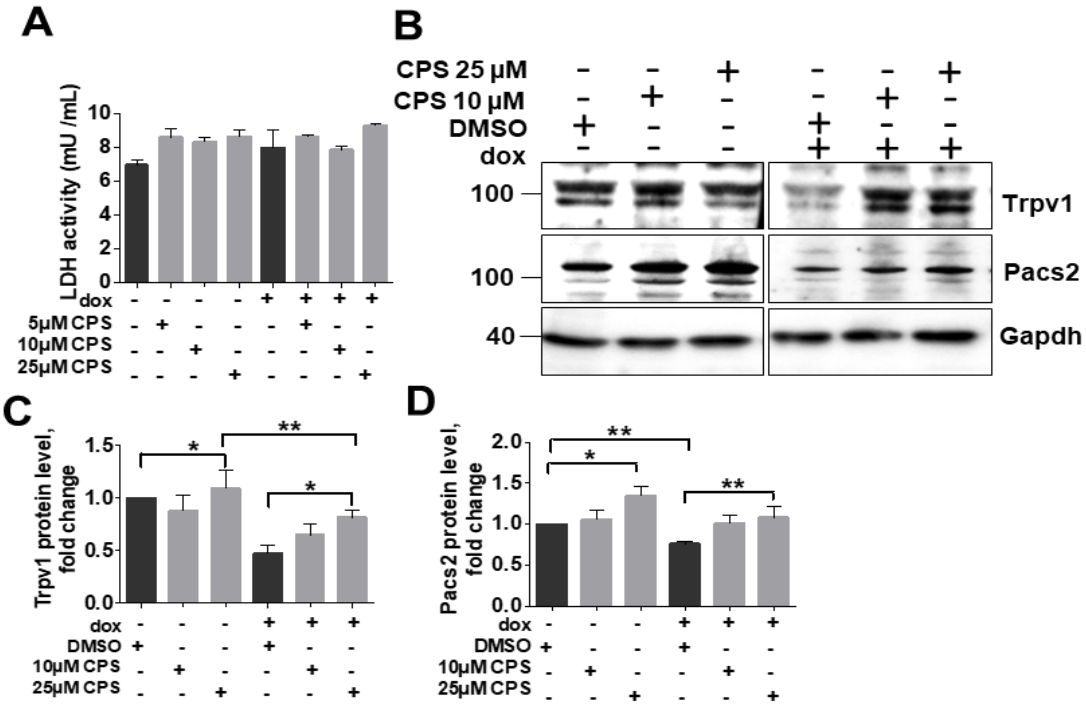

Figure 23 Capsaicin modulates Pacs2-Trpv1 axis

A. Quantification of LDH assay of MLE12 cells overexpressing Chop followed by treatments with different CPS concentrations (5 µM,10 µM, 25 µM). Relative LDH activity were normalized to basal level. **B.** MLE12 Chop cells were either left untreated or treated with dox for 12 h, followed by treatments with DMSO or CPS at indicated concentrations followed by immunoblots for the indicated proteins. **C&D.** Quantification of Trpv1 (**C**) and Pacs2 (**D**) protein expression is shown. Relative protein amounts were normalized to Gapdh and their mean value in respective DMSO treated controls was set as one. Analysis from n=3 independent experiments are shown. P values were not significant between the groups. Statistical significance is indicated as: *p ≤ 0.05, **p ≤ 0.01.

protein levels in Chop induced cells. This effect of CPS treatment on Pacs2 is also observed in non-*Chop* induced cells (**Figure 23 B&D**).

Likewise, PLA was performed in order to investigate if exposure to CPS can improve ER-Mitochondria tethering. As expected, treatment with Trpv1 agonist 25 µM CPS led to a significant improvement in ER-mitochondrial contacts. *Chop* overexpressing cells treated with 25µM CPS displayed similar punctae compared to non-*Chop* induced MLE12 (**Figure 24 A&B**).

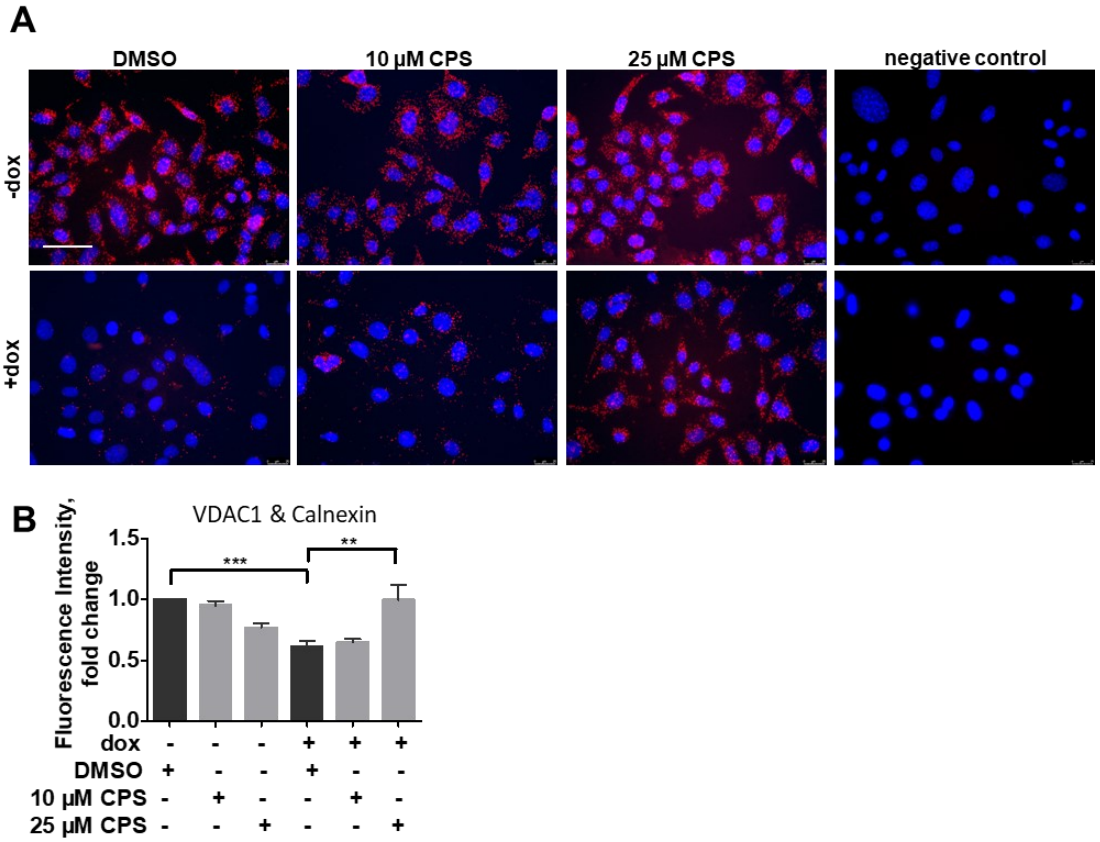

Figure 24 CPS improves ER-mitochondria tethering in cells with *Chop* induction

A. Representative fluorescence images following proximity ligation assay with antibodies against Calnexin and VDAC1, cells treated with CPS at the indicated concentrations or DMSO upon Chop induction are shown, scale bar = 60 µm. **B.** Fluorescence intensity was quantified using ImageJ, its intensity in –dox, DMSO treated cells was set to one. 'n' of three independent experiments were performed and statistical significance is indicated as: $^{**}p \leq 0.01$, $^{***}p \leq 0.001$.

5.4 Regulation of ER-mitochondria tethering in SP-C mutant cells

5.4.1 ER-mitochondria tethering in cells overexpressing SP-C$^{\Delta exon4}$

Until now, we observed a reduced ER-mitochondrial tethering under ER stress situation induced by Chop overexpression. We next asked if any pathological ER stress induction could also result in a decreased ER-mitochondrial tethering. It has been well-documented that overexpression of *SP-C$^{\Delta exon4}$* both, *in vitro* in human embryonic kidney (HEK) cells and in mice *in vivo*, results in ER stress. In humans, a heterozygous mutation of A to G in the first base of intron 4 of the human SP-C gene (c.460+1A>G) results in the absence of mature SP-C protein [Wang, W.-J. et al. 2003]. The underlying reason is a spliced deletion of exon 4 resulting in the removal of the conserved cysteine in the C-terminal flanking propeptide, which leads to the generation of a misfolded SP-C protein, with toxic gain of function. Patients with such a mutation are reported to develop familial interstitial lung disease [Mulugeta, S. et al. 2005]. *In vitro*, overexpression of *SP-C$^{\Delta exon4}$* results in ER stress and caspase 4 mediated apoptosis in AECII like cell lines (A549, MLE12) [Beers, M.F. et al. 1998, Mulugeta, S. et al. 2007]. Hence in order to investigate, if the decrease in ER-mitochondrial tethering is a result of an increased CHOP protein or if it may be due to pathological increase in ER stress, like overexpression of *SP-C$^{\Delta exon4}$*, human melanoma cell lines (MEL188) were stably overexpressed for wild type (WT) surfactant protein C (SP-C^{WT}) or the pathological mutation in the exon 4 region of human SP-C (SP-C$^{\Delta exon4}$) by Gene Splicing by Overlap Extension (SOEing). For generating SP-C$^{\Delta exon4}$, deletion of exon 4 from *SP-C^{WT}* was achieved by overlap extension PCR. First, exons 1-3 were amplified by single PCR and next, exon 5 was amplified through the 3' untranslated Poly A tail using a forward primer containing complete overlap with the 3' end of the reverse primer used to amplify exon 3. These two overlapping primary products were then fused together in a SOEing PCR (**Figure 25 A**). Either the *SP-C^{WT}* or the *SP-C$^{\Delta exon4}$* plasmid was stably transfected in MEL188. MEL188 cell line have human origin, possess lamellar bodies and express the 21 kDa pro SP-C protein on mRNA level. Like MLE12 cells, these cells also do not cleave SP-C to its mature form. Stable transfection using these plasmids were performed and positive colonies were screened using routine selection procedure, as described in the methods section. For verification of stable transfection semi-quantitative PCR was performed using given primers and compared to expression of β-actin **(Figure 25 B**). Additionally, western blot for stably transfected cells for GFP and SP-C was performed (**Figure 26 A**).

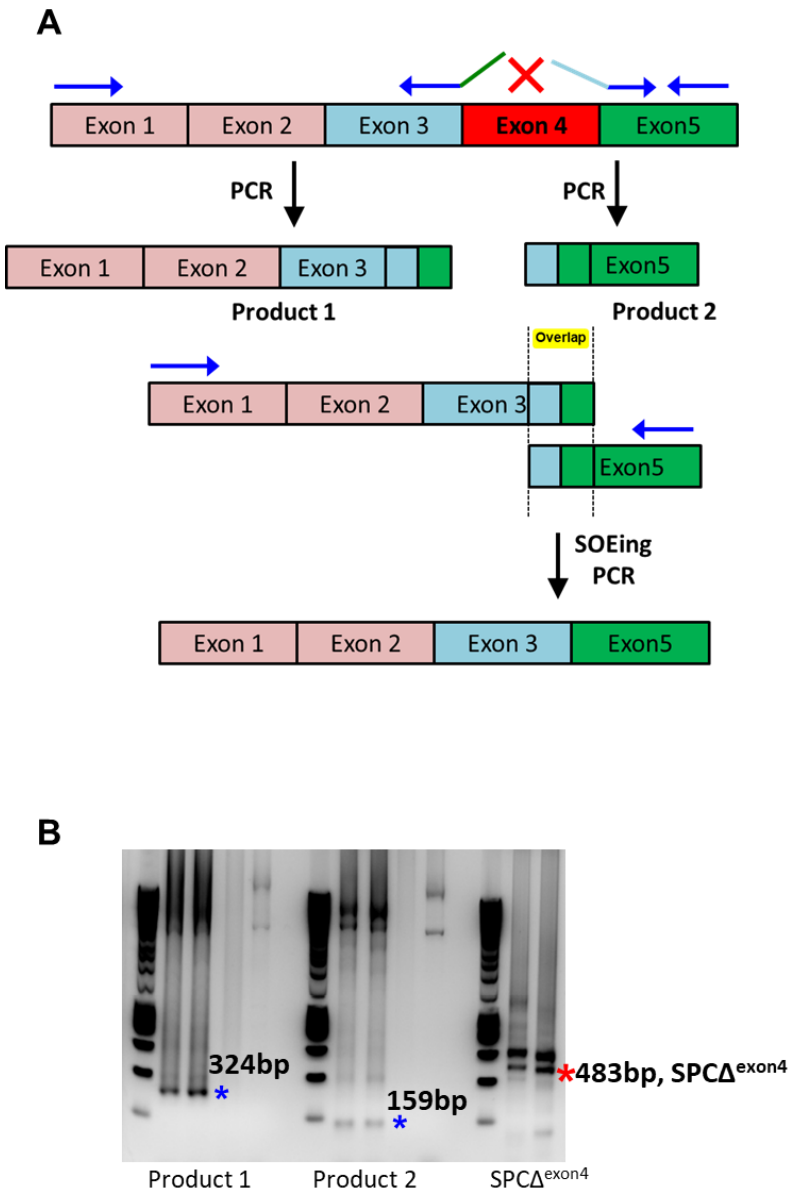

Figure 25 SOEing PCR for generation of SP-C$^{\Delta exon4}$ engineered cell lines

A. For generating of SP-C$^{\Delta exon4}$, deletion of exon 4 from SP-C^{WT} was achieved by overlap extension PCR. First exons 1-3 were amplified by single PCR and next exon 5 was amplified through the 3' untranslated Poly A tail using a forward primer containing complete overlap with the 3' end of the reverse primer used to amplify exon 3. These two overlapping primary products were then fused together in a SOEing PCR. **B.** Agarose gel picture showing Product 1 (324 bp) and Product 2 (159 bp) and the fused product (483 bp) resulting in *SP-C$^{\Delta exon4}$*.

An increase in CHOP protein in cells overexpressing *SP-C$^{\Delta exon4}$* as compared to control cells or *SP-C^{WT}* overexpressing cells compared to controls was observed, indicating an increased ER stress in these cells (**Figure 26 A&B**). Similar to our observation in Chop induced cells, cells overexpressing *SP-C$^{\Delta exon4}$* also showed a significant reduction in PACS2 protein levels (**Figure 26 A&C**). These data collectively imply for a decreased PACS2 expression in ER stress conditions. However, in contrast to MEL12 cells with Chop induction, TRPV1 protein level in *SP-C$^{\Delta exon4}$* stably transfected MEL188 cells is increased in comparison to non-transfected or stably transfected *SP-C^{WT}* MEL188 cells (**Figure 26 A&D)**. This result is in line with a previous study by Guo et al., who demonstrated an increase in TRPV1 staining as well as its mRNA in bleomycin induced lung injury in a guinea pig model [Guo, Y. et al. 2019].

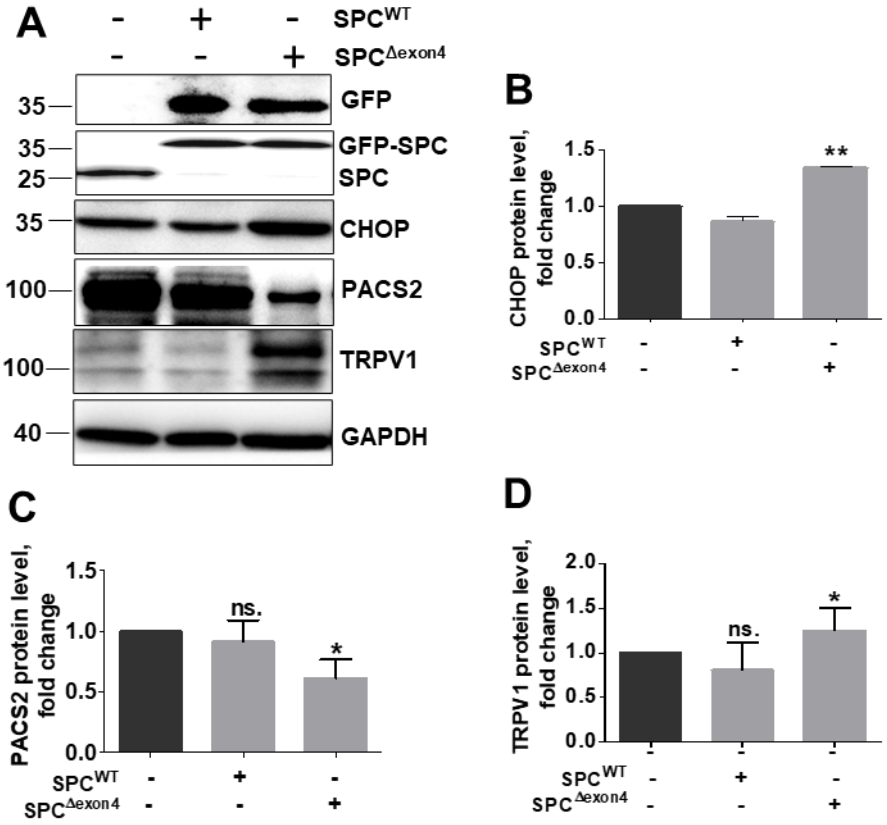

Figure 26 PACS2 protein levels in *SP-C$^{\Delta exon4}$* cells

A. MEL188 cells were stably transfected with either SP-C^{WT} or SP-C$^{\Delta exon4}$ plasmids or left un-transfected, followed by immunoblots for the given proteins. **B.-D**. Quantification of CHOP (**B**), PACS2 (**C**) and TRPV1 (**D**) proteins levels are shown. Relative protein amounts were normalized to GAPDH and their mean value in untransfected cells was set as one. Statistical significance is indicated as: *p ≤ 0.05, **p ≤ 0.01, ns.= not significant.

Next, we performed a PLA assay again and observed that ER-mitochondrial tethering was disrupted in *SP-C$^{\Delta exon4}$* stably transfected MEL188 cells in a similar manner as in *Chop* overexpressing MLE12 cells (**Figure 27 A&B**). These analyses reaffirm that altered PACS2 and TRPV1 protein levels caused disrupted ER-mitochondria tethering under ER stress conditions as well as in SP-C mutant MEL188 cells. Therefore, it validates the hypothesis that disrupted ER-mitochondria tethering is caused by altered PACS2 protein level under ER-stress conditions.

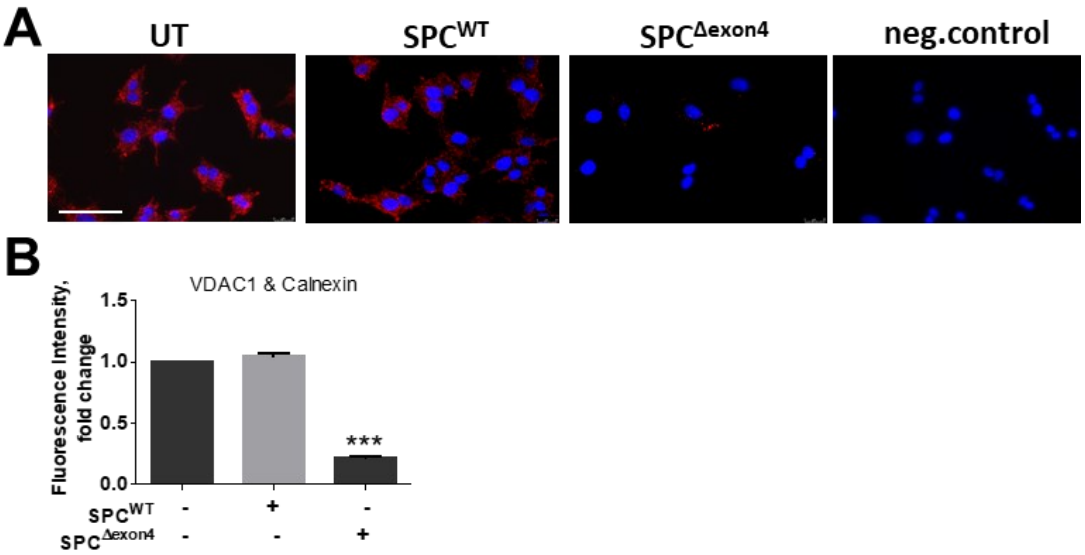

Figure 27 Unpaired ER-mitochondrial tethering in *SP-C$^{\Delta exon4}$* cells

A. Representative fluorescence microscopy images following proximity ligation assay with antibodies against Calnexin and VDAC1 in SP-C^{WT} or SP-C$^{\Delta exon4}$ overexpressing cells, scale bar = 60 µm. **B.** Fluorescence intensity was quantified using ImageJ, its intensity in untransfected cells was set to one and statistical significance is indicated as: ***$p \leq 0.01$

5.4.2 CPS rescues ER-mitochondrial tethering in SP-C$^{\Delta exon4}$ MEL188 cells

Since we observed a beneficial effect upon CPS treatment in cells with Chop induction, we also treated the *SP-C^{WT}* and *SP-C$^{\Delta exon4}$* cells with CPS. Like in *Chop* overexpressing cells, treatment of *SP-C$^{\Delta exon4}$* cells with CPS also resulted in an increase in PACS2 protein levels (**Figure 28 A&B**). Interestingly, results of western blot analysis for TRPV1 protein level showed a significantly decrease in *SP-C$^{\Delta exon4}$* stably transfected MEL188 under CPS treatment, even lower than in control (**Figure 28 A&C**). The protein level of cleaved PARP1 as an apoptotic marker has not been changed under CPS treatment so far.

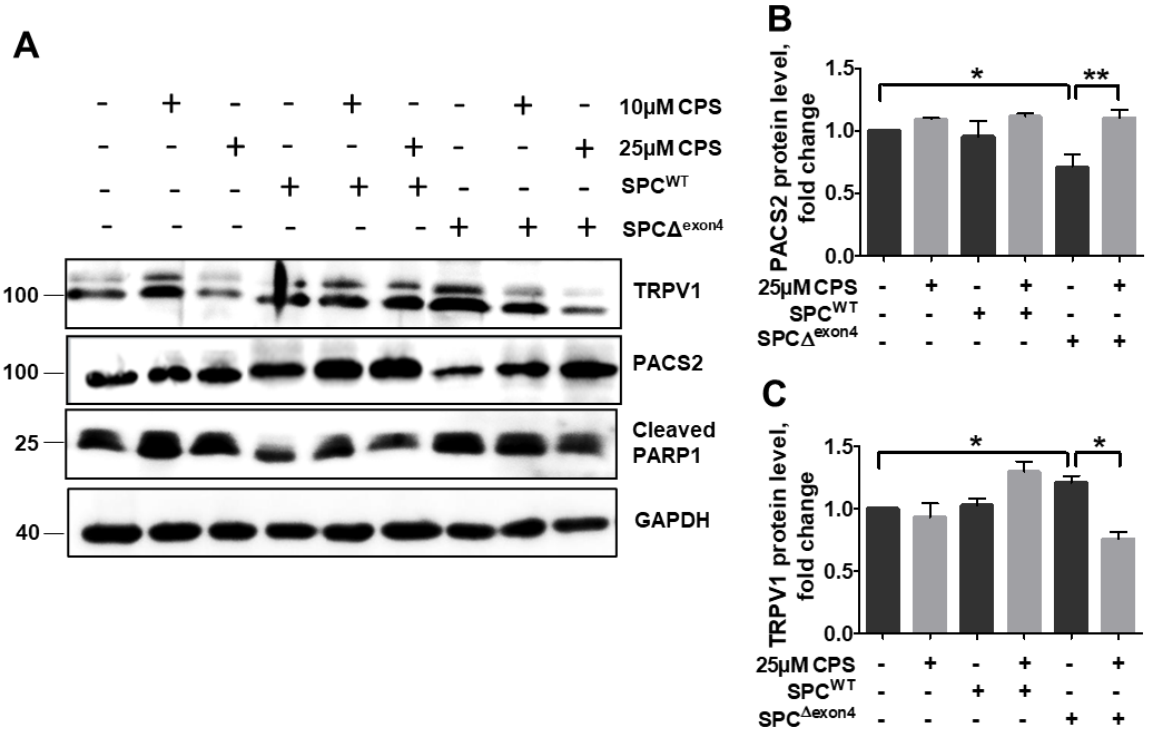

Figure 28 Modulation of TRPV1 in *SP-C$^{\Delta exon4}$* cells by CPS treatment

A. Cells stably expressing SP-C^{WT} or SP-C$^{\Delta exon4}$ or control cells were treated with DMSO or CPS, followed by immunoblotting of PACS2 and TRPV1. **B.,C.** Quantification of PACS2 (**B**) and TRPV1 (**C**) is shown. Relative protein amounts were normalized to GAPDH and its mean value in control cells was set as one. Statistical significance is indicated as: *p ≤ 0.05, **p ≤ 0.01.

To further verify whether increased PACS2 protein level improves ER-mitochondria tethering, PLA was performed, displaying tighter connection between ER and mitochondria under CPS treatment in all three settings. In the same line, ER-mitochondrial contacts increased under 25 µM CPS treatment in *SP-C$^{\Delta exon4}$* stably transfected MEL188 cells, as compared to DMSO treated cells (**Figure 29 A&B**). Cells overexpressing *SP-C^{WT}* did not show any differences in TRPV1 or PACS2 protein levels, nor did they exhibit any decrease in ER-mitochondrial tethering. Results until this point indicated that both CHOP induction as well as pathological ER stress induction, resulted in decreased protein levels of PACS2 and a decrease in ER-mitochondrial contacts. The TRPV1 modulating drug CPS reversed these effects. These unsuspected results with regard to TRPV1 protein levels led to the assumption that TRPV1 activation by CPS may balance dysregulated TRPV1 protein levels in a way that it can interact with PACS2 properly. Even so the TRPV1 protein level is decreased under CPS treatment, the PACS2 protein level is increased and improves ER-mitochondrial tethering in *SP-C$^{\Delta exon4}$*.

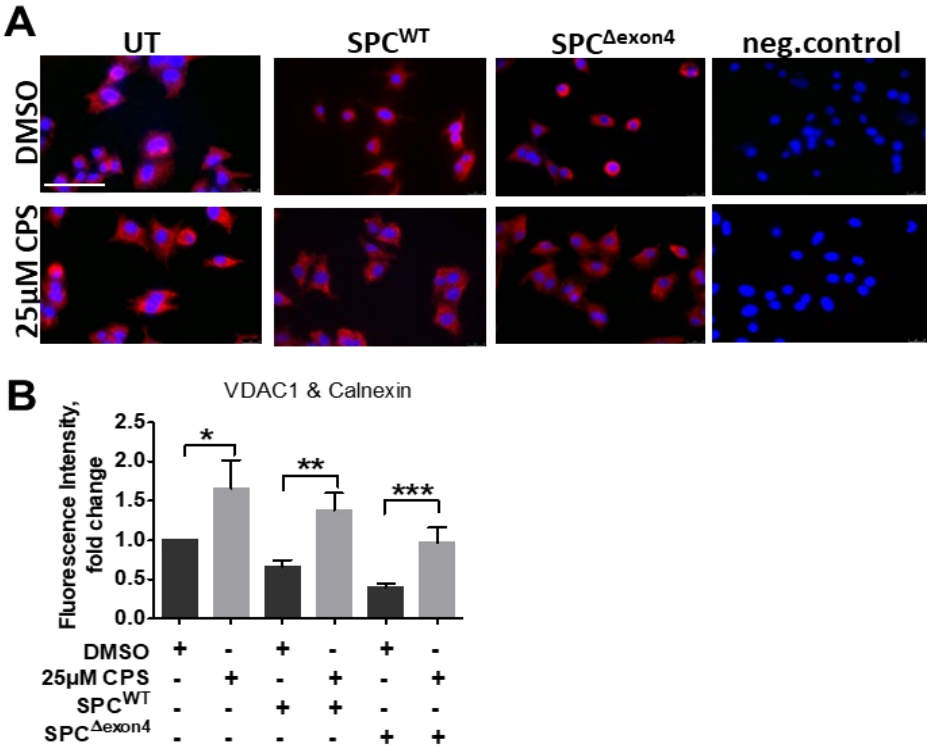

Figure 29 Modulating TRPV1 rescues ER-mitochondrial tethering in cells overexpressing *SP-C$^{\Delta exon4}$* overexpression

A. Fluorescence microscopy images following proximity ligation assay with antibodies against Calnexin and VDAC1 in control cells or in cells overexpressing SP-C^{WT} or SP-C$^{\Delta exon4}$, followed by DMSO or CPS treatments at the indicated doses, scale bar = 60 µm. **B.** Fluorescence intensity was quantified using ImageJ, its intensity in untreated control cells was set as one. 'n' of three independent experiments were performed and statistical significance is indicated as: *p ≤ 0.05, **p ≤ 0.01, ***p ≤ 0.001.

5.5 Regulation of ER-mitochondria interaction in IPF patients

5.5.1 PACS2 protein and ER-mitochondrial tethering are decreased in IPF AECII

In order to further understand the ER-mitochondrial tethering under clinical situation, MAM proteins in IPF as compared to healthy donor lungs were analyzed. ER stress is a well-documented pathomechanistic feature of IPF and an upregulation of ER stress signature molecules, namely ATF6, ATF4, BiP and CHOP in the AECII of IPF patients was reported by us and by others [Bertolotti, A. et al. 2000, Günther, A. et al. 2012, Korfei, M. et al. 2008, Lawson, W.E. et al. 2008, Schröder, M. et al. 2005, Zhang, L. et al. 2017].

The findings of this study showing an important role of PACS2 in maintaining ER-mitochondrial tethering under ER stress conditions let us hypothesize that PACS2 is altered in the AECII of IPF patients, thereby altering ER-mitochondrial contacts. To test this, we first analyzed the protein levels of the MAM proteins namely PACS2, SigmaR1 and IP3R3 as well as the cation channel TRPV1 in total lung homogenates of IPF versus donors. In coherence with our previous results, PACS2 levels were significantly decreased in IPF lung homogenates in comparison to healthy donor lungs (**Figure 30 A&B**) while protein levels of IP3R3 and SigmaR1 did not alter greatly **(Figure 30 D&E**).

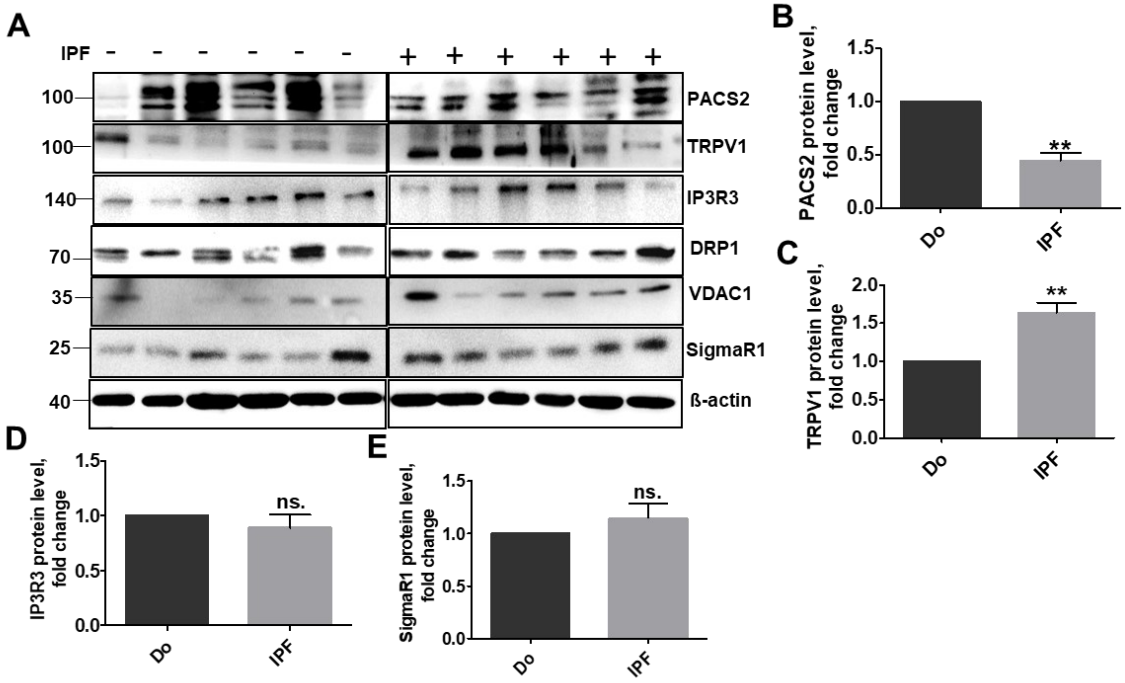

Figure 30 Altered MAM proteins in IPF patients

A. Western blot analysis was performed from IPF and Donor lungs homogenates for the given proteins n=7. **B-E.** Quantification of PACS2 (**B**), TRPV1 (**C**), IP3R3 (**D**) and SigmaR1 (**E**) protein expression is shown. Relative protein amounts were normalized to β-actin and their mean value in Donor was set as one.'n' of seven independent patients' lung were used. Statistical significance is indicated as: ** $p \leq 0.05$, ns.=not significant.

Interestingly, TRPV1 protein levels increased significantly in IPF lung homogenates as compared to those of donors (**Figure 30 A&C**).

Next, in order to study the protein levels of PACS2 in the AECII of IPF patient lungs, we performed immunofluorescence for PACS2 (red) and ABCA3 as ACEII marker (green) on paraffin sections that revealed a decreased PACS2 staining in the AECII of IPF patients (**Figure 31 A&B**), fully supporting the western blot results from IPF and donor lung homogenates.

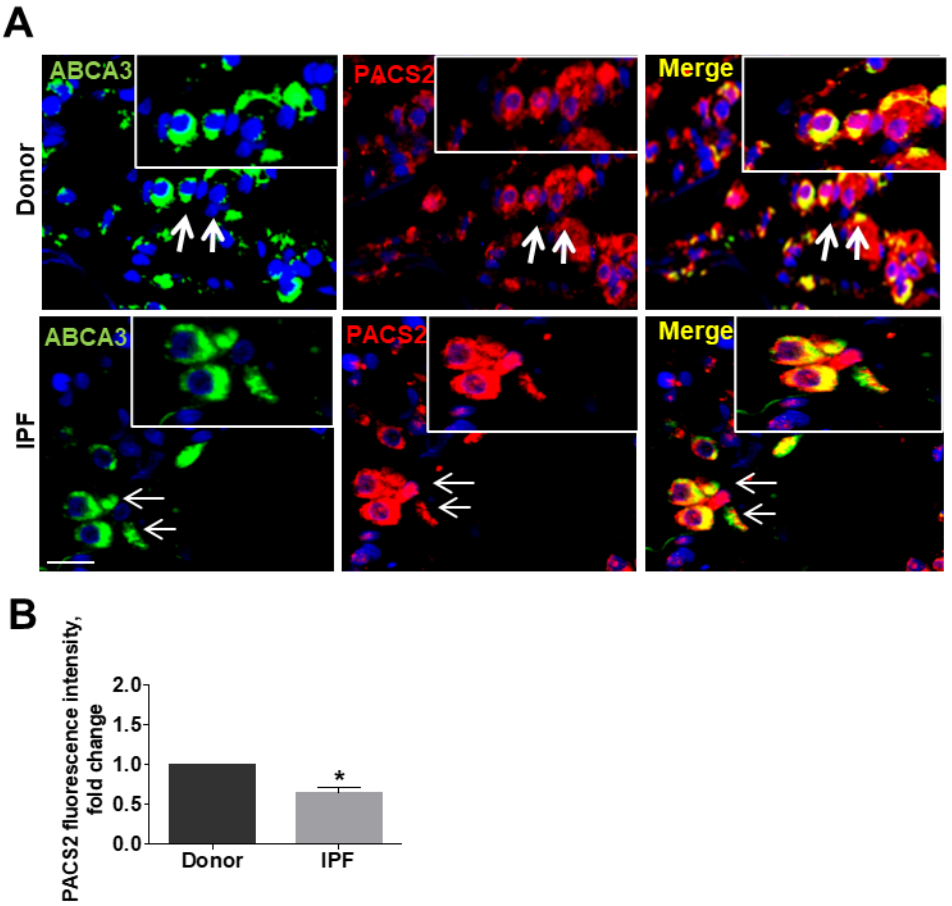

Figure 31 PACS2 is decreased in IPF

A. Representative immunofluorescence images for PACS2 (red) and ABCA3 (green) in IPF and donor lung sections, nuclei were stained with DAPI (blue) scale bar = 25µm. **B.** Fluorescence intensity of PACS2 was quantified using ImageJ, its intensity in donor sections was set as one. Lung sections from 7 IPF and 7 donors were used for staining. Statistical significance is indicated as: * $p \leq 0.5$

In order to understand if the ER-mitochondrial contacts are disturbed in IPF lung AECIIs, we next performed ultrastructural analysis of IPF and donor lungs via electron microscopy. In some areas, the membrane of the ER approached the outer membrane of the mitochondria in a way that there were no ribosomes between them and the membranes were separated from each other by a very thin leaflet of cytosol. In these contact regions the distance between the membranes was only a few nanometers. Based on these considerations the MAMs could be easily identified by ultrastructural criteria. As indicated in **Figure 32**, electron microscopy analysis demonstrated that in IPF AECIIs, the contact zones were more point shaped and the ER appeared to be locally widened. In

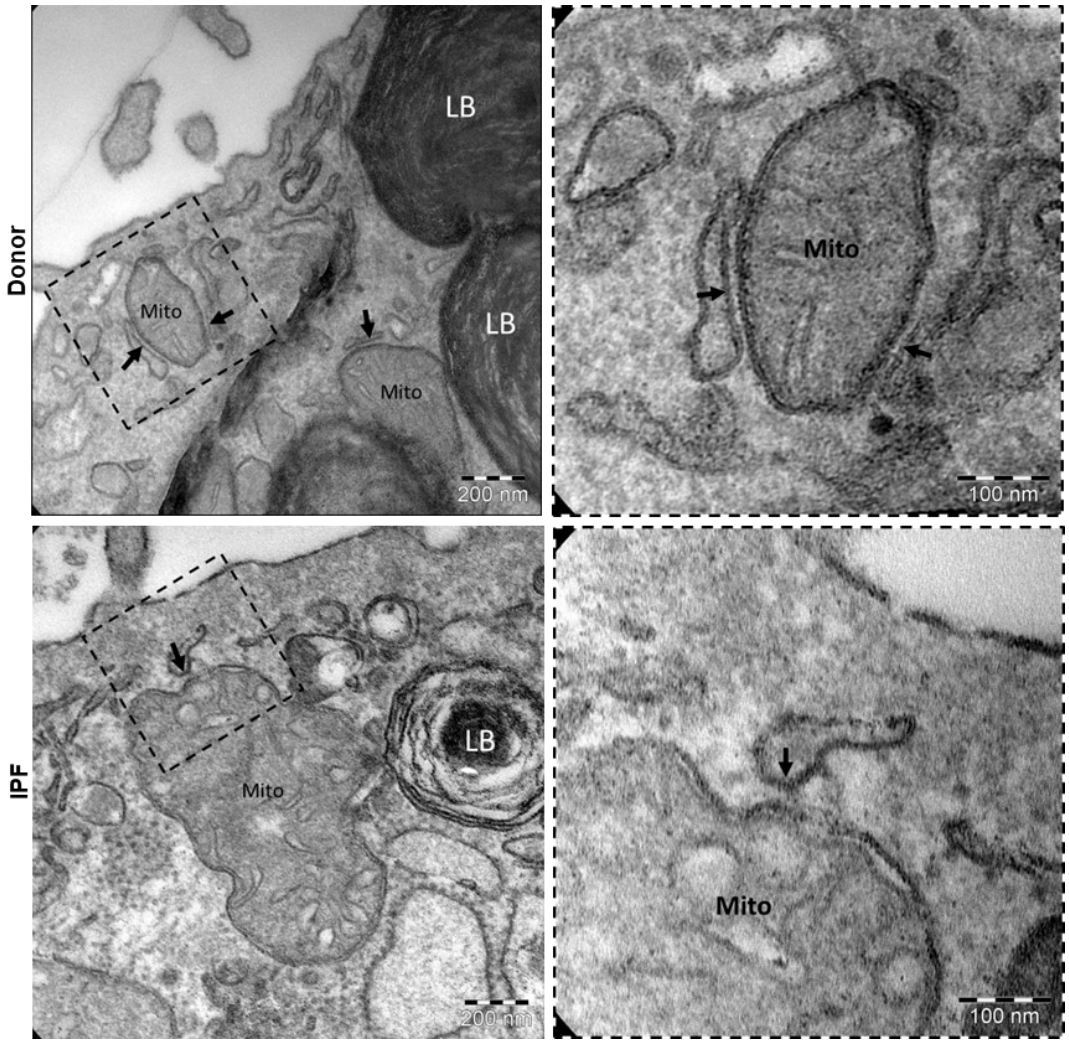

Figure 32 ER-mitochondrial tethering is decreased in IPF

Representative transmission electron microscopic images of alveolar epithelial type II cells (characterized by the presence of lamellar bodies (LB)) are shown. At ultrastructural level the appearance of the contact zones between ER and mitochondria (Mito) in IPF differed from the healthy control. The closest contacts (arrows) appeared to be rather point shaped with the ER piston-like widened in IPF. In healthy controls the contacts were in general elongated and more laminar so that the ER and mitochondrial membranes had a parallel run.

AECII from healthy appearing lung tissue (donors) the contact zones between ER and mitochondria were rather laminar than point shaped and the ER was not widened.

5.5.2 Activation of TRPV1 decreases apoptosis and COLA1A level in IPF PCLS

In order to determine the effect of PACS2-TRPV1 axis modulation in IPF, the 3D precision cut lung slices (PCLS) culture septum from explanted IPF lungs was exploited. IPF PCLS were treated in cell culture with DMSO, 10 or 25 µM CPS or 25 µM Nintedanib followed by immunoblotting or immunofluorescence. Nintedanib (Nin) is a well-known drug for the treatment of IPF [Varone, F. et al. 2018] and is used here for comparison. Western blot data of PCLS confirmed the effect of CPS on PACS2 protein levels: a significant increase in PACS2 protein levels was observed in IPF PCLS treated with 25 µM CPS as compared to DMSO treatment (**Figure 33 A&B**). In addition, a reduction in the apoptosis marker cleaved caspase 3 (**Figure 33 A&C**) was also observed.

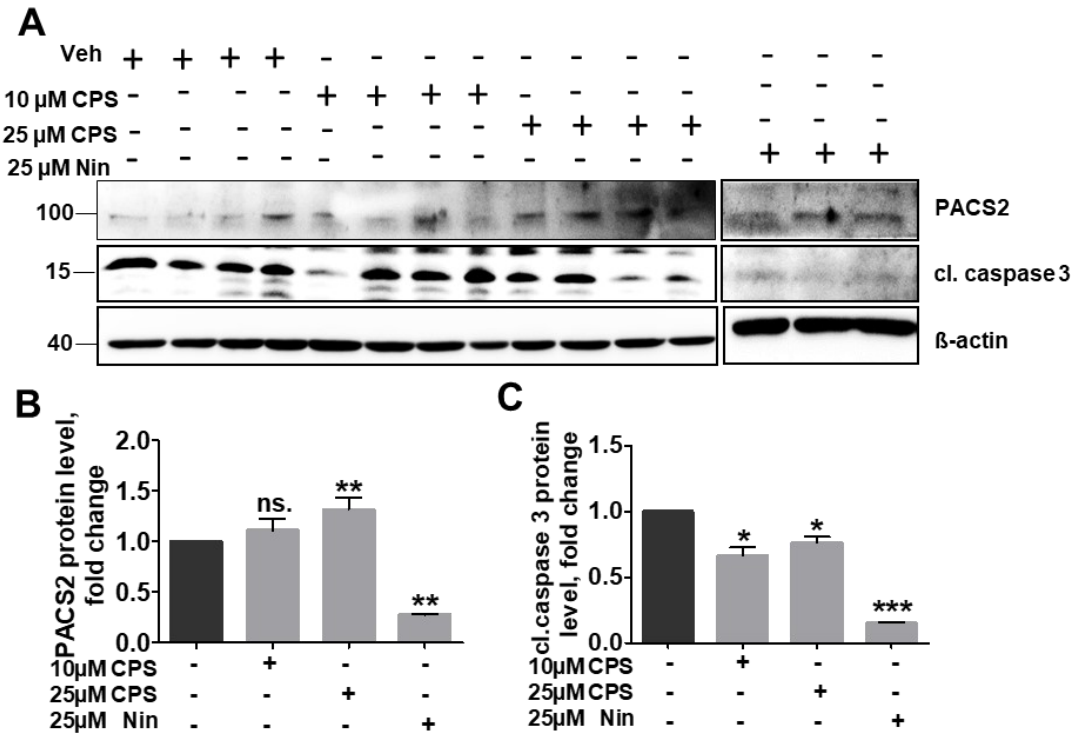

Figure 33 Modulation of TRPV1 by CPS in IPF PCLS

A. PCLS from explanted IPF patient lungs were treated either with DMSO or CPS with the indicated concentrations for 8 h, followed by immunoblot analysis for PACS2, TRPV1, cleaved caspase 3 and β-actin. **B&C.** Quantification of PACS2 (**B**) and cl. caspase3 (**C**) protein levels are shown. Relative protein amounts were normalized to β-actin and their mean value in DMSO treated PCLS was set as one. Statistical significance is indicated as: * p≤ 0.5; **p≤ 0.05, ***p≤ 0.01, ns.= not significant.

In full support, quantification of immunofluorescence stainings for cleaved caspase 3 also showed a decrease in CPS treated PCLS (**Figure 34 A&B**).

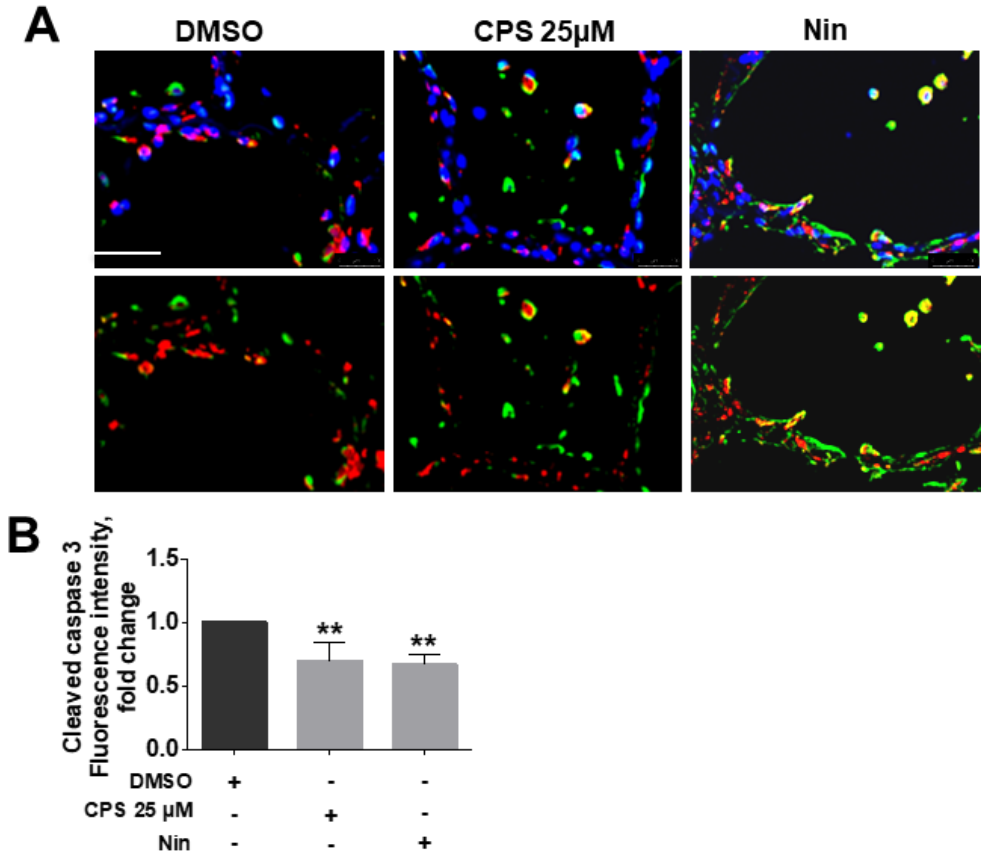

Figure 34 Activation of TRPV1 decreases apoptosis in IPF PCLS

A. Immunofluorescence staining for cl. caspase 3 (red) in AECII (ABCA3, green) on IPF PCLS upon DMSO, CPS or Nin treatment for 8 h. Nuclei were stained with DAPI (blue), scale bar = 60 µm. **B.** Fluorescence intensity of cleaved caspase 3 in ABCA3 positive cells was quantified using ImageJ, its intensity in DMSO treated cells was set as one. Stainings and analysis were performed in PCLS performed from three IPF patients and significance is indicated as: **$p \leq 0.01$

Further, we asked if treatment of IPF PCLS with CPS would have any effect on extracellular matrix protein, collagen1A1 (COL1A1), which is usually higher in IPF tissues due to the excessive deposition of extracellular matrix. Immunofluorescence analysis revealed a significant decrease in COL1A1 (red) in IPF PCLS treated with 25 µM CPS as compared to DMSO treated PCLS (**Figure 35 A&B**). A similar reduction of COL1A1 was observed upon incubation with clinically approved anti-fibrotic drug Nintedanib.

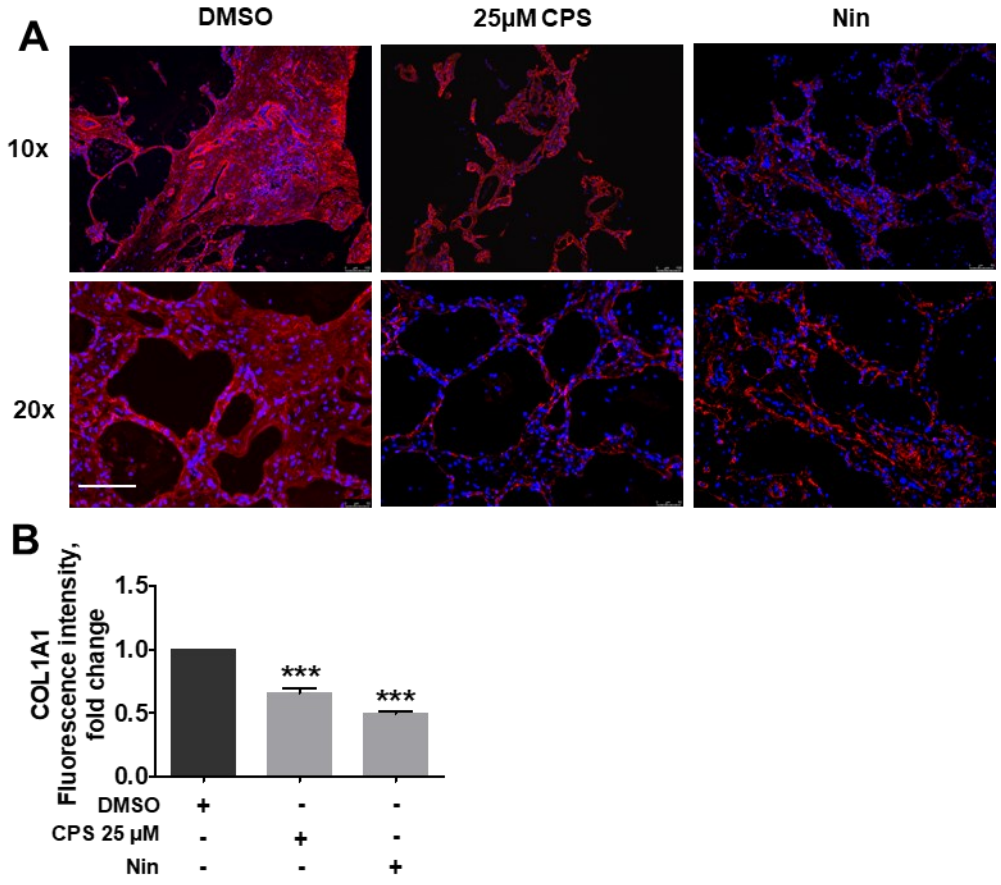

Figure 35 Activation of TRPV1 decreases COLA1A level in IPF PCLS

A. Immunofluorescence staining for COLA1A on IPF PCLS upon Veh, CPS or Nin treatment for 8 h. Nuclei were stained with DAPI (blue), scale bar = 60 µm. **B.** Fluorescence intensity of COLA1A was quantified using ImageJ, its intensity in DMSO treated cells was set as one. Stainings and analysis were performed in PCLS performed from three IPF patients and significance is indicated as: ***$p \leq 0.001$.

5.6 Mitochondrial dysfunction in Chop Cells

ER-mitochondrial miscommunication effect varied cellular functions which may contribute to cell death mechanisms. On the one hand, decreased ER-mitochondrial tethering leads to mitochondrial dysfunction. On the other hand, it may lead to the induction of autophagy, a self-eating mechanism of a cell. In view of our results that revealed decreased ER-mitochondrial tethering under conditions of ER stress, we next performed, the analysis of mitochondrial membrane proteins, PTEN-induced kinase 1 (Pink1) and Parkin. Both these proteins were significantly decreased upon Chop overexpression (**Figure 36 A-C**). It is well-known that Pink1 and Parkin are important mitochondrial proteins that regulate mitophagy, a process of autophagy-lysosome mediated mitochondrial degradation and apoptosis of mitochondria [Gegg, M.E. et al. 2010, Matsuda, N. et al. 2010].

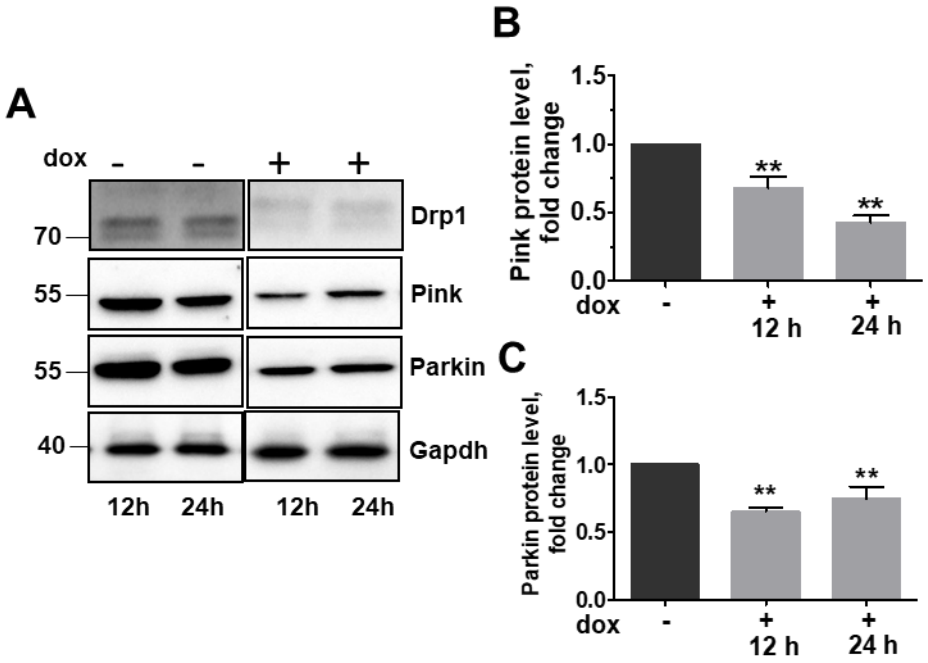

Figure 36 Mitochondria protein upon Chop overexpression

A. MLE12 Chop cells were either not induced or were induced with 1 µg/mL doxycycline for *Chop* expression for 12 and 24 hours, followed by Western blots for the given proteins from total lysate. The positions of molecular weight markers are shown**. B.& C.** Quantification of Pink1 protein levels (**B**) and Parkin protein level (**C**) upon Chop induction. Relative protein amounts were normalized to Gapdh and their level in not induced was set as one. Statistical significance is indicated as: **$p \leq 0.01$

These results give a hint towards an impaired mitochondrial homeostasis upon Chop overexpression. To prove this hypothesis, we next performed immunofluorescence microscopy. MLE12 Chop cells that were treated with doxycycline for 24 h and labelled active mitochondria with Mitotracker® dye (**Figure 37 A**). We observed a significant decrease in Mitotracker® labelling, in *Chop* overexpressing MLE12 cells (**Figure 37 B**). All together this confirms that mitochondrial homeostasis is impaired upon *Chop* overexpression.

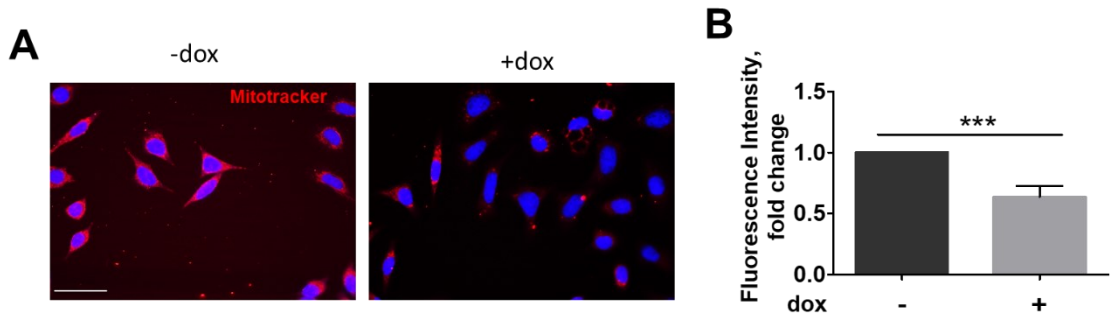

Figure 37 Defective mitochondria upon Chop overexpression

A. Representative immunofluorescence images of mitochondria (Mitotracker®, red) in –dox or + dox treated cells for 24 hours. Nuclei were stained with DAPI (blue), scale bar = 60 µm. **B.** Fluorescence intensity was quantified using ImageJ, its intensity in -dox cells was set to one. Blots and analysis were performed from n=3 experiments and statistical significance is indicated as: ***p ≤ 0.001

5.6.1 Impaired mitochondrial respiration in Chop Cells

In view of decreased mitochondrial proteins, namely Pink1 and Parkin, and the decreased mitochondria activity upon *Chop* overexpression, we next performed mitochondrial respiration measurement in these cells using an ororboros system. The measurement illustrated lower oxygen concentration in +dox treated cells for 24 h in comparison to -dox treated cells (**Figure 38 A&B**). The quantification of spare respiration confirmed a significant decrease of mitochondrial function (**Figure 38 C**). Furthermore, the quantification of oxygen consumption was performed to dive deeper into the mitochondria respiration chain. The data deciphers an impaired function of the mitochondrial respiration chain in nearly all sub units (**Figure 38 D**). Altogether, the data points towards dysfunctional mitochondria upon ER stress due to *Chop* overexpression.

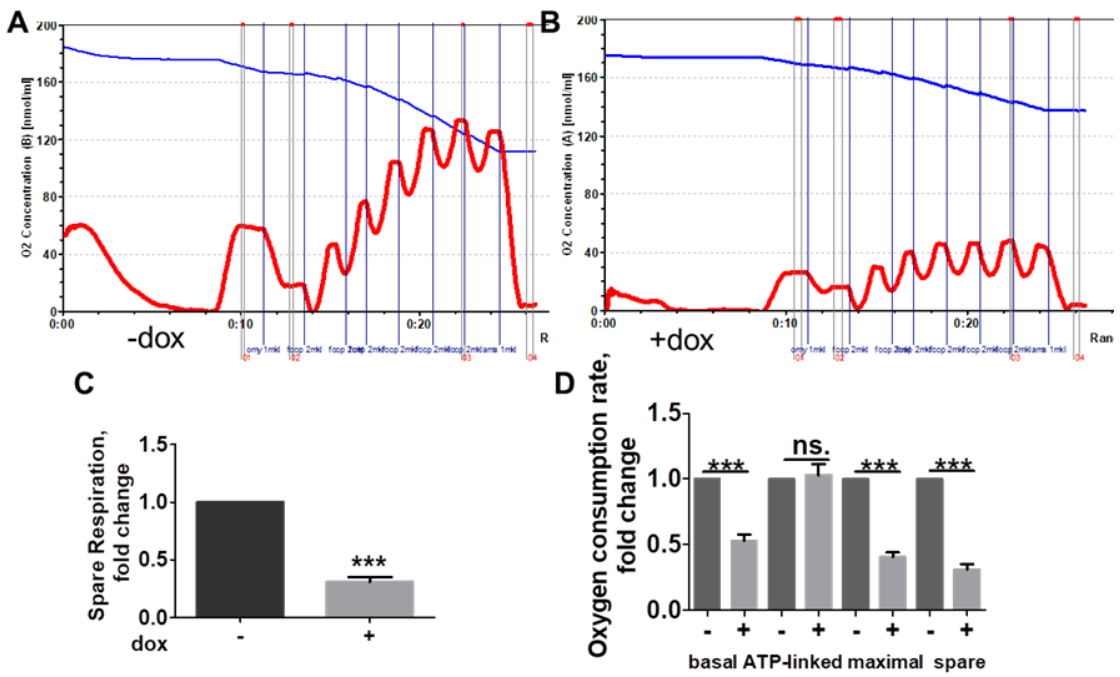

Figure 38 Mitochondrial dysfunction upon Chop overexpression

A.&B. Representative graph of oxygen consumption rate of MLE12 cells either uninduced (**A**) or induced (**B**) with doxycycline for *Chop* expression for 24 hours n=10. **C.&D.** Quantification of oxygen consumption rate (**C**) and spare respiration (**D**). Level of non-induced Chop cells was set as one. Statistical significance is indicated as: *** $p \leq 0.001$, ns= not significant.

5.7 Autophagy in MLE12 Chop cells

5.7.1 *Chop* overexpression results in impaired autophagy

Insufficient autophagy in the AECII of IPF patients is a well-reported finding. Especially, mitophagy that is mediated via Pink1-Parkin pathway has been shown be defective in IPF AECII. In this study, we also observed a decrease in both Pink1 and Parkin proteins. We hence next analyzed autophagy in response to *Chop* overexpression. MLE12 cells were either not induced or were induced with doxycycline for *Chop* expression for 12 and 24 hours, followed by western blots analysis (**Figure 39 A**). Overexpression of *Chop* resulted in a significant increase in the autophagy marker protein Microtubule associated protein 1A/1B Light Chain 3B II (LC3BII) (**Figure 39 B**) and in LC3BI to LC3BII conversion (**Figure 39 C**). These results, in parallel with an increased p62 protein level (**Figure 39 D**), implied altered autophagy upon Chop overexpression.

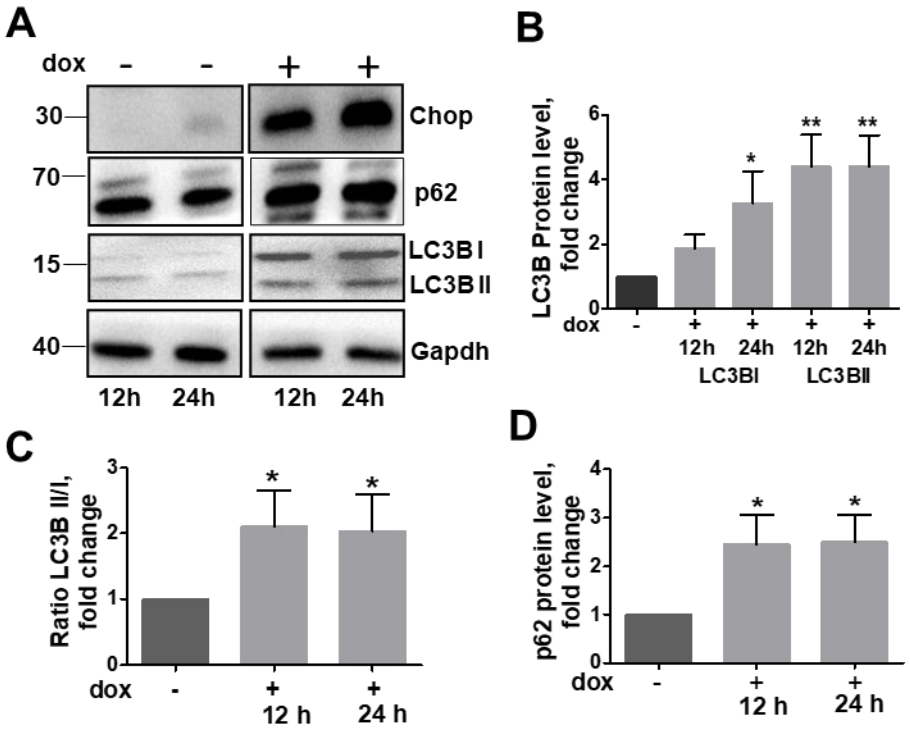

Figure 39 *Chop* overexpression results in impaired autophagy

A. MLE12 Chop cells were either not induced or were induced with 1 µg/mL doxycycline for *Chop* expression for 12 and 24 hours, followed by western blots for the given proteins from total lysates. The positions of molecular weight markers are shown. **B.-D.** Quantification of LC3B (**B**), Ratio of LC3BI to LC3BII conversion (**C**) and p62 (**D**) upon Chop induction obtained from (**A**). Relative protein amounts were normalized to Gapdh and their level in not induced was set as one. Statistical significance is indicated as: *p ≤ 0.05, **p ≤ 0.01.

In addition to these distal autophagy proteins, a significant increase in Beclin1 was also observed in response to *Chop* overexpression (**Figure 40 A**). Also, the lysosomal proteins Lysosomal associated membrane protein 1 (Lamp1) and Lamp2 were also find to be increased significantly upon Chop induction (**Figure 40 A**). Cathepsin D, a lysosome related stress marker, decreased significantly in these cells (**Figure 40 B)**. Of note, the transcription factor EB (TFEB), which is a master regulator of several autophagy genes and for the members of coordinated lysosomal expression and regulation (CLEAR) network, significantly increased upon *Chop* overexpression (**Figure 40 C**).

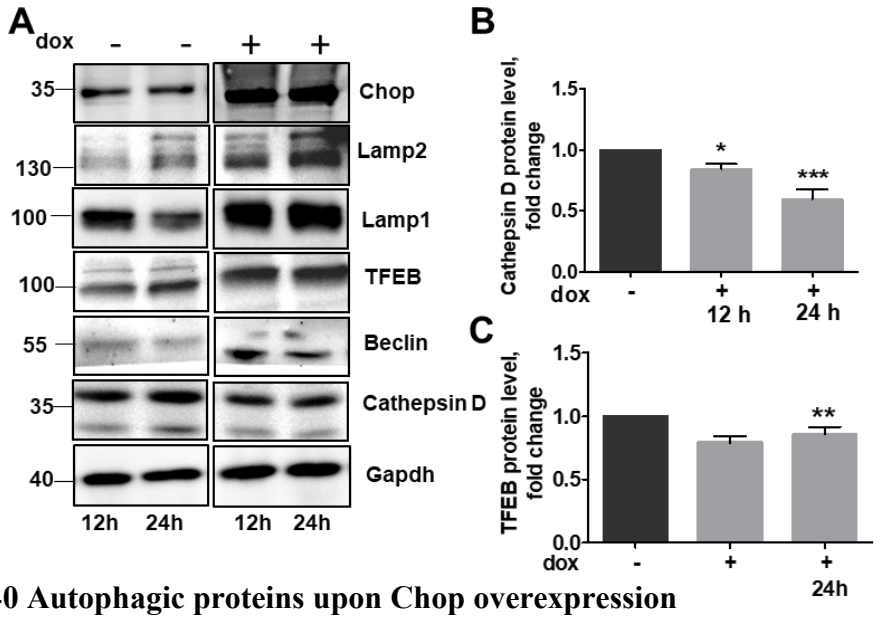

Figure 40 Autophagic proteins upon Chop overexpression

A. MLE12 Chop cells were either not induced or were induced with 1 µg/mL doxycycline for *Chop* expression for 12 and 24 hours, followed by western blots for the given proteins from total lysates. The positions of molecular weight markers are shown. **B&C.** Quantification of Cathepsin D (**B**) and TFEB (**C**) upon Chop induction obtained from (**A**). Relative protein amounts were normalized to Gapdh and their level in not induced was set as one. Statistical significance is indicated as: *p ≤ 0.05, **p ≤ 0.01, ***p ≤ 0.001.

5.7.2 *Chop* overexpression induces nuclear translocation of TFEB

We next performed cytosolic and nuclear extracts to analyse if the observed increase in TFEB corresponds to nuclear TFEB. In normal conditions, TFEB is localized to the cytoplasm, but stress conditions rapidly induce TFEB nuclear translocation [Settembre, C. et al. 2011]. Therefore, it is reasonable to speculate that TFEB is required for the enhanced autophagy/lysosomes activity in the ER. Interestingly, we observed a significantly increased TFEB in nuclear fraction of Chop induced cells. In fact, we observed a double band in this lane (**Figure 41 A&B**). Since phosphorylation of TFEB is a well-known event in regulating several autophagy related genes, we next performed western blots for p-TFEB in these cells and observed an increase in phosphorylation in cells with Chop induction (**Figure 41 C**).

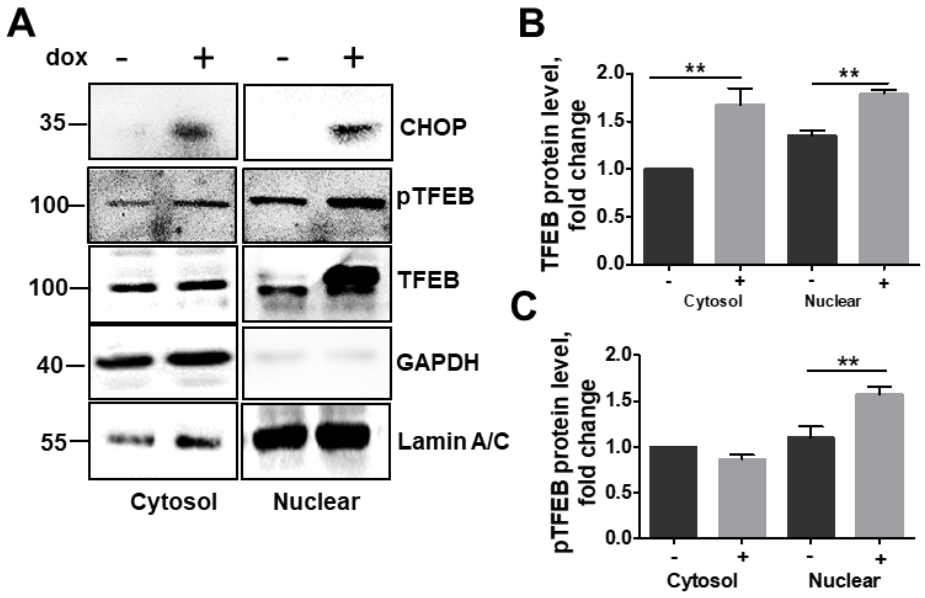

Figure 41 Chop overexpression induces nuclear translocation and phosphorylation of TFEB

A. MLE12 Chop cells were either left uninduced or were induced with doxycycline for *Chop* expression for 12 and 24 hours, followed by western blots from cytosolic and nuclear extracts. **B&C.** Quantification TFEB (**B**) and pTFEB (**C**) after *Chop* induction. Statistical significance is indicated as: **p ≤ 0.01.

To further confirm this results immunofluorescence was performed. Cells overexpressing Chop (green) displays increased fluorescence intensity of TFEB (red) in the nucleus (blue). These results revealed increased nuclear translocation of TFEB (**Figure 42 A&B**). In conclusion TFEB is translocated to the nucleus upon pro-apoptotic ER stress and there activates transcription biogenesis factors of the lysosome. Taken all results together, Chop overexpression leads to an increase in autophagosome formation and increased lysosomal biogenesis via TFEB, but, at the same time, also impaired autophagy in those cells.

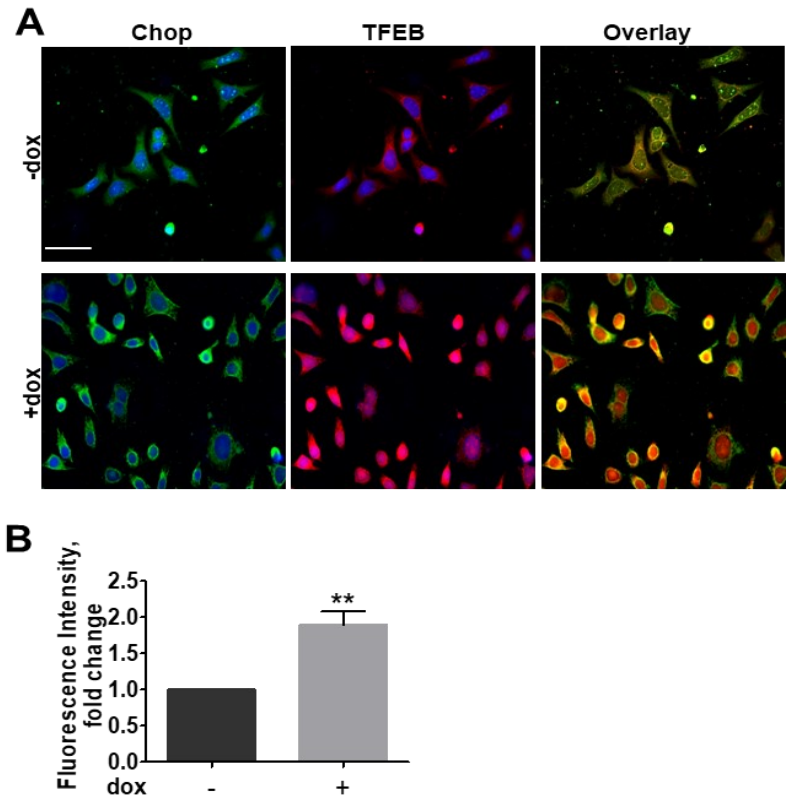

Figure 42 Nuclear translocation of TFEB in Chop overexpressing cells

A. Immunofluorescence for TFEB indicated nuclear translocation of TFEB (red) upon *Chop* expression (green) Nuclei were stained with DAPI (blue), scale bar = 60 µm. **B.** Fluorescence intensity of co-localization was quantified using ImageJ, its intensity in uninduced cells was set to one. Statistical significance is indicated as: **$p \leq 0.01$.

5.7.3 Induction of Chop leads to blocked autophagic flux

Since several autophagy proteins are increased and the master regulator TFEB was also found to be increased upon Chop induction, we hypothesized that autophagy is increased in cells with Chop induction. We measured autophagy flux using the inhibitor of vacuolar H^+-ATPase bafilomycin A1 and chloroquine, which mainly inhibits autophagy by impairing autophagosome fusion with lysosomes. MLE12 Chop cells were pretreated with one of the lysosomal inhibitors for 1 h, followed by dox-treatment for 6 h to induce *Chop* or left untreated. Western blot analysis showed increased LC3BI and LC3BII protein levels in Chop induced cells compared to non-induced cells (as also shown in **Figure 39**), but no significant change in LC3BI and LC3BII protein levels upon additional treatment with lysosomal inhibitors compared to vehicle treatment upon *Chop* overexpression (**Figure 43 A&B**). Additionally, p62 protein levels also did not seem to be affected upon chloroquine treatment (**Figure 43 A**).

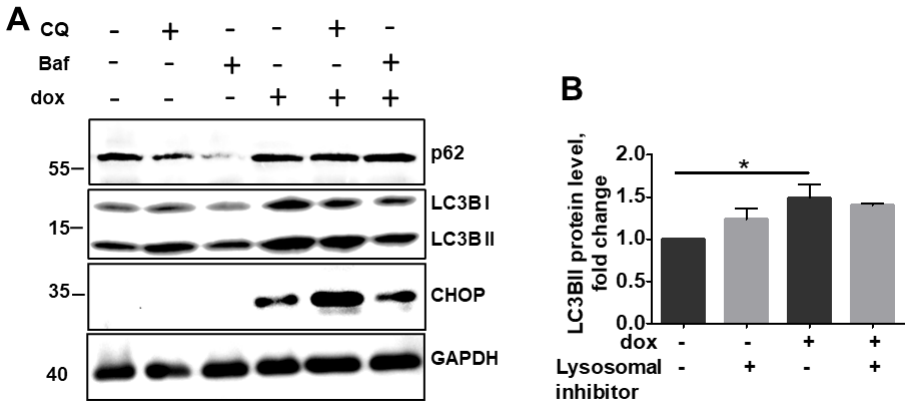

Figure 43 Impaired autophagic flux upon Chop overexpression

A. MLE12 Chop cells were pretreated with either chloroquine or bafilomycin A1 or vehicle for 1h followed by non-induction or induction with 1 µg/mL doxycycline for *Chop* expression for 6 hours, followed by western blots for the given proteins from total lysates. **B.** Quantification of LC3BII protein level. Relative protein amounts were normalized to Gapdh and their level in controls was set as one Statistical significance is indicated as: *$p \leq 0.05$

Next, cells were transfected with tandem fluorescence LC3B plasmid (mRFP-GFP-LC3B, tfLC3B) (**Figure 44 A**). LC3B is tandemly fused to acid-insensitive mCherry and acid-sensitive GFP to measure the formation of autolysosomes and their degradation. In autophagosomes both tags emit fluorescent light resulting in a yellow fluorescence. However, the fusion of autophagosomes to acidic lysosomes results in low pH, where the GFP gets degraded and the green fluorescence is lost and only the red fluorescence of mCherry is visible. Subsequently, the red fluorescence from mCherry is lost when the double tagged protein is degraded in the autolysosome [Hansen, T.E. et al. 2011]. MLE12 Chop cells were transfected with tfLC3B followed by *Chop* induction for 16 h or were not induced. Immunofluorescence analysis revealed no significant change in green fluorescence intensity of GFP-LC3B (**Figure 44 B**), but a significant decrease in red fluorescence intensity of mCherry in dox treated cells compared to untreated cells (**Figure 44 C**). This suggested proper generation of autophagosome (green), but defective fusion with the lysosome (red), leading to an accumulation of autophagosomes upon *Chop* induction and therefore a blockade in autophagic flux.

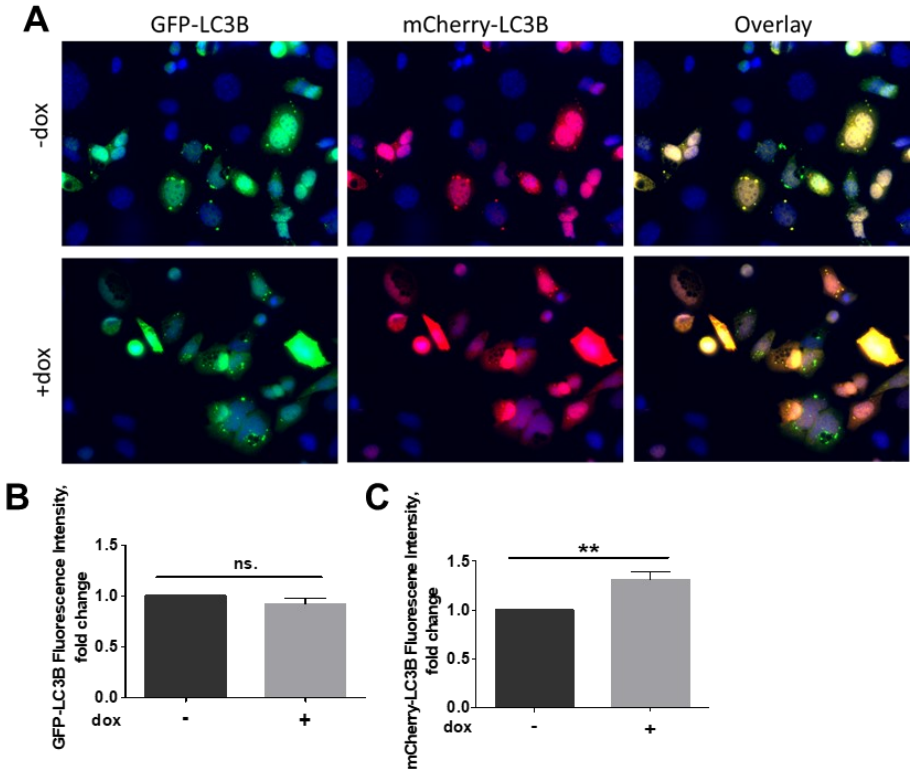

Figure 44 Autophagic flux is blocked upon *Chop* overexpression

A. Representative immunofluorescence of MLE12 Chop cells either non-induced or induced with doxycycline for *Chop* expression for 24 hours transfected with tfLC3B. Nuclei were stained with DAPI (blue), scale bar = 60 µm. **B.,C.** Fluorescence intensity of GFP-LC3B (**B**) and mCherry-LC3B (**C**) was quantified using ImageJ, its intensity in uninduced cells was set to one. Statistical significance is indicated as: **p ≤ 0.01, ns. =not significant.

6 Discussion

This study reveals impaired ER-mitochondrial tethering under three different conditions: 1. upon overexpression of the terminal ER stress inducer, Chop, 2. upon overexpression of the IPF associated mutation, SP-C $^{\Delta exon4}$ and 3. in the lungs of IPF patient lungs. Under all three conditions, we observed a decrease in the MAM protein PACS2. "Therapeutic", transient overexpression of PACS2 in our ER stress models restored ER-mitochondrial tethering. In addition, we observed an interaction between PACS2 and the calcium channel TRPV1. Therapeutic targeting of TRPV1 by capsaicin restored levels of TRPV1 as well as PACS2 in our in vitro models as well as in the PCLS of IPF patients. Of note, such capsaicin treatment not only restored TRPV1 and PACS2 levels, it also resulted in a reduction of epithelial apoptosis and reduction of collagen expression – key processes in the development of lung fibrosis. Altogether, these readouts signify the critical role of ER-mitochondrial contacts in maintaining cellular homeostasis during ER stress and lung fibrosis.

6.1 MAM contribution in response of pro-apoptotic ER stress

6.1.1 ER stress and mitochondrial signaling in lung fibrosis

Several studies have revealed the importance of chronic ER stress in AECII apoptosis in lung fibrosis in general and in IPF in particular. AECII apoptosis is an established key event in the pathogenesis of sporadic as well as familial forms of IPF [Korfei, M. et al. 2008, Lawson, W.E. et al. 2008]. CHOP is increased particularly in the AECII of sporadic IPF patient lungs alongside with a significant increase in other major ER stress signature molecules, GRP78, ATF4, ATF6α and spliced XBP [Korfei, M. et al. 2008, Lawson, W.E. et al. 2008]. It has been proven, that chronic ER stress induces upregulation of CHOP [Zinszner, H. et al. 1998]. And such overexpression of CHOP leads to AECII apoptosis [Klymenko et al. 2016], while its knockdown protects cells from ER-stress induced apoptosis [Oyadomari, S. et al. 2002]. Such ER stress has also been reported in several animal models of lung fibrosis [Ahuja, S. et al. 2016, Kesireddy, V.S. et al. 2019, Yao, Y. et al. 2016]. Besides, overexpression of the BRICHOS domain mutants of SP-C, SP-C $^{\Delta exon4}$ and SP-C^{L188Q} in lung epithelial cell line A549 and in human embryonic kidney (HEK) cells elicited pro-apoptotic ER stress signaling, again asserting the importance of ER stress in the epithelial cell apoptosis in lung fibrosis [Maguire, J.A. et al. 2011, Mulugeta, S. et al. 2005]. Complimenting these studies, we here observed

increased ER stress signaling upon overexpression of SP-C $^{\Delta exon4}$ in human melanoma cell lines (MEL188). IPF has a remarkable age-related onset, hence several hallmarks of aging have been reported in IPF patients. Mitochondrial dysfunction is one such characteristic feature and mitochondria-mediated AECII apoptosis has been reported in IPF and in idiopathic interstitial pneumonias (IIPs) [Kuwano, K. et al. 2002]. In detail, the release of cytochrome c and activation of caspase 9 was shown in patients with IIPs in addition to condensed mitochondria in the apoptotic epithelium [Kuwano, K. et al. 2002]. The contextual role of reactive oxygen species (ROS) as part of adaptive or maladaptive responses in several tissues has been discussed and such evidence has been reported in asbestos-related lung fibrosis [Liu, G. et al. 2010]. A direct role of dysfunctional mitochondria in AECII apoptosis and IPF was first shown in a study that revealed low expression of PINK1 in IPF lungs. Increased expression of pro-fibrotic factors and depolarized, dysmorphic mitochondria were reported upon PINK1 knockdown. Since PINK1 is an active mediator of mitochondrial autophagy, both autophagy and mitophagy related cellular quality control was also effected due to its knockdown [Bueno, M. et al. 2015].

6.1.2 ER -mitochondrial crosstalk in ER stress and lung fibrosis

The pathological roles of ER stress and dysfunctional mitochondria in AECII apoptosis and lung fibrosis have been very well established. However, under normal conditions, these fundamental organelles are highly interconnected, both physically and functionally [Csordás, G. et al. 2006]. Studies thus far in IPF, ILDs or in animal models of lung fibrosis did not focus on the crosstalk of these two organelles.

In the last decade, the importance of interaction between the ER and mitochondria in cellular homeostasis has been described [American Thoracic Society. 2000, Lynch, D.A. et al. 2018]. Altered ER-mitochondrial crosstalk has been observed in various cell types and tissues under pathological conditions [Hedskog, L. et al. 2013]. The ER-mitochondria associated membrane (MAM) have been shown to play an important role in calcium signaling, mitochondrial fragmentation and in the dynamics of the ER and the mitochondria. Key regulators of the physical interactions between mitochondria and the ER are, amongst others, MAM proteins SigmaR1, IP3R3, calnexin and PACS2, which is anchored to calnexin, as well as ER chaperones [Fan, Y. et al. 2019]. An important role of MAM is calcium transport. The outer mitochondrial membrane (OMM) ion channel voltage-dependent anion channel (VDAC) and the ER calcium channel inositol 1,4,5-

triphosphate receptor (IP3R) form a complex, stabilized by the chaperone protein glucose-regulated protein 75 (GRP75) to facilitate calcium exchange from the ER to mitochondria [Thoudam, T. et al. 2016].

The sarcoplasmic reticulum (SR), a special part of the ER, is the main internal store of calcium ions. SigmaR1 facilitates calcium transfer by chaperoning IP3R3 [Hayashi, T. et al. 2007]. Under ER stress, SigmaR1 can also stabilize the UPR sensor protein IRE1α at the MAM. These findings suggest that SigmaR1 is not only involved in stabilization of calcium channels, but also in maintaining ER cell functions [Bernard-Marissal, N. et al. 2015]. Additionally, the knockdown of SigmaR1 promotes pro-apoptotic ER stress by defective calcium exchange. SigmaR1 seems to be a potential MAM modulator. In line with this in the current study, IHC of AECII in IPF demonstrated increased staining of SigmaR1 and IP3R3 in comparison to IHC of AECII in donor lungs.

As a consequence of this close contact of ER and mitochondria and the excessive calcium exchange, prolonged ER stress leads to calcium overload in mitochondria and subsequent calcium depletion, therefore to mitochondrial and ER dysfunction. This dysfunction can result in cell death signaling mechanisms [Wei, Y. et al. 2009]. The Ca^{2+} exchange through IP3Rs and SigmaR1 as well as VDAC1 maintains Ca^{2+} homeostasis and normal cellular function. However, upon pro-apoptotic ER stress the MAM proteins can induce apoptotic pathways by facilitating Ca^{2+} release from mitochondria and induce pro-apoptotic factors [Joseph, S.K. et al. 2007]. First of all, UPR is a survival mechanism to restore and maintain cellular homeostasis by the transfer of misfolded or unfolded proteins into the cytosol, where they are properly folded by chaperones. However, if this mechanism fails, the ERAD pathway will be activated and misfolded proteins will be ubiquitinated and degraded via proteasome. The ER also undergoes expansion in such conditions to create more space for misfolded proteins. The expanded ER will then be degraded by autophagy due to its larger size (as autophagosomes can accommodate such large organelles) after the stress response. This process is called ER-phagy [Khaminets, A. et al. 2015]. All of these processes take high energy and Ca^{2+} consumption and therefore also compromise mitochondria function [Kincaid, M.M. et al. 2007]. Pinton et al. have argued that disrupted ER contributes to damaged mitochondrial function and finally results in induction of apoptosis [Pinton, P. et al. 2006]. Agreeing to this, in our current study, we observed impaired mitochondrial respiration in cells with the induction of CHOP protein.

If dysfunctional mitochondria are not able to cope with cellular stress, they undergo fragmentation and will be degraded via mitophagy, resulting in vulnerability of the cell to further injury. In this context, MAM also plays an important role during mitochondrial fission and fusion processes to maintain their homeostasis. The process of fusion is controlled by MFN1 and MNF2. After stress reaction, mitochondria undergo fusion to recover mitochondria functions. Mitochondria, which are not able to fuse, will be degraded via mitophagy or under severe mitochondrial stress, they undergo apoptosis [Archer, S.L. 2013]. The fission process of mitochondria could lead to apoptosis. This process is started by enveloping the damaged mitochondria by the MAM, this triggers dynamin-related protein 1 (DRP1) translocation to the MAM interface, where it then starts the fission of mitochondria and the damaged mitochondria will then undergo mitophagy [Böckler, S. et al. 2014].

This concept could be supported by the observation of dysregulated mitochondrial proteins like DRP1, MNF2 and PINK1 in mitochondrial fraction upon *Chop* overexpression as well as impaired mitochondrial respiration capacity similar to the findings in IPF. Although PINK1-regulated mitochondrial quality control still remains elusive, it is known that, under ER stress conditions, PINK1 recruits Parkin from the cytoplasm to damaged mitochondria to initiate the autophagic degradation of damaged mitochondria. In stress conditions, PINK1 is able to relocate to MAMs to promote the formation of mitochondrial autophagosomes. The mitochondrial localization of PINK1 is linked to decreased mitochondrial potential [Matsuda, N. et al. 2010]. A decreased PINK1 protein level upon *Chop* overexpression in our study indicated a potential dysregulated mitochondrial quality control and impaired mitophagy.

6.1.3 PACS2: A key player in ER-mitochondrial tethering

PACS2 is a multifunctional sorting protein, which is located in many tissues, such as skeletal muscle, heart, brain and liver tissues. PACS2 transfers several cargo proteins to respective organelles and is therefore involved in membrane trafficking as well as in organelle communication, especially between ER and mitochondria. In cells, PACS2 controls the cohesion of mitochondria with ER. It is located in between the MAM and is bound to calnexin and therefore plays an important role in the communication between ER and mitochondria. It is known that PACS2 plays an integral part in membrane trafficking, as its identifier and binds to cargo proteins, e.g. calnexin, and then transfers these cargo proteins to corresponding organelles. Thus PACS2 controls the distribution

of calnexin to MAM [Youker, R.T. et al. 2009]. As it acts with calnexin, PACS2 might also be involved in the transfer of other chaperone to MAMs [Veeresh, P. et al. 2019]. Recent studies have therefore focused on PACS2 as a therapeutical target for different diseases [Li, C. et al. 2020, Moulis, M. et al. 2019, Yu, S. et al. 2019].

However, certain debates exist. Li et al. showed that PACS2 has an essential role on ER homeostasis as PACS2 depletion induces UPR [Li, C. et al. 2020]. A direct regulation between CHOP and PACS2 proteins, however, had not been investigated so far. But it has been reported that in response to ER stress inducers like staurosporin and tunicamycin PACS2 protein is translocated from cytosol [Simmen, T. et al. 2005]. Upon ER stress PACS2 is translocated to MAM contacts sites in order to increase ER–mitochondria contact formation, thereby restoring cell homeostasis [Fan, Y. et al. 2019]. Additionally, Joseph et al. have identified a potential PACS2-binding site on IP3R3, so PACS2 may redirect this ion channel on the ER membrane and hence depletion of PACS2 may lead to mislocalization of IP3R3 into ER, resulting in disrupted calcium transfer and at least ER stress and apoptosis [Hajnóczky, G. et al. 2000, Joseph, S.K. et al. 2007, Köttgen, M. et al. 2005]. Another interesting observation demonstrates extended tubulation of the peripheral ER by electron microscopy of PACS2 depleted cells. This observation could give a hint towards a role of PACS2 in the modulation of ER shape, correct folding and ER-phagy, as depletion of PACS2 leads to uncontrolled extension of the ER [Nakajima, K. et al. 2004, Piccini, M. et al. 1998].

However, when these attempts to restore homeostasis is fail, the apoptotic pathway is initiated. Under such apoptotic conditions PACS2 translocates to mitochondria, thereby recruiting pro-apoptotic factors like Bid to mitochondria [Simmen, T. et al. 2005]. It has been also demonstrated that TNF-related apoptosis-inducing ligand (TRAIL) dephosphorylates Ser437 of PACS2 to facilitate interaction with Bid, Bid will be then translocated to the mitochondria, where it will be cleaved. Truncated Bid (tBid) itself triggers cytochrome C release leading to the induction of apoptosis. TRAIL also induces lysosomal membrane permeabilization, this will be mediated by PACS2 [Aslan, J.E. et al. 2009, Barroso-González, J. et al. 2016].

Taking these observations together, there are two paradoxical findings about PACS2 depletion. On the one hand the absence of PACS2 showed mitochondrial fragmentation and thereby uncoupling of the mitochondria from the ER. As a consequence of uncoupling the MAM were disrupted and this - in turn - leads to ER stress [Pitts, K.R. et

al. 1999]. On the other hand as PACS2 induces TRAIL-depended apoptosis, the depletion of PACS2 may lead to a reduction of apoptosis [Simmen, T. et al. 2005]. Whether PACS2 depletion is beneficial or harmful for the cells depends on the MAM conditions and dynamics.

A contradictory study by Arruda et al. showed that the interaction of ER and mitochondria is highly dynamic, the MAM are able to adapt to physiological conditions. Especially under acute ER stress the ER membrane wraps around the mitochondria, thereby increasing MAM contact sites. This indicates a short-term adaptive process to increase mitochondrial function by increased Ca^{2+} exchange [Arruda, A.P. et al. 2014, Zhao, L. et al. 2017]. Upon chronic ER stress the increased MAM contact site facilitates higher Ca^{2+} intake by the mitochondria, but a prolonged uptake leads to mitochondrial dysregulation and apoptosis. In conclusion, excessive MAM formation during ER stress through altered Ca^{2+} signaling to mitochondria leads to mitochondrial dysfunction and apoptosis. In such situations knockdown of PACS2 reduces the MAM contact site and improves mitochondrial function. All these studies indicate that an increase or a decrease in ER-mitochondrial interaction above or below physiologically accepted levels leads to mitochondrial dysfunction.

In this study, we demonstrated that a downregulation of Pacs2 is - at least in part - responsible for the decreased apposition of ER and mitochondria as well as for the increased apoptosis in *Chop* overexpressing MLE12, SP-C mutant (SP-$C^{\Delta exon4}$) model as well as in AECII of IPF patients. Although we did not show how depletion of PACS2 may result in apoptosis of alveolar epithelial cells, we did show that its overexpression restores ER stress induced epithelial cell apoptosis.

In contrast to some previous studies, in this study Pacs2 was decreased upon ER-Stress conditions. One straight forward explanation for this observation could be that our study focused on models where single overexpression of Chop or SP-$C^{\Delta exon4}$ was performed, which might have different effects on MAM or PACS2 regulation than in models where general ER stress has been studied. To our knowledge, both these models were not used to study MAMs or PACS2 regulation so far. In addition, our study is the first to show that the physical distance between ER and mitochondria in IPF is decreased via ultrastructural analysis and to study the regulation of MAMs or PACS2 protein in IPF. In any case, dox induced cells (*Chop* overexpression) with *Myc-PACS2* overexpression demonstrated no significant change in cl. caspase 3 level compared to non-induced cells. In summary, these

results provide strong evidence for Pacs2 to be a crucial player in maintaining ER-mitochondrial crosstalk in our models of ER stress and in the AECII of IPF lungs.

6.1.4 cIAPs mediate ubiquitination of PACS2

The cellular inhibitor of apoptosis proteins (cIAPs) are involved in a variety of cellular processes, first of all as repressors of apoptosis [Salvesen, G.S. et al. 2002]. Through their E3 ubiquitin ligase domain cIAPs ubiquitinate their substrates and via K48 polyubiquitination the substrates are degraded via proteasome [Gyrd-Hansen, M. et al. 2010]. Guicciardi et al. provided evidence that PACS2 is a target of such cIAP1 and cIAP2 mediated proteasomal degradation of PACS2 in hepatobiliary cancer cells [Guicciardi, M.E. et al. 2014]. In the same study it was demonstrated that the depletion of both cIAP1 and cIAP2 leads to PACS2 accumulation, lysosomal membrane permeabilization (LMP) and TRAIL-induced apoptosis [Guicciardi, M.E. et al. 2011]. As previously described, TRAIL induced apoptosis is also mediated by PACS2. Immunoprecipitation assays also identified an interaction between PACS2 and cIAP1 and cIAP2 [Guicciardi, M.E. et al. 2014]. However, in our current study MLE12 cells with *Chop* induction showed a reduction in Pacs2, but this was not accompanied by alterations in the protein level of ciAP or protein ubiquitination. In addition, proteasomal inhibition with MG132 did not result in PACS2 accumulation. According to this observation, Pacs2 reduction in MLE12 CHOP seems not to be caused by ciAP E3 ligase activity.

6.1.5 TRPV1-PACS2 axis effects ER-mitochondrial tethering

Both PACS1 and PACS2 were shown to be involved in the trafficking of polycystin-2, a member of the TRPP2 ion channel family [Köttgen, M. et al. 2005]. A recurrent de novo mutant of PACS2 (p.Glu209Lys) interacts to a greater extent with TRPV1 than the wild type PACS2, implicating the importance of PACS2 in channelopathies [Olson, H.E. et al. 2018]. In the same line, in the current study, we observed an interaction between PACS2 and TRPV1 by co-immunoprecipitation experiments. TRPV1 is a well-characterized, non-selective cation channel present in several peripheral sensory neurons involved in pain and heat sensation [Caterina, M.J. et al. 1997]. It can also be activated by alkaloid pungent food ingredients such as capsaicin (CPS), the ingredient of hot chili peppers, causing burning sensation by contact [Nilius, B. et al. 2014]. CPS is a highly selective TRPV1 agonist and has a wide range of medical benefits. It is a major component of topical application for pain therapies [Tandan, R. et al. 1992] and high concentration CPS patches are approved and well-tolerated for neuropathic pain [Abrams, R.M.C. et al.

2021]. Its anti-hypertensive [Hayes, A.G. et al. 1981], anti-tumorigenic [Mori, A. et al. 2006] and anti-inflammatory [Frydas, S. et al. 2013] properties are well documented. CPS has inhibitory effects in hepatic fibrosis [Sheng, J. et al. 2020] and prevents renal damage in acute kidney injury [Zhang, S. et al. 2018]. In the lung, CPS has been shown to reduce pulmonary remodeling and collagen fibrils in vessels and lung tissues of animals with chronic lung inflammation [Prado, C.M. et al. 2011]. Further it was shown that low doses of CPS improves bleomycin-induced lung fibrosis via inhibiting ERK1/2/eIF3a signaling in the alveolar epithelial cells [Lu, L.M. et al. 2020]. Besides its health benefits, CPS is reported to be acutely toxic and is a powerful natural irritant. But its medical benefits outweigh its risks. Due to its lipophilic feature, it can pass the cell membrane and bind to TRPV1 on the intracellular surface [Jung, J. et al. 1999]. CPS stabilizes the open state of TRPV1 by "pull-and-contact" interaction with the S4-S5 linker [Yang, F. et al. 2017]. Regulation of TRPV1 activity can be modulated by phosphorylation of several key residues, which leads to increased sensitivity of the ion channel [Nilius, B. et al. 2014]. TRPV1 is highly sensitive and selective for CPS, therefore it is also called CPS receptor. With the binding of CPS, TRPV1 is activated and gets more permeable for sodium (Na^+) and calcium (Ca^{2+}) ions flowing through TRPV1 into the cell to depolarize it, leading to an analgetic effect mostly due to channel desensitization [Caterina, M.J. et al. 1997, Elokely, K. et al. 2016]. TRPV1 builds a multimeric complex with several proteins which regulate the location and function of the channel [Novakova-Tousova, K. et al. 2007]. Migration of TRPV1 to the cell surface is mediated by interacting proteins, majorly the inflammation mediators [Camprubí-Robles, M. et al. 2009]. TRPV1 antagonists are utilized for pain relief and also TRPV1 agonist are taken into concern as a potential therapeutic agent, due to the calcium-mediated inactivation or desensitization of TRPV1 [Vyklický, L. et al. 1999].

Due to its function and expression in both the plasma membrane and the ER membrane TRPV1 regulates cellular Ca^{2+} homeostasis and also ER stress [Sukumaran, P. et al. 2016]. The most important functions for ER such as protein synthesis, proper folding of proteins and their post-translational modifications, are all Ca^{2+}dependent. Therefore disruption of Ca^{2+} homeostasis leads to disturbed folding of proteins and leads to the accumulation of unfolded/misfolded proteins in the ER lumen causing activation of the UPR pathway [Senft, D. et al. 2015]. TRPV1 is essential for Ca^{2+} homeostasis by facilitating the release of Ca^{2+} from the sarcoplasmic reticulum (SR), the main source of intracellular Ca^{2+} stores. Hence the functions of a dysregulated TRPV1 channel could

also lead to ER stress [Abramowitz, J. et al. 2009]. Because ER stress and autophagy are Ca^{2+} dependent processes, Ca^{2+} is involved in those processes as well and forms the basis of the crosstalk between these two processes. Overall, Ca^{2+}also acts as a second messenger [Berridge, M.J. et al. 2003].

In another study it has been shown that TRPV1 is increased in bleomycin-induced lung fibrosis in guinea pigs [Guo, Y. et al. 2019]. Overall, TRP channels were suggested to contribute to lung repair processes [Dietrich, A. 2019] and agreeing to this, we here showed that modulating TRPV1 using CPS influences PACS2 protein levels and aids in restoring the ER-mitochondrial crosstalk.

6.1.6 TRPV1 modulation and ER stress response

TRPV1 plays an important role in lung functions, as it is expressed in C-fibers, which innervate the respiratory tract. Both lung epithelial cells and bronchial smooth muscle cells have been shown to express TRPV1. Thomas et al. have demonstrated that cells of the conducting airways, alveoli, and pulmonary capillaries of humans and mice express TRPV1 and that its agonist nonivamide activated ER stress by disrupting ER Ca^{2+} homeostasis [Jara-Oseguera, A. et al. 2008]. TRPV1 agonist activates TRPV1 channel and causes Ca^{2+} release from the ER into the nucleus. Due to its function as a second messengers it increases the expression of stress response genes like CHOP and BiP mRNA [Thomas, K.C. et al. 2007]. Furthermore, treatment with lipopolysaccharide (LPS), which is widely used to induce inflammation and acute lung injury, triggers the production of endogenous TRPV1 agonists, thus leading to ER stress and CHOP expression by Ca^{2+} release [Thomas, K.C. et al. 2012]. Further work indicated that the TRPV1 agonist CPS may trigger ER stress through the activation of TRPV1-mediated ROS generation, which disrupted ER redox homeostasis [Farfariello, V. et al. 2012]. However, not only the TRPV1 agonist seems to promote ER stress, Wang et al. have demonstrated that a TRPV1 antagonist, DWP05195, induced caspase-dependent apoptosis. DWP05195 increased ROS production and its intracellular accumulation, leading to ER stress. Upon ER stress, the expression of CHOP was upregulated, thereby inducing apoptosis [Wang, Y.-Y. et al. 2020]. Further work by Wei et al. has indicated that in diabetic nephropathy increased MAM, resulting in prolonged mitochondrial Ca^{2+} overload, is observed in podocytes. This in turn leads to mitochondrial dysfunction. In this disease condition activation of TRPV1 by CPS could improve mitochondrial

dysfunction by reducing Ca^{2+} transfer from ER to mitochondria and MAM contact sites [Wei, X. et al. 2020].

However, contradictory studies have also been published. Amantini et al. have reported that thymocytes treated with CPS inhibit UPR and apoptosis, displaying a reduction of BiP and Grp94 [Amantini, C. et al. 2017]. All these results draw a line towards TRPV1 as a modulator for MAM contact sites and Ca^{2+} flux in order to promote cell viability.

Adding to this, in this study we show that Trpv1 protein levels are decreased in cells overexpressing *Chop*. Treating these cells (and non Chop overexpression cells) with 25 µM CPS resulted in increased Trpv1 as well as Pacs2 protein levels. These results may be explained by taking a study published by Olson et al. [Olson, H.E. et al. 2018] into consideration. There, a binding site of PACS2 for TRPV1 was described, suggesting an interaction between these proteins. In our current study where we also report an interaction between these proteins. Adding to this, our results also show that restoration of TRPV1 and PACS2 improved ER-mitochondrial tethering.

However, PACS2-TRPV1 interaction represents only a small part of the organelle interaction. Not only mitochondria, but also ER stress has also been linked to the autophagy pathway [Ogata, M. et al. 2006]. In the context of our study, CPS treatment has been shown to inhibit UPR and apoptosis in thymocytes as well as to increase the gene expression of ERAD and autophagy related genes. Although not proven directly here, CPS induced autophagy may be a consequence of the ER stress, like previously shown by other groups [Amantini, C. et al. 2017].

6.2 ER-Stress and Autophagy are linked via MAMs

As mention before, cellular stress conditions or pathological settings like nutrient starvation and hypoxia induce autophagy in order to obtain cell survival [Ogata, M. et al. 2006, Zhang, J. 2015]. It is well known that autophagy has a pro-survival function, but autophagy could also lead to apoptosis by degrading necessary cellular components. Due to this, a balanced autophagy is required for cell homeostasis. The ER contains several autophagy related proteins, which could play a role in autophagosome formation [Lamb, C.A. et al. 2013]. Hamasaki et al. have indicated that MAMs are a source of autophagosome formation [Hamasaki, M. et al. 2013] and several studies have shown that autophagosome formation on the MAMs is essential for the removal of defective proteins of the ER, thus contributing towards the normal function of the ER [Klionsky, D.J. et al.

2016, Ogata, M. et al. 2006]. PACS2 also plays an important role in the autophagosome formation at MAMs, as the knockdown of PACS2 results in the disruption of MAMs and leads to defective autophagosome formation [Lamb, C.A. et al. 2013]. In addition, the depletion of PACS2 resulted in disrupted mitophagosome formation at MAMs and therefore impaired mitophagy and increased apoptosis. In line with this, repression of PACS2 promotes cell survival by an increased in the mitophagy on MAM contact site [Moulis, M. et al. 2019]. These observations are in line with our observation that autophagy is impaired in the ER stress model of Chop overexpression. Whether this impaired autophagy is directly due to a decrease in Pacs2 or Trpv1 protein levels needs to be studied further.

6.2.1 Regulation of autophagy via TFEB

The transcription factor EB (TFEB) has been reported to promote lysosomal biogenesis. Most lysosomal genes (22 out of 23 genes tested) are regulated by TFEB. Furthermore, TFEB promotes the upregulation of genes belonging to the Coordinated Lysosomal Expression and Regulation (CLEAR) network, which are involved in major steps of the autophagic pathway, such as autophagosome formation, autophagosome-lysosome fusion and degradation. Under normal conditions, TFEB is localized at the cytoplasm. Under stress conditions, like starvation or pathological conditions, TFEB is translocated to the nucleus, where it activates its target genes and induces autophagy [Sardiello, M. et al. 2009]. Settembre et al. demonstrated in stably TFEB overexpressing HeLa cells a significantly increase in autophagosomes formation [Settembre, C. et al. 2011]. Further work has demonstrated that TFEB overexpression leads to a reduction in expression of ATF4 and CHOP, two key players of ER stress pathway. On the other hand, knockdown of TFEB showed an upregulation of ATF4 and CHOP [Yoneshima, E. et al. 2016]. These findings indicate that TFEB could improve cell viability by supressing ER stress. As mentioned before, misfolded proteins, which accumulate in the ER and induce ER stress, will be degraded by autophagy, thereby giving rise to the concept that TFEB is involved in increased autophagy leading to enhanced clearance of the accumulated proteins in the ER. Likewise, depletion of TFEB promotes ER stress and leads to increased apoptosis [Yoneshima, E. et al. 2016]. Recent studies have also showed that lysosomal Ca^{2+} signaling regulates TFEB expression and therefore also autophagy genes. Lysosomal Ca^{2+} release promotes binding of calcineurin to TFEB, this in turn leads to TFEB dephosphorylation and nuclear translocation [Medina, D.L. et al. 2015].

Our results here show that TFEB is increased in Chop overexpressing cells. In fact, we also identified an increased nuclear translocation of TFEB in Chop overexpressing cells. Although these observations are in line with previous studies, one intriguing observation is that, in spite of the TFEB nuclear translocation, autophagy is impaired in Chop overexpressing cells as observed in our study. One explanation, although not proven in this study is that TFEB upregulates autophagy / lysosomal genes and autophagy is induced but Chop overexpression may lead to a late block of autophagy, meaning that the fusion between lysosomes and autophagosomes is impaired. However, without further in depth studies focussing on structural interactions between these organelles, such conclusions remains speculation.

6.3 Insufficient cellular quality in IPF AECII

A key factor in the development of IPF is disrupted AECII quality control. In IPF the UPS, UPR, macroautophagy and mitophagy are impaired. All this results in pro-apoptotic ER stress, mitochondrial dysfunction and, finally, epithelial apoptosis, which ultimately drive fibrotic remodelling in the lungs [Beers, M.F. et al. 2017]. Various intrinsic (e.g. genetic) and extrinsic (e.g. infection) factors promote the vulnerability of AECIIs. As mentioned before there are different quality control systems to remove misfolded proteins: The UPR signaling facilitates correct protein folding by expanding ER and attenuated translation. Autophagy removes then the misfolded protein aggregates which could not be proper folded and damaged organelles, like mitochondria (mitophagy). Another quality control system is the ERAD, in which misfolded protein polyubiquitinated via lysine-48, leading to their degradation via proteasome. However, overall failure of all cell quality systems leads to susceptibility of secondary injurious stimuli and this promotes maladaptive ER stress and ultimately cell death. Dysfunctional AECII influence other cell types, like fibroblasts, finally leading to progressive fibrotic remodelling [Katzen, J. et al. 2020]. Such a failure in quality control mechanisms is also reported in familial forms of pulmonary fibrosis as well as in animal models of lung fibrosis [Ahuja, S. et al. 2016, Beers, M.F. et al. 1998, Birkelbach, B. et al. 2015, Brasch, F. et al. 2004, Kesireddy, V.S. et al. 2019, Mahavadi, P. et al. 2015, Wang, K. et al. 2018]. Recent studies have demonstrated that prolonged mutant *SFTPC* expression, like SP-$C^{\Delta exon4}$ mutation impairs both quality control mechanisms, inhibited UPS and autophagy leading to activation of apoptosis [Maguire, J.A. et al. 2011]. These impaired quality control mechanisms leads to impaired clearance of the ubiquitinated aggregates and

accumulation in a time-dependent manner. When the ER capacity for accumulated proteins is exhausted, the mutant proteins are then retro-translocated to the cytosol where aggregates are formed [Maguire, J.A. et al. 2012, Mulugeta, S. et al. 2005]. Further work has demonstrated *SFTPC* BRICHOS mutants increase the expression of the chaperone BiP and UPR to facilitate proper folding of the protein [Mulugeta, S. et al. 2005]. In addition, murine models of *SFTPC* BRICHOS mutants have displayed that this toxic gain of function leads to disrupted AECII and thereby fibrosis [Bridges, J.P. et al. 2003, Katzen, J. et al. 2019].

Non-BRICHOS mutations of *SFTPC* also displayed disturbed trafficking of misfolded pro SP-C and accumulation of these aggregates in the lysosomal compartment, resulting in blocked autophagy flux [Hawkins, A. et al. 2015]. Interestingly, this non-BRICHOS mutation resulted in a loss of mitochondrial transmembrane potential ($\Delta\psi$) and impaired mitophagy [Hawkins, A. et al. 2015]. As mention before, previous ER stress in AECII promotes a reduction in PINK1, an important protein in mitochondrial homeostasis. Of note, intracellular Ca^{2+} regulates surfactant secretion in AECII by stimulating the fusion of laminar bodies to the plasma membrane [Jennings, P. et al. 2005]. Further investigations are required to study if TRPV1 could interfere in this process.

Such mitochondrial dysfunction was also observed in our current study in cells overexpressing Chop and stably cells overexpressing SP-$C^{\Delta exon4}$, next to an upregulation UPR related proteins. Furthermore, MEL188 cells stably overexpressing SP-$C^{\Delta exon4}$ displayed decreased PACS2 and increased TRPV1 as well. These observations are in line with the observations in IPF patients. Accordingly, CPS treatment recovered ER-mitochondrial tethering in all models that we used. This positive effect of CPS treatment could be explained by activation of TRPV1, which in turn could bind to PACS2 and influence PACS2 protein level or activity. Both Chop and SP-$C^{\Delta exon4}$ overexpressing cells showed improved ER-mitochondrial tethering and restoration of PACS2 protein levels upon exposure to the TRPV1 modulating drug, CPS, supporting cell quality control and avoiding apoptosis. While it is clear that ER-mitochondrial tethering is restored, the effect of CPS on autophagy and/or mitophagy in our models still needs to be studied. CPS is known to activate autophagy in several cell types [Chu, H. et al. 2019, Farfariello, V. et al. 2012, Lin, Y.-T. et al. 2017, Qiao, Y. et al. 2021]. Although not show here, it is conceivable that CPS treatment might result in increased autophagy flux, thereby degrading the cellular aggregates and relieving cellular stress events. However,

experimental evidence is required to conclude the additional beneficial effects of CPS in lung fibrosis. Our study also does not fully explain if and how increased TRPV1 protein level interacted with ER stress mechanisms.

6.4 Conclusion

In summary, the results of our current study suggest that the modulation of TRPV1-PACS2 axis by CPS represents a potential therapeutic target for lung fibrosis, proved in two different cell line models (*Chop* overexpression and *SP-C*$^{\Delta exon4}$ overexpressing cells) as well as ex vivo in PCLS derived from IPF patients. CPS not only modulates TRPV1, but also restores PACS2 protein levels and improves ER-mitochondrial tethering. This study provides important insights into the regulation of ER-mitochondrial communication by the TRPV1-PACS2 axis. Our study also shows that targeting this TRPV1-PACS2 axis results in improved AECII survival and reduced collagen deposition, outlining the translational and therapeutic relevance of this axis for lung fibrosis.

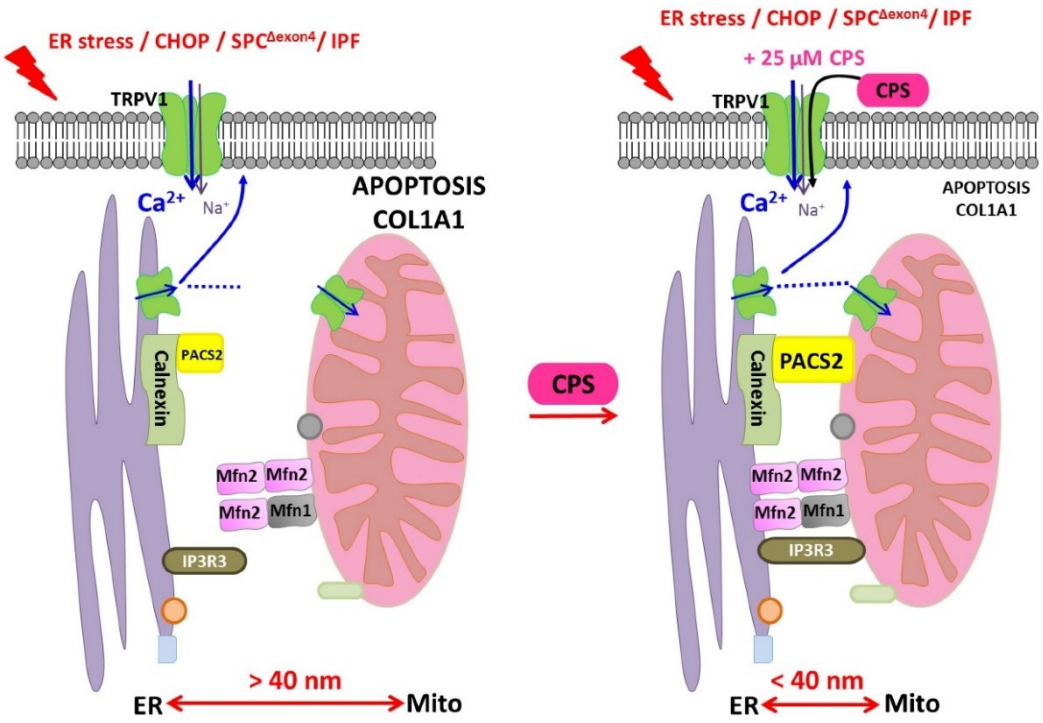

Figure 45 PACS2-TRPV1 axis is required for ER-mitochondrial tethering during ER stress and lung fibrosis

Diagrams summarizing the results of this study: Left side: Upon ER stress / CHOP induction, SP-C$^{\Delta exon4}$ overexpression or in IPF AECII where persistent pro-apoptotic ER stress is observed, this mediates i) Ca^{2+} release from the ER to mitochondria promoting apoptotic signaling pathway, ii) PACS2 reduction leading to disrupted ER-mitochondria tethering and increased distance of over 40nm and iii) altered TRPV1 protein levels. Right side: Upon treatment with CPS, a TRPV1 modulator, PACS2 protein levels are restored, ER-mitochondrial tethering is rescued (10–40 nm) and this supports the inter-organelle communication again and ER and mitochondria are capable to handle ER stress and cell homeostasis can be restored together with a decrease in AECII apoptosis and COL1A1.

Summary

About 20% of mitochondria in a cell are juxtaposed to the ER forming mitochondria associated membranes (MAMs). These dynamic, physical, proteinaceous contacts between ER-mitochondria are required for several physiological functions including Ca^{2+} transfer and signaling molecules that are important to govern critical cell fate decisions. However, under conditions of ER stress, mitochondria relocate to the perinuclear region to tighten their contact with the ER and display an increase in Ca^{2+} uptake, ATP production and oxygen consumption. Upon persistent ER stress, when the unfolded protein response (UPR) fails to resolve such stress, pro-apoptotic signals are triggered leading to apoptotic cell death and these mechanisms have been linked to alterations in the MAMs and MAM proteins. Characteristic MAM proteins involved are inositol 1,4,5-triphosphate receptors (IP_3R), sigma 1 receptor (SigmaR1), calnexin. Certain core mitochondrial proteins, namely dynamin-related protein 1 (DRP1) and mitochondrial fission and fusion regulating proteins, Mitofusin 1 and 2 (MNF1/MFN2) respectively, are also involved in modulating interaction between these two organelles. Another multifaceted sorting protein, phosphofurin acidic cluster sorting protein-2 (PACS2), is also located at the ER-mitochondria interface. An absence of PACS2 leads to mitochondrial fragmentation and uncoupling from the ER.

Persistent ER stress and mitochondrial dysfunction are well-documented pathological mechanisms in the lung alveolar epithelial cells type II (AECII) of patients with idiopathic pulmonary fibrosis (IPF). Although multiple cell types are indicated to contribute to the pathogenesis, chronic injury to the AECII is an accepted key event that triggers the disease process in IPF. In this regard, extensive ER stress signature molecules in the AECII of sporadic IPF patients is reported and that induction of the terminal ER stress pro-apoptotic transcription factor CHOP is sufficient enough to drive lung epithelial cell apoptosis and pro-fibrotic signaling. Supporting this, in familial cases with mutations in the surfactant protein C (SP-C) gene which leads to its protein misfolding, a ‘maladaptive’ pro-apoptotic ER stress has been reported.

In this study, the contribution of MAM proteins towards apoptosis in response to ER stress have been analyzed. The induction of CHOP or pathological ER stress resulted in a decrease in ER-mitochondrial contacts in addition to a decrease in PACS2 as well as a dysregulation of its interactor, TRPV1 which in turn drove cells to apoptosis. A similar reduction in PACS2 as well as altered TRPV1 proteins were observed in cells stably

overexpressing pathologic mutation SP-C$^{\Delta exon4}$ and in AECII of IPF patients. Finally, treatment of *ex-vivo*, three-dimensional lung slices or precision cut lung slices (PCLS) of IPF patients with the TRPV1 modulating drug CPS decreased apoptosis and restored both TRPV1 and PACS2 protein levels. In conclusion, this study shows that targeting of the PACS2-TRPV1 axis represents an interesting novel, epithelial-protective approach in IPF.

Zusammenfassung

Ungefähr 20% der Mitochondrien in einer Zelle sind dicht mit dem ER verbunden. Diese Strukturen werden Mitochondrien assoziierte ER-Membranen (MAM) genannt und sind für viele physiologische Funktionen, unter anderem für den Transfer von Calcium (Ca^{2+}) und kritischen Signalmolekülen verantwortlich. In ER Stress Situationen verlagern sich die Mitochondrien in die perinukleare Region, um die Verbindung mit dem ER zu verstärken. Dadurch erhöhen sich die Ca^{2+} Aufnahme sowie die ATP-Produktion und der Sauerstoffverbrauch in den Mitochondrien. Wenn die "unfolded protein response" (UPR, Antwort ungefaltete Proteine) diesen ER Stress nicht auflösen kann und der ER Stress anhält, werden pro-apoptotische Signale hervorgerufen, die zum Zelltod führen. Dieser Mechanismus führt zu Veränderungen an den MAM und den MAM Proteinen. Zu den charakteristischen MAM Proteinen zählen Inositol 1,4,5,-Triphosphat Rezeptoren (IP3R), Sigma1 Rezeptoren (SigmaR1), Calnexin, Calreticulin, ERp57 und ERp4. Auch mitochondriale Kernproteine, wie Dynamin ähnliches Protein 1 (DRP1) und Mitofusin 1 und 2 (MNF1/MNF2), die mitochondriale Spaltung und Fusionierung regulieren, sind in der Regulierung der beiden Organellen involvieret. Ein weiteres multifunktionales Sortierungsprotein Phosphofurin Acides Cluster Sortierungsprotein 2 (PACS2), befindet sich auch an der Schnittstelle zwischen ER und Mitochondrien. Die Abwesenheit von PACS2 verursacht Fragmentierung der Mitochondrien und Abspaltung vom ER.

Anhaltender ER-Stress und mitochondriale Funktionsstörung in Alveolarepithelzellen Typ II (AECII) der Lungen von Patienten mit idiopathische Lungenfibrose (IPF) sind anerkannte pathologische Mechanismen. Auch wenn viele verschiedene Zelltypen in Zusammenhang mit der Erkrankung stehen, gilt die chronische Schädigung der AECII als anerkanntes Schlüsselereignis für die Entstehung von IPF. Diesbezüglich wurden auch charakteristische Moleküle für extensiven ER-Stress in AECII in Patienten mit sporadischer IPF gefunden. Die Aktivierung des pro-apoptotischen terminalen ER Stress Transkriptionsfaktors CHOP allein ist ausreichend, um Apoptose von Lungenepithelzellen und pro-fibrotische Signalwege anzustoßen. Diese Aussage wird unterstützt durch die Beobachtung, dass es in familiären Fällen, in denen Mutationen des Surfacant Protein C (SP-C) Gen vorliegt, zur fehlerhaften Faltung des Proteins kommt und "maladapitver" pro-apoptotischer ER-Stress entsteht.

In dieser Studie wurden MAM-Proteine im Hinblick auf, durch ER Stress ausgelöste, Apoptose analysiert. Die Aktivierung von CHOP oder pathologischer ER Stress resultiert

in einer Abnahme von ER-mitochondrialem Kontakt. Darüber hinaus wurden auch eine Abnahme von PACS2 und eine fehlerhafte Regulation von seinem Zusammenspieler TRPV1 beobachtet, was wiederum zu Zelltod führt. Ebenso wurden in der stabilen Zelllinie, die eine pathologische Mutation von SP-C (SP-C$^{\Delta exon4}$) überexprimiert, als auch in AECII von IPF Patienten ähnliche Ergebnisse beobachtet. Als letztes wurde festgestellt, dass die Behandlung von *ex vivo*, dreidimensionale Lungenschnitten, auch precision cut lung slices (PCLS) genannt, von IPF Patienten mit TRPV1 Modulator CPS die Apoptose verringert und das Proteinlevel von TRPV1 und PACS2 wiederherstellt. Abschließend lässt sich sagen, dass diese Studie einen interessanten neuen protektiven Ansatz auf das Epithel in IPF darlegt.

List of abbreviations

AB	Antibody
ABCA3	ATP-binding cassette transporter protein A3
AD	Amidarone
AECII	Alveolar epithelial cells type II
AP	Alkalic phosphatase
APS	Ammoniumperoxodisulfate
ARDS	Adult Respiratory Distress Syndrome
ATF6	Activating Transcription Factor 6
ATCC	American Type Culture Collection
Bad	Bcl-2 agonist of cell death
Bak	Bcl-2 homologous antagonist killer
BAL	Bronchoalveolar lavage
Bax	Bcl-2-associated X protein
BCA	Bicinchoninic acid
Bcl-2	B-cell lymphoma 2
Bid	Bcl-2 interacting domain death agonist
BiP	Binding immunoglobulin protein
BLM	Bleomycin
bp	Base pairs
BSA	Bovine Serum Albumin
cDNA	Complementary deoxyribonucleic acid
$CaCl_2$	Calcium chloride
$C_6H_5Na_3O_7$*2 H_2O	Tri-sodium citrate dihydrate
CHOP	CCAAT/ enhancer binding proteins (C/EBP) homologous protein
CT	Computed Tomography
CVD	Collagen-vascular diseases
CPS	Capsaicin
CQ	Chloroquine
DAPI	4′,6-Diamidin-2-phenylindole
DMEM	Dulbecco's Modified Eagle's Medium
DMSO	Dimethylsulfoxid
DNA	Deoxyribonucleic acid

DPLD	Diffuse parenchymal lung disease
dsDNA	Double-strand DNA
DTT	Dithiothreitol
dNTP	Desoxyribonucleosidtriphosphate
ECL	Enhanced Chemiluminescence
ECM	Extracellular matrix
EDEM	ER-degradation enhancing α-mannosidase-like protein
EDTA	Ethylendiamintetraacetate
elF2α	Eukaryotic translation initiation factor 2 subunit alpha
ER	Endoplasmic reticulum
ERAD	ER-associated protein degradation
ERSE	ER Stress response elements
FBS	Fetal Bovine Serum
FCCP	Carbonyl cyanide 4-(trifluoromethoxy) phenylhydrazone
FCS	Fetal Calf Serum
FIP	Familial interstitial pneumonia
FIPF	Familial idiopathic pulmonary fibrosis
GADD 153	Growth arrest and DNA damage 153
GRP78	Glucose regulated protein 78
h	Hours
HEPES	2-(4-(2-Hydroxyethyl)-1-piperazinyl)-ethansulfonic acid
HPS	Hermansky-Pudlak syndrome
HRP	Horseradish Peroxidase
IIP	Idiopathic interstitial pneumonia
IHC	Immunohistochemistry
ILD	Interstitial Lung Disease
IP	Immunoprecipitation
IPF	Idiopathic Pulmonary Fibrosis
IRE1α	Inositol-requiring enzyme 1 alpha
kDa	Kilo Dalton
LB	Luria Bertani
MAM	ER-Mitochondria associated membranes
MEM	Minimum Essential Media
MEM NEAA	MEM Non-Essential Amino Acids Solution

mA	Milliampere
min	Minutes
MNF2	Mitofusin 2
NaOH	Sodium Hydroxide
NaCl	Sodium Chloride
$Na_2HPO_4•2H_2O$	Di-Sodium hydrogenphosphate dehydrate
NCBI	National Center for Biotechnology Information
nt	Nucleotids
KCl	Potassium chloride
KH_2PO_4	Potassium dihydrogenphosphate
LAMP	Lysosome Associated Membrane Protein
LRO	Lysosome related organelles
PBS	Phosphate Buffered Saline
PERK	Protein kinase RNA-like ER kinase
PCR	Polymerase Chain Reaction
PFA	Paraformaldehyde
PMSF	Phenylmethylsulfonylfluorid
PVDF	Polyvinylidene fluoride
RD	Restriction digested
RPMI	Roswell Park Memorial Institute
RNA	Ribonucleic acid
RNase	Ribonuclease
RT	Reverse Transcription
RT	Room Temperature
SDS	Sodium dodecyl sulfate
SDS-PAGE	Sodium dodecyl sulfate polyacrylamide gel electrophoresis
SFTPA2	Surfactant Protein A, gene
SFTPC	Surfactant Protein C, gene
SNARE	Soluble N-ethylmaleimide-sensitive factor-attachment receptor
SP	Surfactant Protein
SP-C	Surfactant Protein C
$SP\text{-}C^{WT}$	Surfactant Protein C, wild type
$SP\text{-}C^{\Delta exon4}$	Surfactant Protein C, deletion exon4 mutant

SR	Sarcoplasmic reticulum
PARP1	Poly(ADP-ribose)-Polymerase 1
TAE	Tris base, acetic acid and EDTA
TC Disch	Tissue Culture Dish
TEMED	N,N,N',N'-Tetramethyl ethylenediamine
TERC	Telomerase RNA component,
TERT	Telomerase reverse transcriptase
Tris	Tris(hydroxymethyl)-aminomethane
UIP	Usual interstitial pneumonia
un	Untreated
UPR	Unfolded protein response
UPS	Ubiquitin/proteasome system
WB	Western Blot
XBP-1	X-box-binding protein 1

List of figures

List of tables

References

Abramowitz, J. et al. Physiology and pathophysiology of canonical transient receptor potential channels. FASEB j. 2009 **23.**(2):297–328

Abrams, R.M.C. et al. A critical review of the capsaicin 8% patch for the treatment of neuropathic pain associated with diabetic peripheral neuropathy of the feet in adults. Expert Rev Neurother. 2021 **21.**(3):259–266

Ahuja, S. et al. MAP1LC3B overexpression protects against Hermansky-Pudlak syndrome type-1-induced defective autophagy in vitro. Am J Physiol Lung Cell Mol Physiol. 2016 **310.**(6):L519-31

Amantini, C. et al. The TRPV1 ion channel regulates thymocyte differentiation by modulating autophagy and proteasome activity. Oncotarget. 2017 **8.**(53):90766–90780

American Thoracic Society. Idiopathic pulmonary fibrosis: diagnosis and treatment. International consensus statement. American Thoracic Society (ATS), and the European Respiratory Society (ERS). Am J Respir Crit Care Med. 2000 **161.**(2 Pt 1):646–664

Amin, R.S. et al. Surfactant protein deficiency in familial interstitial lung disease. J Pediatr. 2001 **139.**(1):85–92

Andreeva, A.V. et al. Regulation of surfactant secretion in alveolar type II cells. Am J Physiol Lung Cell Mol Physiol. 2007 **293.**(2):L259-71

Araya, J. et al. Insufficient autophagy in idiopathic pulmonary fibrosis. Am J Physiol Lung Cell Mol Physiol. 2013 **304.**(1):L56-69

Archer, S.L. Mitochondrial dynamics--mitochondrial fission and fusion in human diseases. N Engl J Med. 2013 **369.**(23):2236–2251

Armanios, M.Y. et al. Telomerase mutations in families with idiopathic pulmonary fibrosis. N Engl J Med. 2007 **356.**(13):1317–1326

Arruda, A.P. et al. Chronic enrichment of hepatic endoplasmic reticulum-mitochondria contact leads to mitochondrial dysfunction in obesity. Nat Med. 2014 **20.**(12):1427–1435

Ashkenazi, A. et al. Death receptors: signaling and modulation. Science. 1998 **281.**(5381):1305–1308

Aslan, J.E. et al. Akt and 14-3-3 control a PACS-2 homeostatic switch that integrates membrane traffic with TRAIL-induced apoptosis. Mol Cell. 2009 **34.**(4):497–509

Axe, E.L. et al. Autophagosome formation from membrane compartments enriched in phosphatidylinositol 3-phosphate and dynamically connected to the endoplasmic reticulum. J Cell Biol. 2008 **182.**(4):685–701

Azuma, A. Shared mechanisms of lung injury and subsequent fibrosis: role of surfactant proteins in the pathogenesis of interstitial pneumonia in Hermansky-Pudlak Syndrome. Intern Med. 2005 **44.**(6):529–530

B Moore, B. et al. Animal models of fibrotic lung disease. Am J Respir Cell Mol Biol. 2013 **49.**(2):167–179

Baek, H.A. et al. Involvement of endoplasmic reticulum stress in myofibroblastic differentiation of lung fibroblasts. Am J Respir Cell Mol Biol. 2012 **46.**(6):731–739

Barbarin, V. et al. The role of pro- and anti-inflammatory responses in silica-induced lung fibrosis. Respir Res. 2005 **6**:112

Barkauskas, C.E. et al. Type 2 alveolar cells are stem cells in adult lung. J Clin Invest. 2013 **123.**(7):3025–3036

Barkauskas, C.E. et al. Cellular mechanisms of tissue fibrosis. 7. New insights into the cellular mechanisms of pulmonary fibrosis. Am J Physiol , Cell Physiol. 2014 **306.**(11):C987-96

Barroso-González, J. et al. PACS-2 mediates the ATM and NF-κB-dependent induction of anti-apoptotic Bcl-xL in response to DNA damage. Cell Death Differ. 2016 **23.**(9):1448–1457

Baumgartner, K.B. et al. Cigarette smoking: a risk factor for idiopathic pulmonary fibrosis. Am J Respir Crit Care Med. 1997 **155.**(1):242–248

B'chir, W. et al. Dual role for CHOP in the crosstalk between autophagy and apoptosis to determine cell fate in response to amino acid deprivation. Cell Signal. 2014 **26.**(7):1385–1391

Beers, M.F. et al. Synthetic processing of surfactant protein C by alevolar epithelial cells. The COOH terminus of proSP-C is required for post-translational targeting and proteolysis. J Biol Chem. 1998 **273.**(24):15287–15293

Beers, M.F. et al. When Is an Alveolar Type 2 Cell an Alveolar Type 2 Cell? A Conundrum for Lung Stem Cell Biology and Regenerative Medicine. Am J Respir Cell Mol Biol. 2017 **57.**(1):18–27

Beike, L. et al. Surfactant dysfunction and alveolar collapse are linked with fibrotic septal wall remodeling in the TGF-β1-induced mouse model of pulmonary fibrosis. Lab Invest. 2019 **99.**(6):830–852

Bernard-Marissal, N. et al. Dysfunction in endoplasmic reticulum-mitochondria crosstalk underlies SIGMAR1 loss of function mediated motor neuron degeneration. Brain. 2015 **138.**(Pt 4):875–890

Berridge, M.J. The endoplasmic reticulum: a multifunctional signaling organelle. Cell Calcium. 2002 **32.**(5-6):235–249

Berridge, M.J. et al. Calcium signalling: dynamics, homeostasis and remodelling. Nat Rev Mol Cell Biol. 2003 **4.**(7):517–529

Bertolotti, A. et al. Dynamic interaction of BiP and ER stress transducers in the unfolded-protein response. Nat Cell Biol. 2000 **2.**(6):326–332

Bilgili, H. et al. Telomere Abnormalities in the Pathobiology of Idiopathic Pulmonary Fibrosis. J Clin Med. 2019 **8.**(8)

Birkelbach, B. et al. Linking progression of fibrotic lung remodeling and ultrastructural alterations of alveolar epithelial type II cells in the amiodarone mouse model. Am J Physiol Lung Cell Mol Physiol. 2015 **309.**(1):L63-75

Böckler, S. et al. Mitochondrial ER contacts are crucial for mitophagy in yeast. Developmental Cell. 2014 **28.**(4):450–458

Bonner, J.C. Lung fibrotic responses to particle exposure. Toxicol Pathol. 2007 **35.**(1):148–153

Bouman, L. et al. Parkin is transcriptionally regulated by ATF4: evidence for an interconnection between mitochondrial stress and ER stress. Cell Death Differ. 2011 **18.**(5):769–782

Braakman, I. et al. Protein folding and modification in the mammalian endoplasmic reticulum. Annual review of biochemistry. 2011 **80**:71–99

Brasch, F. et al. Interstitial lung disease in a baby with a de novo mutation in the SFTPC gene. Eur Respir J. 2004 **24.**(1):30–39

Bravo, R. et al. Increased ER-mitochondrial coupling promotes mitochondrial respiration and bioenergetics during early phases of ER stress. Journal of Cell Science. 2011 **124.**(14):2511

Bridges, J.P. et al. Expression of a human surfactant protein C mutation associated with interstitial lung disease disrupts lung development in transgenic mice. J Biol Chem. 2003 **278.**(52):52739–52746

Brito, O.M. de et al. An intimate liaison: spatial organization of the endoplasmic reticulum-mitochondria relationship. EMBO J. 2010 **29.**(16):2715–2723

Brush, M.H. et al. Growth arrest and DNA damage-inducible protein GADD34 targets protein phosphatase 1 alpha to the endoplasmic reticulum and promotes dephosphorylation of the alpha subunit of eukaryotic translation initiation factor 2. Mol Cell Biol. 2003 **23.**(4):1292–1303

Bueno, M. et al. PINK1 deficiency impairs mitochondrial homeostasis and promotes lung fibrosis. J Clin Invest. 2015 **125.**(2):521–538

Bueno, M. et al. ATF3 represses PINK1 gene transcription in lung epithelial cells to control mitochondrial homeostasis. Aging Cell. 2018 **17.**(2)

Bueno, M. et al. Mitochondria dysfunction and metabolic reprogramming as drivers of idiopathic pulmonary fibrosis. Redox Biol. 2020 **33**:101509

Cameron, H.S. et al. A common mutation in the surfactant protein C gene associated with lung disease. J Pediatr. 2005 **146.**(3):370–375

Camprubí-Robles, M. et al. Differential contribution of SNARE-dependent exocytosis to inflammatory potentiation of TRPV1 in nociceptors. FASEB j. 2009 **23.**(11):3722–3733

Castro, J. et al. A small component of the endoplasmic reticulum is required for store-operated Ca2+ channel activation in liver cells: evidence from studies using TRPV1 and taurodeoxycholic acid. Biochem J. 2009 **418.**(3):553–566

Caterina, M.J. et al. The capsaicin receptor: a heat-activated ion channel in the pain pathway. Nature. 1997 **389.**(6653):816–824

Chu, H. et al. Capsaicin induces apoptosis and autophagy in human melanoma cells. Oncol Lett. 2019 **17.**(6):4827–4834

Committee on Fetus and Newborn et al. Respiratory support in preterm infants at birth. Pediatrics. 2014 **133.**(1):171–174

Conkright, J.J. et al. Secretion of surfactant protein C, an integral membrane protein, requires the N-terminal propeptide. J Biol Chem. 2001 **276.**(18):14658–14664

Csordás, G. et al. Structural and functional features and significance of the physical linkage between ER and mitochondria. J Cell Biol. 2006 **174.**(7):915–921

Cuervo, A.M. et al. A receptor for the selective uptake and degradation of proteins by lysosomes. Science. 1996 **273.**(5274):501–503

Davis, G.S. Pathogenesis of silicosis: current concepts and hypotheses. Lung. 1986 **164.**(3):139–154

Deegan, S. et al. Stress-induced self-cannibalism: on the regulation of autophagy by endoplasmic reticulum stress. Cell Mol Life Sci. 2013 **70.**(14):2425–2441

Deerinck, T.J. et al. Enhancing Serial Block-Face Scanning Electron Microscopy to Enable High Resolution 3-D Nanohistology of Cells and Tissues. Microsc Microanal. 2010 **16.**(S2):1138–1139

Dietrich, A. Modulators of Transient Receptor Potential (TRP) Channels as Therapeutic Options in Lung Disease. Pharmaceuticals (Basel). 2019 **12.**(1)

Ding, W.-X. et al. Differential effects of endoplasmic reticulum stress-induced autophagy on cell survival. J Biol Chem. 2007 **282.**(7):4702–4710

Ding, W.-X. et al. Mitophagy: mechanisms, pathophysiological roles, and analysis. Biol Chem. 2012 **393.**(7):547–564

Djafarzadeh, S. et al. Isolation of Intact Mitochondria from Skeletal Muscle by Differential Centrifugation for High-resolution Respirometry Measurements. J Vis Exp. 2017(121)

Earnshaw, W.C. et al. Mammalian caspases: structure, activation, substrates, and functions during apoptosis. Annual review of biochemistry. 1999 **68**:383–424

Elokely, K. et al. Understanding TRPV1 activation by ligands: Insights from the binding modes of capsaicin and resiniferatoxin. Proc Natl Acad Sci U S A. 2016 **113.**(2):E137-45

Fader, C.M. et al. Autophagy and multivesicular bodies: two closely related partners. Cell Death Differ. 2009 **16.**(1):70–78

Fan, Y. et al. Mechanistic Connections between Endoplasmic Reticulum (ER) Redox Control and Mitochondrial Metabolism. Cells. 2019 **8.**(9)

Farfariello, V. et al. Transient receptor potential vanilloid 1 activation induces autophagy in thymocytes through ROS-regulated AMPK and Atg4C pathways. J Leukoc Biol. 2012 **92.**(3):421–431

Frank, S. et al. The Role of Dynamin-Related Protein 1, a Mediator of Mitochondrial Fission, in Apoptosis. Developmental Cell. 2001 **1.**(4):515–525

Frydas, S. et al. Impact of capsaicin on mast cell inflammation. Int J Immunopathol Pharmacol. 2013 **26.**(3):597–600

Fulton, A.B. Genetic defects and clinical characteristics of patients with a form of oculocutaneous albinism (Hermansky-Pudlak syndrome) correction of (Hennansky-Pudlak). Arch Ophthalmol. 1999 **117.**(2):251–252

Gavory, G. et al. Minimum length requirement of the alignment domain of human telomerase RNA to sustain catalytic activity in vitro. Nucleic Acids Res. 2002 **30.**(20):4470–4480

Gegg, M.E. et al. Mitofusin 1 and mitofusin 2 are ubiquitinated in a PINK1/parkin-dependent manner upon induction of mitophagy. Hum Mol Genet. 2010 **19.**(24):4861–4870

Gorman, A.M. et al. Stress management at the ER: regulators of ER stress-induced apoptosis. Pharmacol Ther. 2012 **134.**(3):306–316

Greider, C.W. et al. A telomeric sequence in the RNA of Tetrahymena telomerase required for telomere repeat synthesis. Nature. 1989 **337.**(6205):331–337

Griese, M. Pulmonary surfactant in health and human lung diseases: state of the art. Eur Respir J. 1999 **13.**(6):1455–1476

Guicciardi, M.E. et al. Cellular inhibitor of apoptosis 1 (cIAP-1) degradation by caspase 8 during TNF-related apoptosis-inducing ligand (TRAIL)-induced apoptosis. Exp Cell Res. 2011 **317.**(1):107–116

Guicciardi, M.E. et al. Cellular Inhibitor of Apoptosis (cIAP)-Mediated Ubiquitination of Phosphofurin Acidic Cluster Sorting Protein 2 (PACS-2) Negatively Regulates Tumor Necrosis Factor-Related Apoptosis-Inducing Ligand (TRAIL) Cytotoxicity. PLoS ONE. 2014 **9.**(3)

Günther, A. et al. Unravelling the progressive pathophysiology of idiopathic pulmonary fibrosis. Eur Respir Rev. 2012 **21.**(124):152–160

Guo, Y. et al. Increased expression of lung TRPV1/TRPA1 in a cough model of bleomycin-induced pulmonary fibrosis in Guinea pigs. BMC Pulm Med. 2019 **19.**(1):27

Gyrd-Hansen, M. et al. IAPs: from caspase inhibitors to modulators of NF-kappaB, inflammation and cancer. Nat Rev Cancer. 2010 **10.**(8):561–574

Hajnóczky, G. et al. The machinery of local Ca2+ signalling between sarco-endoplasmic reticulum and mitochondria. J Physiol. 2000 **529 Pt 1**:69–81

Haller, T. et al. Dynamics of surfactant release in alveolar type II cells. Proc Natl Acad Sci U S A. 1998 **95.**(4):1579–1584

Hamasaki, M. et al. Autophagosomes form at ER-mitochondria contact sites. Nature. 2013 **495.**(7441):389–393

Hamvas, A. et al. Progressive lung disease and surfactant dysfunction with a deletion in surfactant protein C gene. Am J Respir Cell Mol Biol. 2004 **30.**(6):771–776

Han, J. et al. ER-stress-induced transcriptional regulation increases protein synthesis leading to cell death. Nat Cell Biol. 2013 **15.**(5):481–490

Hansen, T.E. et al. Following autophagy step by step. BMC Biol. 2011 **9**:39

Harding, H.P. et al. Perk Is Essential for Translational Regulation and Cell Survival during the Unfolded Protein Response. Mol Cell. 2000 **5.**(5):897–904

Haspel, J.A. et al. Autophagy: a core cellular process with emerging links to pulmonary disease. Am J Respir Crit Care Med. 2011 **184.**(11):1237–1246

Hawkins, A. et al. A non-BRICHOS SFTPC mutant (SP-CI73T) linked to interstitial lung disease promotes a late block in macroautophagy disrupting cellular proteostasis and mitophagy. Am J Physiol Lung Cell Mol Physiol. 2015 **308.**(1):L33-47

Hayashi, T. et al. Sigma-1 receptor chaperones at the ER-mitochondrion interface regulate Ca(2+) signaling and cell survival. Cell. 2007 **131.**(3):596–610

Hayashi-Nishino, M. et al. A subdomain of the endoplasmic reticulum forms a cradle for autophagosome formation. Nat Cell Biol. 2009 **11.**(12):1433–1437

Hayes, A.G. et al. Effects of single doses of capsaicin on nociceptive thresholds in the rodent. Neuropharmacology. 1981 **20.**(5):505–511

Hedskog, L. et al. Modulation of the endoplasmic reticulum-mitochondria interface in Alzheimer's disease and related models. Proc Natl Acad Sci U S A. 2013 **110.**(19):7916–7921

Hetz, C. The unfolded protein response: controlling cell fate decisions under ER stress and beyond. Nat Rev Mol Cell Biol. 2012 **13.**(2):89–102

Hiller, M.M. et al. ER degradation of a misfolded luminal protein by the cytosolic ubiquitin-proteasome pathway. Science. 1996 **273.**(5282):1725–1728

Hom, J.R. et al. Thapsigargin induces biphasic fragmentation of mitochondria through calcium-mediated mitochondrial fission and apoptosis. J Cell Physiol. 2007 **212.**(2):498–508

Horton, R.M. PCR-mediated recombination and mutagenesis. SOEing together tailor-made genes. Mol Biotechnol. 1995 **3.**(2):93–99

Høyer-Hansen, M. et al. Connecting endoplasmic reticulum stress to autophagy by unfolded protein response and calcium. Cell Death Differ. 2007 **14.**(9):1576–1582

Itakura, E. et al. The hairpin-type tail-anchored SNARE syntaxin 17 targets to autophagosomes for fusion with endosomes/lysosomes. Cell. 2012 **151.**(6):1256–1269

Jäger, R. et al. The unfolded protein response at the crossroads of cellular life and death during endoplasmic reticulum stress. Biol Cell. 2012 **104.**(5):259–270

Jara-Oseguera, A. et al. TRPV1: on the road to pain relief. Curr Mol Pharmacol. 2008 **1.**(3):255–269

Jennings, P. et al. Ca2+ induced surfactant secretion in alveolar type II cultures isolated from the H-2Kb-tsA58 transgenic mouse. Cell Physiol Biochem. 2005 **15.**(1-4):159–166

Johnston, J.A. et al. Aggresomes: a cellular response to misfolded proteins. J Cell Biol. 1998 **143.**(7):1883–1898

Joseph, S.K. et al. IP3 receptors in cell survival and apoptosis: Ca2+ release and beyond. Apoptosis. 2007 **12.**(5):951–968

Jung, J. et al. Capsaicin Binds to the Intracellular Domain of the Capsaicin-Activated Ion Channel. The Journal of neuroscience : the official journal of the Society for Neuroscience. 1999 **19.**(2):529–538

Kabore, A.F. et al. Biosynthesis of surfactant protein C: characterization of aggresome formation by EGFP chimeras containing propeptide mutants lacking conserved cysteine residues. Journal of Cell Science. 2001 **114.**(Pt 2):293–302

Kalchiem-Dekel, O. et al. Interstitial Lung Disease and Pulmonary Fibrosis: A Practical Approach for General Medicine Physicians with Focus on the Medical History. J Clin Med. 2018 **7.**(12):476

Karanasios, E. et al. Autophagy initiation by ULK complex assembly on ER tubulovesicular regions marked by ATG9 vesicles. Nat Commun. 2016 **7**:12420

Katzen, J. et al. An SFTPC BRICHOS mutant links epithelial ER stress and spontaneous lung fibrosis. JCI Insight. 2019 **4.**(6)

Katzen, J. et al. Contributions of alveolar epithelial cell quality control to pulmonary fibrosis. J Clin Invest. 2020 **130.**(10):5088–5099

Keane, M.P. et al. Inflammation and angiogenesis in fibrotic lung disease. Semin Respir Crit Care Med. 2006 **27.**(6):589–599

Kesireddy, V.S. et al. Susceptibility of microtubule-associated protein 1 light chain 3β (MAP1LC3B/LC3B) knockout mice to lung injury and fibrosis. FASEB J. 2019 **33.**(11):12392–12408

Khaminets, A. et al. Regulation of endoplasmic reticulum turnover by selective autophagy. Nature. 2015 **522.**(7556):354–358

Kim, K.K. et al. Alveolar epithelial cell mesenchymal transition develops in vivo during pulmonary fibrosis and is regulated by the extracellular matrix. Proc Natl Acad Sci U S A. 2006 **103.**(35):13180–13185

Kincaid, M.M. et al. ERADicate ER stress or die trying. Antioxid Redox Signal. 2007 **9.**(12):2373–2387

Klionsky, D.J. et al. Guidelines for the use and interpretation of assays for monitoring autophagy (3rd edition). Autophagy. 2016 **12.**(1):1–222

Klymenko et al. Regulation and role of the pro-apoptotic transcription factor C/EBP homologous protein (CHOP) in type II cells apoptosis and Idiopathic Pulmonary Fibrosis (IPF). 2016

Klymenko, O. et al. Regulation and role of the ER stress transcription factor CHOP in alveolar epithelial type-II cells. J Mol Med. 2019 **97.**(7):973–990

Korfei, M. et al. Epithelial endoplasmic reticulum stress and apoptosis in sporadic idiopathic pulmonary fibrosis. Am J Respir Crit Care Med. 2008 **178.**(8):838–846

Kota, A. et al. Autophagy and airway fibrosis: Is there a link? F1000Res. 2017 **6**:409

Kotani, T. et al. The Atg2-Atg18 complex tethers pre-autophagosomal membranes to the endoplasmic reticulum for autophagosome formation. Proc Natl Acad Sci U S A. 2018 **115.**(41):10363–10368

Köttgen, M. et al. Trafficking of TRPP2 by PACS proteins represents a novel mechanism of ion channel regulation. EMBO J. 2005 **24.**(4):705–716

Kuwano, K. et al. Mitochondria-mediated apoptosis of lung epithelial cells in idiopathic interstitial pneumonias. Lab Invest. 2002 **82.**(12):1695–1706

Lai, C.K. et al. Histopathology of pulmonary fibrotic disorders. Semin Respir Crit Care Med. 2006 **27.**(6):613–622

Lamb, C.A. et al. The autophagosome: origins unknown, biogenesis complex. Nat Rev Mol Cell Biol. 2013 **14.**(12):759–774

Larson-Casey, J.L. et al. Macrophage Akt1 Kinase-Mediated Mitophagy Modulates Apoptosis Resistance and Pulmonary Fibrosis. Immunity. 2016 **44.**(3):582–596

Lawson, W.E. et al. Endoplasmic reticulum stress in alveolar epithelial cells is prominent in IPF: association with altered surfactant protein processing and herpesvirus infection. Am J Physiol Lung Cell Mol Physiol. 2008 **294.**(6):L1119-26

Lawson, W.E. et al. Endoplasmic reticulum stress enhances fibrotic remodeling in the lungs. Proc Natl Acad Sci U S A. 2011 **108.**(26):10562–10567

Lee, A.S. The ER chaperone and signaling regulator GRP78/BiP as a monitor of endoplasmic reticulum stress. Methods. 2005 **35.**(4):373–381

Li, C. et al. PACS-2: A key regulator of mitochondria-associated membranes (MAMs). Pharmacological research. 2020 **160**:105080

Li, W. et al. Microautophagy: lesser-known self-eating. Cell Mol Life Sci. 2012 **69.**(7):1125–1136

Li, X. et al. Mesenchymal stem cells in idiopathic pulmonary fibrosis. Oncotarget. 2017 **8.**(60):102600–102616

Lin, J.H. et al. Endoplasmic reticulum stress in disease pathogenesis. Annu Rev Pathol. 2008 **3**:399–425

Lin, Y.-T. et al. Capsaicin Induces Autophagy and Apoptosis in Human Nasopharyngeal Carcinoma Cells by Downregulating the PI3K/AKT/mTOR Pathway. Int J Mol Sci. 2017 **18.**(7)

Liu, C.Y. et al. Ligand-independent dimerization activates the stress response kinases IRE1 and PERK in the lumen of the endoplasmic reticulum. J Biol Chem. 2000 **275.**(32):24881–24885

Liu, G. et al. Molecular mechanisms of asbestos-induced lung epithelial cell apoptosis. Chem Biol Interact. 2010 **188.**(2):309–318

Liu, G. et al. Use of precision cut lung slices as a translational model for the study of lung biology. Respir Res. 2019 **20.**(1):162

Lok, S.S. et al. Murine gammaherpes virus as a cofactor in the development of pulmonary fibrosis in bleomycin resistant mice. Eur Respir J. 2002 **20.**(5):1228–1232

Lu, L.M. et al. Effect of small dose capsaicin for treatment of pulmonary fibrosis in mice and its mechanism. Zhongguo Ying Yong Sheng Li Xue Za Zhi. 2020 **36.**(3):216–222

Lv, X. et al. Autophagy and Pulmonary Fibrosis. Adv Exp Med Biol. 2020 **1207**:569–579

Lynch, D.A. et al. Diagnostic criteria for idiopathic pulmonary fibrosis: a Fleischner Society White Paper. The Lancet Respiratory Medicine. 2018 **6.**(2):138–153

Ma, Y. et al. Two Distinct Stress Signaling Pathways Converge Upon the CHOP Promoter During the Mammalian Unfolded Protein Response. Journal of Molecular Biology. 2002 **318.**(5):1351–1365

Maguire, J.A. et al. Endoplasmic reticulum stress induced by surfactant protein C BRICHOS mutants promotes proinflammatory signaling by epithelial cells. Am J Respir Cell Mol Biol. 2011 **44.**(3):404–414

Maguire, J.A. et al. Multiple ways to die: delineation of the unfolded protein response and apoptosis induced by Surfactant Protein C BRICHOS mutants. Int J Biochem Cell Biol. 2012 **44.**(1):101–112

Mahavadi, P. Role of impaired lysosomal trafficking in the development of lung fibrosis in a murine model of Hermansky-Pudlak syndrome. 2009

Mahavadi, P. et al. Altered surfactant homeostasis and alveolar epithelial cell stress in amiodarone-induced lung fibrosis. Toxicol Sci. 2014 **142.**(1):285–297

Mahavadi, P. et al. Regulation of macroautophagy in amiodarone-induced pulmonary fibrosis. J Pathol Clin Res. 2015 **1.**(4):252–263

Matsuda, N. et al. PINK1 stabilized by mitochondrial depolarization recruits Parkin to damaged mitochondria and activates latent Parkin for mitophagy. J Cell Biol. 2010 **189.**(2):211–221

McCullough, K.D. et al. Gadd153 sensitizes cells to endoplasmic reticulum stress by down-regulating Bcl2 and perturbing the cellular redox state. Mol Cell Biol. 2001 **21.**(4):1249–1259

Medina, D.L. et al. Lysosomal calcium signalling regulates autophagy through calcineurin and TFEB. Nat Cell Biol. 2015 **17.**(3):288–299

Mi, S. et al. Blocking IL-17A promotes the resolution of pulmonary inflammation and fibrosis via TGF-beta1-dependent and -independent mechanisms. J Immunol. 2011 **187.**(6):3003–3014

Moore, B.B. et al. Murine models of pulmonary fibrosis. Am J Physiol Lung Cell Mol Physiol. 2008 **294.**(2):L152-60

Mora, A.L. et al. Mitochondria in the spotlight of aging and idiopathic pulmonary fibrosis. J Clin Invest. 2017 **127.**(2):405–414

Moretti, F. et al. TMEM41B is a novel regulator of autophagy and lipid mobilization. EMBO Rep. 2018 **19.**(9)

Mori, A. et al. Capsaicin, a component of red peppers, inhibits the growth of androgen-independent, p53 mutant prostate cancer cells. Cancer Res. 2006 **66.**(6):3222–3229

Moulis, M. et al. The Multifunctional Sorting Protein PACS-2 Controls Mitophagosome Formation in Human Vascular Smooth Muscle Cells through Mitochondria-ER Contact Sites. Cells. 2019 **8.**(6)

Mueller-Mang, C. et al. What every radiologist should know about idiopathic interstitial pneumonias. Radiographics. 2007 **27.**(3):595–615

Mulugeta, S. et al. A surfactant protein C precursor protein BRICHOS domain mutation causes endoplasmic reticulum stress, proteasome dysfunction, and caspase 3 activation. Am J Respir Cell Mol Biol. 2005 **32.**(6):521–530

Mulugeta, S. et al. Misfolded BRICHOS SP-C mutant proteins induce apoptosis via caspase-4- and cytochrome c-related mechanisms. Am J Physiol Lung Cell Mol Physiol. 2007 **293.**(3):L720-9

Mulugeta, S. et al. Lost after translation: insights from pulmonary surfactant for understanding the role of alveolar epithelial dysfunction and cellular quality control in fibrotic lung disease. Am J Physiol Lung Cell Mol Physiol. 2015 **309.**(6):L507-25

Murrow, L. et al. Autophagy as a stress-response and quality-control mechanism: implications for cell injury and human disease. Annu Rev Pathol. 2013 **8**:105–137

Myhill, N. et al. The subcellular distribution of calnexin is mediated by PACS-2. Mol Biol Cell. 2008 **19.**(7):2777–2788

Nakajima, K. et al. Involvement of BNIP1 in apoptosis and endoplasmic reticulum membrane fusion. EMBO J. 2004 **23.**(16):3216–3226

Nilius, B., Flockerzi, V. Mammalian Transient Receptor Potential (TRP) Cation Channels, vol. 222. Springer Berlin Heidelberg, Berlin, Heidelberg (2014)

Noble, P.W. et al. Back to the future: historical perspective on the pathogenesis of idiopathic pulmonary fibrosis. Am J Respir Cell Mol Biol. 2005 **33.**(2):113–120

Noda, T. et al. Atg14L recruits PtdIns 3-kinase to the ER for autophagosome formation. Autophagy. 2011 **7.**(4):438–439

Nogee, L.M. et al. A mutation in the surfactant protein C gene associated with familial interstitial lung disease. N Engl J Med. 2001 **344.**(8):573–579

Novakova-Tousova, K. et al. Functional changes in the vanilloid receptor subtype 1 channel during and after acute desensitization. Neuroscience. 2007 **149.**(1):144–154

Novoa, I. et al. Feedback inhibition of the unfolded protein response by GADD34-mediated dephosphorylation of eIF2alpha. J Cell Biol. 2001 **153.**(5):1011–1022

Nureki, S.-I. et al. Expression of mutant Sftpc in murine alveolar epithelia drives spontaneous lung fibrosis. J Clin Invest. 2018 **128.**(9):4008–4024

Ogata, M. et al. Autophagy is activated for cell survival after endoplasmic reticulum stress. Mol Cell Biol. 2006 **26.**(24):9220–9231

Oh, S.-H. et al. Endoplasmic reticulum stress-mediated autophagy/apoptosis induced by capsaicin (8-methyl-N-vanillyl-6-nonenamide) and dihydrocapsaicin is regulated by the extent of c-Jun NH2-terminal kinase/extracellular signal-regulated kinase activation in WI38 lung epithelial fibroblast cells. J Pharmacol Exp Ther. 2009 **329.**(1):112–122

Okatsu, K. et al. p62/SQSTM1 cooperates with Parkin for perinuclear clustering of depolarized mitochondria. Genes Cells. 2010 **15.**(8):887–900

Olson, H.E. et al. A Recurrent De Novo PACS2 Heterozygous Missense Variant Causes Neonatal-Onset Developmental Epileptic Encephalopathy, Facial Dysmorphism, and Cerebellar Dysgenesis. Am J Hum Genet. 2018 **102.**(5):995–1007

Oyadomari, S. et al. Targeted disruption of the Chop gene delays endoplasmic reticulum stress-mediated diabetes. J Clin Invest. 2002 **109.**(4):525–532

Patel, A.S. et al. Autophagy in idiopathic pulmonary fibrosis. PLoS ONE. 2012 **7.**(7):e41394

Patel, A.S. et al. Epithelial cell mitochondrial dysfunction and PINK1 are induced by transforming growth factor-beta1 in pulmonary fibrosis. PLoS ONE. 2015 **10.**(3):e0121246

Piccini, M. et al. FACL4, a new gene encoding long-chain acyl-CoA synthetase 4, is deleted in a family with Alport syndrome, elliptocytosis, and mental retardation. Genomics. 1998 **47.**(3):350–358

Pierson, D.M. et al. Pulmonary fibrosis in hermansky-pudlak syndrome. a case report and review. Respiration. 2006 **73.**(3):382–395

Pinton, P. et al. Bcl-2 and Ca2+ homeostasis in the endoplasmic reticulum. Cell Death Differ. 2006 **13.**(8):1409–1418

Pitts, K.R. et al. The dynamin-like protein DLP1 is essential for normal distribution and morphology of the endoplasmic reticulum and mitochondria in mammalian cells. Mol Biol Cell. 1999 **10.**(12):4403–4417

Pradelli, L.A. et al. Mitochondrial control of caspase-dependent and -independent cell death. Cell Mol Life Sci. 2010 **67.**(10):1589–1597

Prado, C.M. et al. Inactivation of capsaicin-sensitive nerves reduces pulmonary remodeling in guinea pigs with chronic allergic pulmonary inflammation. Braz J Med Biol Res. 2011 **44.**(2):130–139

Puthalakath, H. et al. ER stress triggers apoptosis by activating BH3-only protein Bim. Cell. 2007 **129.**(7):1337–1349

Qiao, Y. et al. Capsaicin protects cardiomyocytes against lipopolysaccharide-induced damage via 14-3-3γ-mediated autophagy augmentation. Front Pharmacol. 2021 **12**:659015

Raghu, G. et al. An official ATS/ERS/JRS/ALAT statement: idiopathic pulmonary fibrosis: evidence-based guidelines for diagnosis and management. Am J Respir Crit Care Med. 2011 **183.**(6):788–824

Rainbolt, T.K. et al. Stress-responsive regulation of mitochondria through the ER unfolded protein response. Trends Endocrinol Metab. 2014 **25.**(10):528–537

Rashid, H.-O. et al. ER stress: Autophagy induction, inhibition and selection. Autophagy. 2015 **11.**(11):1956–1977

Ricci, A. et al. Decreased expression of autophagic beclin 1 protein in idiopathic pulmonary fibrosis fibroblasts. J Cell Physiol. 2013 **228.**(7):1516–1524

Rizzuto, R. et al. Close contacts with the endoplasmic reticulum as determinants of mitochondrial Ca2+ responses. Science. 1998 **280.**(5370):1763–1766

Roberts, S.N. et al. A novel model for human interstitial lung disease: hapten-driven lung fibrosis in rodents. The Journal of pathology. 1995 **176.**(3):309–318

Rubinsztein, D.C. et al. Mechanisms of autophagosome biogenesis. Curr Biol. 2012 **22.**(1):R29-34

Russo, S.J. et al. Structural requirements for intracellular targeting of SP-C proprotein. Am J Physiol. 1999 **277.**(5):L1034-44

Salvesen, G.S. et al. IAP proteins: blocking the road to death's door. Nat Rev Mol Cell Biol. 2002 **3.**(6):401–410

Sanchez, V.C. et al. Biopersistence and potential adverse health impacts of fibrous nanomaterials: what have we learned from asbestos? Wiley Interdiscip Rev Nanomed Nanobiotechnol. 2009 **1.**(5):511–529

Sardiello, M. et al. A gene network regulating lysosomal biogenesis and function. Science. 2009 **325.**(5939):473–477

Schröder, M. et al. The mammalian unfolded protein response. Annual review of biochemistry. 2005 **74**:739–789

Selman, M. et al. Idiopathic pulmonary fibrosis: misunderstandings between epithelial cells and fibroblasts? Sarcoidosis Vasc Diffuse Lung Dis. 2004 **21.**(3):165–172

Selman, M. et al. Role of epithelial cells in idiopathic pulmonary fibrosis: from innocent targets to serial killers. Proceedings of the American Thoracic Society. 2006 **3.**(4):364–372

Selman, M. et al. Aging and interstitial lung diseases: unraveling an old forgotten player in the pathogenesis of lung fibrosis. Semin Respir Crit Care Med. 2010 **31.**(5):607–617

Senft, D. et al. UPR, autophagy, and mitochondria crosstalk underlies the ER stress response. Trends Biochem Sci. 2015 **40.**(3):141–148

Settembre, C. et al. TFEB links autophagy to lysosomal biogenesis. Science. 2011 **332.**(6036):1429–1433

Shen, J. et al. Dependence of site-2 protease cleavage of ATF6 on prior site-1 protease digestion is determined by the size of the luminal domain of ATF6. J Biol Chem. 2004 **279.**(41):43046–43051

Sheng, J. et al. Capsaicin attenuates liver fibrosis by targeting Notch signaling to inhibit TNF-α secretion from M1 macrophages. Immunopharmacol Immunotoxicol. 2020 **42.**(6):556–563

Shi, J. et al. The ER stress-mediated mitochondrial apoptotic pathway and MAPKs modulate tachypacing-induced apoptosis in HL-1 atrial myocytes. PLoS ONE. 2015 **10.**(2):e0117567

Shibutani, S.T. et al. A current perspective of autophagosome biogenesis. Cell Res. 2014 **24.**(1):58–68

Simmen, T. et al. PACS-2 controls endoplasmic reticulum-mitochondria communication and Bid-mediated apoptosis. EMBO J. 2005 **24.**(4):717–729

Solarin, K.O. et al. Synthesis and post-translational processing of surfactant protein C. Pediatr Pathol Mol Med. 2001 **20.**(6):471–500

Sosulski, M.L. et al. Deregulation of selective autophagy during aging and pulmonary fibrosis: the role of TGFβ1. Aging Cell. 2015 **14.**(5):774–783

Su, J. et al. Bcl-2 family proteins are involved in the signal crosstalk between endoplasmic reticulum stress and mitochondrial dysfunction in tumor chemotherapy resistance. Biomed Res Int. 2014 **2014**:234370

Sukumaran, P. et al. Functional role of TRP channels in modulating ER stress and Autophagy. Cell Calcium. 2016 **60.**(2):123–132

Tanaka, Y. et al. The exacerbating roles of CCAAT/enhancer-binding protein homologous protein (CHOP) in the development of bleomycin-induced pulmonary

fibrosis and the preventive effects of tauroursodeoxycholic acid (TUDCA) against pulmonary fibrosis in mice. Pharmacological research. 2015 **99**:52–62

Tandan, R. et al. Topical capsaicin in painful diabetic neuropathy. Controlled study with long-term follow-up. Diabetes Care. 1992 **15.**(1):8–14

Tanjore, H. et al. Emerging evidence for endoplasmic reticulum stress in the pathogenesis of idiopathic pulmonary fibrosis. Am J Physiol Lung Cell Mol Physiol. 2012 **302.**(8):L721-9

Thomas, A.Q. et al. Heterozygosity for a surfactant protein C gene mutation associated with usual interstitial pneumonitis and cellular nonspecific interstitial pneumonitis in one kindred. Am J Respir Crit Care Med. 2002 **165.**(9):1322–1328

Thomas, K.C. et al. Transient receptor potential vanilloid 1 agonists cause endoplasmic reticulum stress and cell death in human lung cells. J Pharmacol Exp Ther. 2007 **321.**(3):830–838

Thomas, K.C. et al. Contributions of TRPV1, endovanilloids, and endoplasmic reticulum stress in lung cell death in vitro and lung injury. Am J Physiol Lung Cell Mol Physiol. 2012 **302.**(1):L111-9

Thoudam, T. et al. Role of Mitochondria-Associated Endoplasmic Reticulum Membrane in Inflammation-Mediated Metabolic Diseases. Mediators Inflamm. 2016 **2016**:1851420

Uhal, B.D. Cell cycle kinetics in the alveolar epithelium. Am J Physiol. 1997 **272.**(6 Pt 1):L1031-45

van Vliet, A.R. et al. New functions of mitochondria associated membranes in cellular signaling. Biochim Biophys Acta. 2014 **1843.**(10):2253–2262

Vannuvel, K. et al. Functional and morphological impact of ER stress on mitochondria. J Cell Physiol. 2013 **228.**(9):1802–1818

Varone, F. et al. Nintedanib for the treatment of idiopathic pulmonary fibrosis. Expert Opin Pharmacother. 2018 **19.**(2):167–175

Veeresh, P. et al. Endoplasmic reticulum-mitochondria crosstalk: from junction to function across neurological disorders. Ann N Y Acad Sci. 2019 **1457.**(1):41–60

Vyklický, L. et al. Temperature coefficient of membrane currents induced by noxious heat in sensory neurones in the rat. J Physiol. 1999 **517 (Pt 1)**:181–192

Wang, K. et al. Identification of ANXA2 (annexin A2) as a specific bleomycin target to induce pulmonary fibrosis by impeding TFEB-mediated autophagic flux. Autophagy. 2018 **14.**(2):269–282

Wang, W.-J. et al. Deletion of exon 4 from human surfactant protein C results in aggresome formation and generation of a dominant negative. Journal of Cell Science. 2003 **116.**(Pt 4):683–692

Wang, X. The expanding role of mitochondria in apoptosis. Genes & Development. 2001 **15.**(22):2922–2933

Wang, Y. et al. Activation of ATF6 and an ATF6 DNA binding site by the endoplasmic reticulum stress response. J Biol Chem. 2000 **275.**(35):27013–27020

Wang, Y.-Y. et al. TRPV1 Antagonist DWP05195 Induces ER Stress-Dependent Apoptosis through the ROS-p38-CHOP Pathway in Human Ovarian Cancer Cells. Cancers (Basel). 2020 **12.**(6)

Weaver, T.E. et al. Biogenesis of lamellar bodies, lysosome-related organelles involved in storage and secretion of pulmonary surfactant. Semin Cell Dev Biol. 2002 **13.**(4):263–270

Wei, X. et al. Activation of TRPV1 channel antagonizes diabetic nephropathy through inhibiting endoplasmic reticulum-mitochondria contact in podocytes. Metabolism. 2020 **105**:154182

Wei, Y. et al. Reduced endoplasmic reticulum luminal calcium links saturated fatty acid-mediated endoplasmic reticulum stress and cell death in liver cells. Mol Cell Biochem. 2009 **331.**(1-2):31–40

Werneburg, N.W. et al. Tumor necrosis factor-related apoptosis-inducing ligand (TRAIL) protein-induced lysosomal translocation of proapoptotic effectors is mediated by phosphofurin acidic cluster sorting protein-2 (PACS-2). J Biol Chem. 2012 **287.**(29):24427–24437

Wirawan, E. et al. Autophagy: for better or for worse. Cell Res. 2012 **22.**(1):43–61

Wolters, P.J. et al. Pathogenesis of idiopathic pulmonary fibrosis. Annu Rev Pathol. 2014 **9**:157–179

Yang, F. et al. Understand spiciness: mechanism of TRPV1 channel activation by capsaicin. Protein Cell. 2017 **8.**(3):169–177

Yao, Y. et al. Chop Deficiency Protects Mice Against Bleomycin-induced Pulmonary Fibrosis by Attenuating M2 Macrophage Production. Mol Ther. 2016 **24.**(5):915–925

Yildirim, H. et al. Investigation of telomere related gene mutations in idiopathic pulmonary fibrosis. Mol Biol Rep. 2020 **47.**(10):7851–7860

Ylä-Anttila, P. et al. 3D tomography reveals connections between the phagophore and endoplasmic reticulum. Autophagy. 2009 **5.**(8):1180–1185

Yoneshima, E. et al. The Transcription Factor EB (TFEB) Regulates Osteoblast Differentiation Through ATF4/CHOP-Dependent Pathway. J Cell Physiol. 2016 **231.**(6):1321–1333

Yorimitsu, T. et al. Autophagy: molecular machinery for self-eating. Cell Death Differ. 2005 **12 Suppl 2**:1542–1552

Yoshida, H. et al. XBP1 mRNA Is Induced by ATF6 and Spliced by IRE1 in Response to ER Stress to Produce a Highly Active Transcription Factor. Cell. 2001 **107.**(7):881–891

Yoshida, H. ER stress and diseases. FEBS J. 2007 **274.**(3):630–658

Youker, R.T. et al. At the crossroads of homoeostasis and disease: roles of the PACS proteins in membrane traffic and apoptosis. Biochem J. 2009 **421.**(1):1–15

Youle, R.J. et al. Mechanisms of mitophagy. Nat Rev Mol Cell Biol. 2011 **12.**(1):9–14

Yu, S. et al. PACS2 is required for ox-LDL-induced endothelial cell apoptosis by regulating mitochondria-associated ER membrane formation and mitochondrial Ca2+ elevation. Exp Cell Res. 2019 **379.**(2):191–202

Zank, D.C. et al. Idiopathic Pulmonary Fibrosis: Aging, Mitochondrial Dysfunction, and Cellular Bioenergetics. Front Med (Lausanne). 2018 **5**:10

Zhang, J. Teaching the basics of autophagy and mitophagy to redox biologists--mechanisms and experimental approaches. Redox Biol. 2015 **4**:242–259

Zhang, L. et al. Endoplasmic reticulum stress, a new wrestler, in the pathogenesis of idiopathic pulmonary fibrosis. Am J Transl Res. 2017 **9.**(2):722–735

Zhang, S. et al. Role of capsaicin sensitive sensory nerves in ischemia reperfusion-induced acute kidney injury in rats. Biochem Biophys Res Commun. 2018 **506.**(1):176–182

Zhao, L. et al. Enriched endoplasmic reticulum-mitochondria interactions result in mitochondrial dysfunction and apoptosis in oocytes from obese mice. J Anim Sci Biotechnol. 2017 **8**:62

Zinszner, H. et al. CHOP is implicated in programmed cell death in response to impaired function of the endoplasmic reticulum. Genes & Development. 1998 **12.**(7):982–995

Appendix

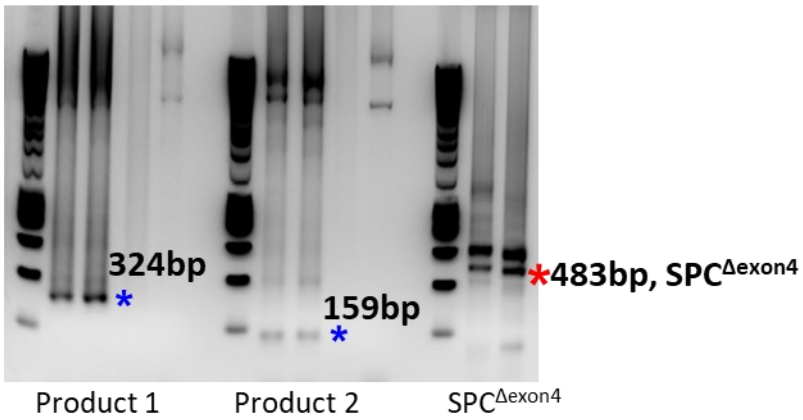

Supplementary figure 1 Gene Splicing by Overlap Extension for generation SP-C$^{\Delta exon4}$

A. Schematic representation of Gene Splicing by Overlap Extension PCR reaction (SOEing PCR) resulting in depletion of Exon 4 of SP-C gene. **B.** Agarose gel picture showing Product 1 (324 bp) and Product 2 (159 bp) and the fused product (483 bp) resulting in *SP-C$^{\Delta exon4}$*.

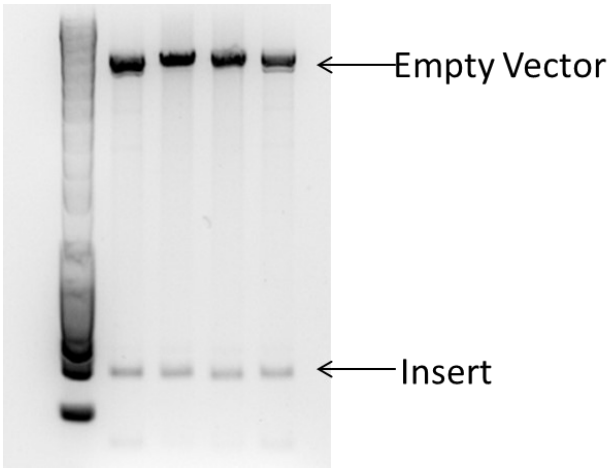

Supplementary figure 2 Insert Release of SP-C$^{\Delta exon4}$

Agarose gel picture showing insert release of positive SP-C$^{\Delta exon4}$ clones.

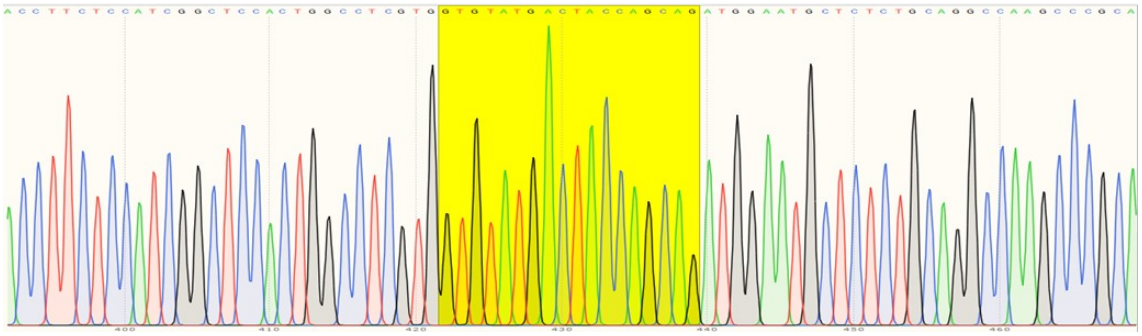

Supplementary figure 3 Sequencing of SP-C$^{\Delta exon4}$
Detail of full sequence of SP-C$^{\Delta exon4}$. Highlighted sequence shows overlap of Product 1 and Product 2

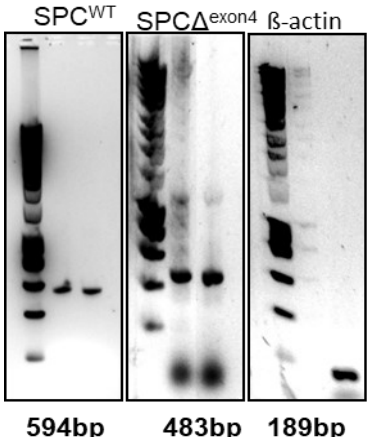

Supplementary figure 4 Semi-quantitative PCR of stable SP-C and SP-C$^{\Delta exon4}$
Agarose gel picture showing SP-C^{WT} (594 bp) and SP-C$^{\Delta exon4}$ (483 bp) and ß-actin (189 bp)

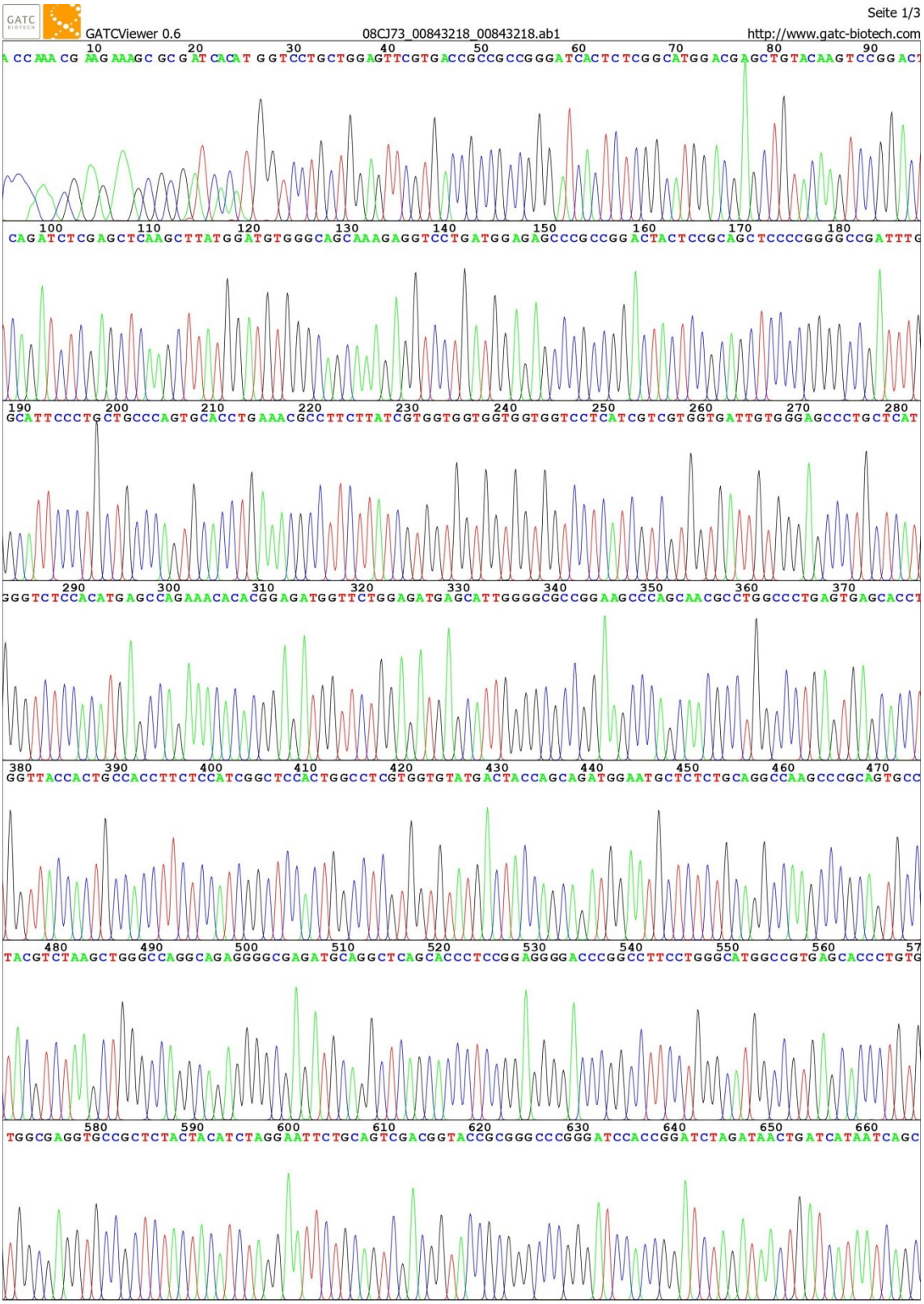
GATCViewer 0.6
08CJ73_00843218_00843218.ab1
http://www.gatc-biotech.com
Seite 1/3

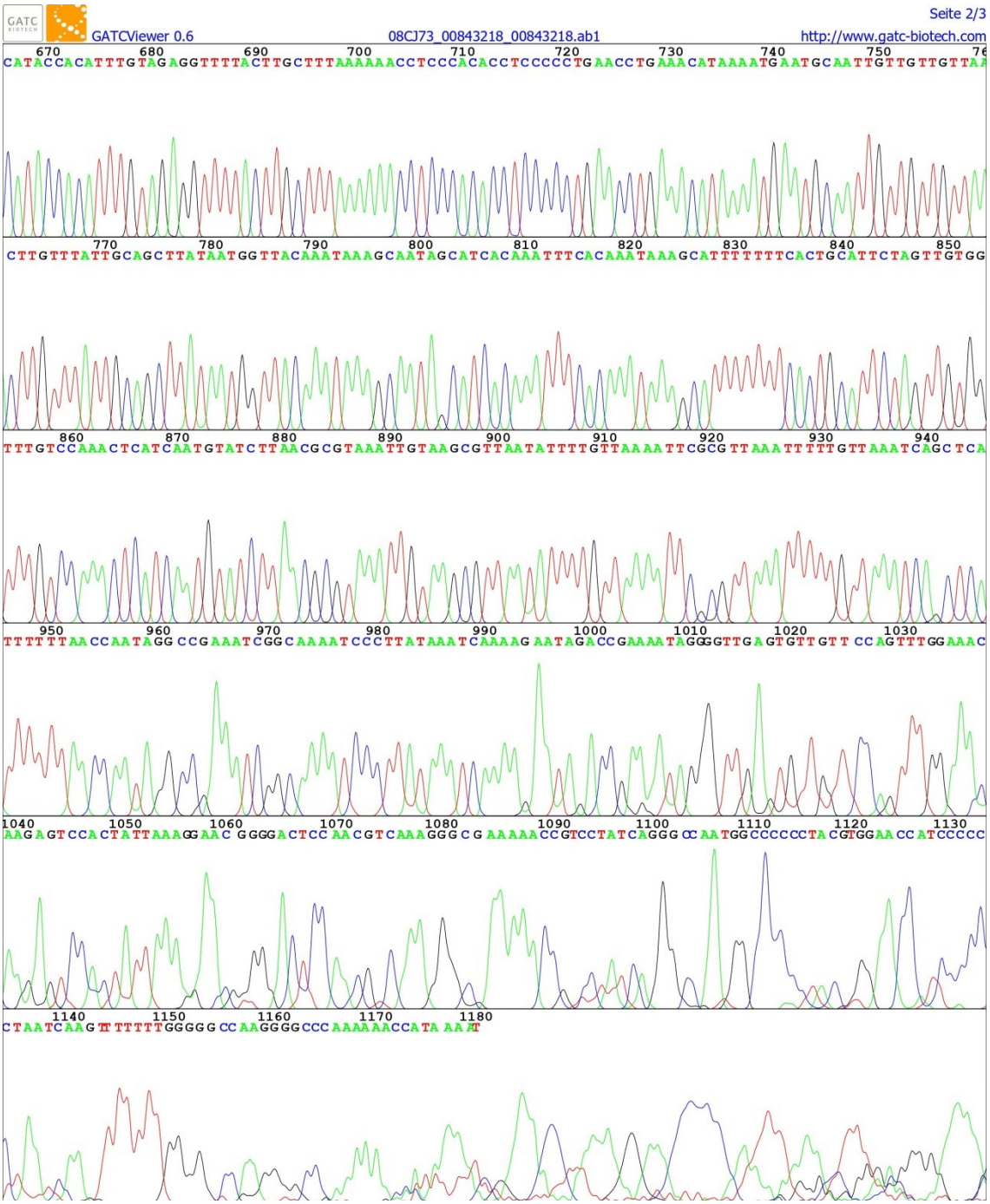

Supplementary figure 5 Full length Sequencing of SP-C$^{\Delta exon4}$

List of publications

Paper

Knoell J. et al. PACS2-TRPV1 axis is required for ER-mitochondrial tethering during ER stress and lung fibrosis. Cell Mol Life Sci. 2022 Feb 25;**79**(3):151

Chillappagari S., Schwarz J., Kesireddy V., **Knoell J.**, Korfei M., Hoetzenecker K., Schmitz M.L., Behl C., Bellusci S., Guenther A., Mahavadi P. Therapeutic induction of Bcl2-associated athanogene 3-mediated autophagy in idiopathic pulmonary fibrosis. Clin Transl Med. 2022 Jul;**12**(7):e935.

Congress contributions

Deutsches Zentrum für Lungenforschung (DZL) Annual Meeting in Heidelberg, 2018 (poster)

Molecular Biology and Medicine of the Lung (MBML) Retreat in Rauischholzhausen, 2018 (poster)

Deutsche Gesellschaft für Pneumologie (DGP) Annual Meeting in Essen, 2018 (poster)

DZL Annual Meeting in Mannheim, 2019 (poster)

DGP Annual Meeting in München, 2019 (poster)

American Thoracic Society (ATS) Conference in Dallas, 2019 (poster)

Cardio-Pulmonary Institute (CPI) Annual Meeting in Bad Nauheim, 2019 (poster+ teaser)

Diffuse Parenchymal Lung Disease (DPLD) Annual Meeting in Hannover, 2019 (poster)

MBML Retreat in Rauischholzhausen, 2019 (presentation)

DZL Annual Meeting in Travemünde, 2020 (poster)

Completion of International Graduate Programme MBML over the period October 2017 to June 2020 (receive three Student Travel Award be attaining once first and twice second place in the Student Examination)

Ehrenwörtliche Erklärung

„Hiermit erkläre ich, dass ich die vorliegende Arbeit selbständig und ohne unzulässige Hilfe oder Benutzung anderer als der angegebenen Hilfsmittel angefertigt habe. Alle Textstellen, die wörtlich oder sinngemäß aus veröffentlichten oder nichtveröffentlichten Schriften entnommen sind, und alle Angaben, die auf mündlichen Auskünften beruhen, sind als solche kenntlich gemacht. Bei den von mir durchgeführten und in der Dissertation erwähnten Untersuchungen habe ich die Grundsätze guter wissenschaftlicher Praxis, wie sie in der „Satzung der Justus-Liebig-Universität Gießen zur Sicherung guter wissenschaftlicher Praxis“ niedergelegt sind, eingehalten sowie ethische, datenschutzrechtliche und tierschutzrechtliche Grundsätze befolgt. Ich versichere, dass Dritte von mir weder unmittelbar noch mittelbar geldwerte Leistungen für Arbeiten erhalten haben, die im Zusammenhang mit dem Inhalt der vorgelegten Dissertation stehen, und dass die vorgelegte Arbeit weder im Inland noch im Ausland in gleicher oder ähnlicher Form einer anderen Prüfungsbehörde zum Zweck einer Promotion oder eines anderen Prüfungsverfahrens vorgelegt wurde. Alles aus anderen Quellen und von anderen Personen übernommene Material, das in der Arbeit verwendet wurde oder auf das direkt Bezug genommen wird, wurde als solches kenntlich gemacht. Insbesondere wurden alle Personen genannt, die direkt und indirekt an der Entstehung der vorliegenden Arbeit beteiligt waren. Mit der Überprüfung meiner Arbeit durch eine Plagiatserkennungssoftware bzw. ein internetbasiertes Softwareprogramm erkläre ich mich einverstanden.“

Ort/Datum

Unterschrift

Acknowledgements

First of all, I would like to express my gratitude to all those who have to encouraged me with their support and suggestions during my doctoral thesis.

I would like to express my sincere acknowledgements to my supervisor Dr. Poornima Mahavadi for her guidance and support in completing my thesis. I also extend sincere thanks to Prof. Dr. Andreas Günther for giving me the opportunity to work in his laboratory. I thank him especially for sharing his expertise and research insights with me. I have gained invaluable knowledge and experience during my time in the laboratory and also at various international conferences.

My special thanks go to Prof. Dr. Werner Seeger and Dr. Rory E. Morty for accepting me into the "Molecular Biology and Medicine of the Lung" programme, where I had the opportunity to gain a lot of knowledge on lung biology and techniques of molecular biology from world-renewed scientist.

I also want to express my thanks to Dr. Martina Korfei for supporting me during my work as well as motivating me.

Finally, I would like to thanks all the member of the laboratory, my family and friends for supporting me during this challenging time.